Study of Multiple-Input Multiple-Output Systems Over Fading Channels

Rongtao XU

Department of Electronic and Information Engineering,
The Hong Kong Polytechnic University

A thesis submitted in partial fulfilment
of the requirements for the
Degree of Doctor of Philosophy

March 2007

CERTIFICATE OF ORIGINALITY

I hereby declare that this thesis is my own work and that, to the best of my knowledge and belief, it reproduces no material previously published or written, nor material that has been accepted for the award of any other degree or diploma, except where due acknowledgement has been made in the text.

____________________ (Signed)

Rongtao XU (Name of student)

For my family

Abstract

Recently, transmitters and receivers with multiple antennas, i.e., multiple-input multiple-output (MIMO) systems, have been proposed for use in wireless communications. The main advantage of MIMO systems over traditional single-input single-output (SISO) systems is that MIMO systems can provide much higher capacities than SISO systems, thus improving the spectral efficiency of the wireless channels. Alternatively, diversity gain can be obtained with the use of MIMO systems and appropriate transmission strategies. In this thesis, we aim to evaluate the analytical performance of MIMO systems over correlated-Rayleigh and Rician channel conditions. We also perform simulations to verify the analytical results.

Multiple-input multiple-output systems can be broadly classified into two types, namely, spatial-multiplexing based and diversity based. For the spatial-multiplexing-based (SM-based) MIMO systems, we will study both the zero-forcing (ZF) detector and the vertical-BLAST (V-BLAST) detecting algorithm. Based on the distribution of the post-detection SNR of the ZF detector, we will derive the bit error rate (BER) expressions for the MIMO systems over correlated-Rayleigh and Rician fading channels. Using the results, the performance degradation due to correlation in a Rayleigh fading channel is expressed in terms of the correlation coefficient. Moreover, we derive a closed-form expression, in terms of the Rician factor and the number of transmit antennas, for the SNR degradation of the Rician channel compared to the independent and identically distributed (i.i.d.) Rayleigh channel.

Further, based on the work done related to ZF detector, the performance of V-BLAST algorithms for the MIMO systems with two transmit antennas is analyzed over correlated-Rayleigh and Rician channels. We will derive the analytical BERs of the first and second detection steps for both optimal- and fixed-detection-ordering schemes. The effect of optimal ordering on the SNR and diversity order will then be discussed. Afterwards, we will investigate the SNR degradation of the detection steps for correlated-Rayleigh and Rician channels over an i.i.d. Rayleigh channel.

We will also evaluate the capacity of the MIMO Rician channel. We will show that the capacity of a MIMO Rician channel can be well-approximated by that of a MIMO correlated-Rayleigh channel and we will derive a close-form expression for the channel capacity. Based on the analytical results, we will study the asymptotic capacities of the Rician channel at low and high SNR regions, and the asymptotic capacity loss of the channel relative to an i.i.d. Rayleigh channel.

Finally, we will investigate thoroughly the performance of diversity-based MIMO systems with antenna selection over an intra-class correlated Rayleigh channel. We will derive the exact BERs of the MIMO systems with three different selection schemes, namely transmit-antenna selection, receive-antenna selection and the full complexity schemes. Then, the asymptotic SNR degradations due to correlation are expressed in terms of the correlation coefficient and the number of antennas. Finally, we evaluate the diversity orders and compare the SNR requirements of different selection schemes at low BER regions.

Acknowledgements

I would like to express my sincere appreciation and gratitude to my supervisor, Dr. F.C.M. Lau for his support and help during my studies. His serious and precise attitude gives me the deepest impression. One thing in my mind will never fade — he modified and improved one of my paper drafts more than ten times by himself. Without his studious efforts, I would never have published any papers. I have to admit that his high standards have greatly improved my Ph.D. research, and will continue to be my guide in the future. Also, I would never have completed this thesis without the guidance, encouragement and patience of Dr. Lau.

Special thanks to Prof. C.K. Tse. He has organized many interesting group activities for us in the past. His skillful leadership and kindness influences me deeply. I also gratefully acknowledge the Research Committee of The Hong Kong Polytechnic University for the financial support of my study.

I am very grateful to Dr. Wai-Man Tam, Dr. Yongxiang Xia, Dr. Dong Dai, Dr. Xiaoqun Wu, Mr. Yi Zhao, Mr. Qingfeng Zhou and Ms. Xia Zheng for their invaluable assistance during my studies at The Hong Kong Polytechnic University, especially in my most difficult times. I really enjoy the harmony atmosphere that has been built by all members in our group. Without them, life would be lusterless.

Finally, my deepest love and gratitude is devoted to my parents. Their love, support and encouragement give the power of my life. To them, I dedicate this thesis.

Publications

Journal Papers

1. R. Xu and F. C. M. Lau, “Performance analysis for MIMO systems using zero forcing detector over fading channels,” *IEE Proc. Communications*, vol. 153, pp. 74–80, Feb. 2006.

2. R. Xu and F. C. M. Lau, “A novel approach to analyzing V-BLAST MIMO systems with two transmit antennas,” *IEEE Transactions on Wireless Communications*, vol. 6, no. 3, pp. 1591–1595, May 2007.

3. R. Xu and F. C. M. Lau, “On the capacity of MIMO Rician channels,” *IEEE Transaction on Wireless Communications*, submitted.

4. R. Xu and F. C. M. Lau, “Performance analysis of MIMO systems with antenna selection over an intra-class correlated Rayleigh fading channel,” *IEEE Transactions on Communications*, submitted.

Conference Papers

1. R. Xu and F. C. M. Lau, “Analytical approach of V-BLAST performance with two transmit antennas,” in *Proc. IEEE Wireless Communications & Networking Conference*, New Orleans, USA, Mar. 2005, vol. 1, pp. 396–401.

2. R. Xu and F. C. M. Lau, “Degradation on the performance of MIMO systems under a correlated sub-channels condition,” in *Proc. IEEE International Symposium on Circuits and Systems*, Kobe, Japan, May 2005, pp. 4967–4970.

3. R. Xu and F. C. M. Lau, “Performance analysis for MIMO systems using zero forcing detector over Rice fading channel,” in *Proc. IEEE International*

Symposium on Circuits and Systems, Kobe, Japan, May 2005, pp. 4955–4958.

Acronyms and Notations

Acronyms

3G	third generation mobile communications systems
AWGN	additive white Gaussian noise
BER	bit error rate
BPSK	binary phase shift keying
BLAST	Bell Labs proposed Layered Space-Time
c.d.f.	cumulative distribution function
CDMA	code division multiple access
c.f.	characteristic function
CSCG	circularly symmetric complex Gaussian
CSI	channel state information
dB	decibel
D-BLAST	diagonal BLAST
DOA	direction of arrival
DOD	direction of departure
DPSK	differential phase-shift-keying
EGC	equal gain combiner
EVD	eigenvalue decomposition
FC-MRC	full complexity maximal ratio combiner
FSK	frequency shift keying
i.i.d.	independent and identically distributed
ISI	inter-stream interference
JEP	joint error probability
LOS	line-of-sight
M-QAM	multi-level quadrature amplitude modulation
MGF	moment generating function

MI	mutual information
MIMO	multiple-input multiple-output
MISO	multiple-input single-output
MMSE	minimum mean-squared-error
MRC	maximal ratio combiner
MSI	multi-stream interference
MSE	mean-squared error
OC	optimal combining
p.d.f.	probability density function
QAM	quadrature amplitude modulation
QPSK	quadrature phase shift keying
RAS-MRC	receive antenna selection with maximal ratio combiner
SC	selective combiner
SER	symbol error rate
SEP	symbol error probability
SISO	single-input single-output
SM	spatial multiplexing
SIMO	single-input multiple-output
SNR	signal-to-noise ratio
STBC	space-time block coding, or space-time block codes
STC	space-time coding, or space-time codes
STTC	space-time trellis coding, or space-time trellis codes
TAS-MRC	transmit antenna selection with maximal ratio combiner
ULA	uniform linear arrays
V-BLAST	vertical BLAST
ZF	zero forcing
ZMCSCG	zero-mean CSCG

Notations

$\mathbf{0}$	matrix with all elements of value 0
$\boldsymbol{X}^+$	pseudo-inverse of matrix $\boldsymbol{X}$
$\boldsymbol{X}^*$	complex conjugate of matrix $\boldsymbol{X}$
$\boldsymbol{X}^T$	transpose of matrix $\boldsymbol{X}$
$\boldsymbol{X}^H$	conjugate transpose of matrix $\boldsymbol{X}$
$\boldsymbol{X} > 0$	$\boldsymbol{X}$ is a positive definite matrix
$\boldsymbol{X} \otimes \boldsymbol{Y}$	kronecker product of matrices $\boldsymbol{X}$ and $\boldsymbol{Y}$
$x \sim$	random variable x is distributed as
$\lvert x\rvert$	absolute value of scalar x, or amplitude of complex x
$\lvert\boldsymbol{X}\rvert$	determinant of square matrix $\boldsymbol{X}$
$[\boldsymbol{X}]_{ij}$	element in the ith row and jth column of matrix $\boldsymbol{X}$
$\lvert\boldsymbol{X}\rvert_{\hat{\alpha}_k}^{\hat{\alpha}_k}$	determinant of row subset $\hat{\alpha}_k$ and column subsets $\hat{\alpha}_k$ of $\boldsymbol{X}$
$\boldsymbol{X}(m \times n)$	matrix of size $m \times n$
$n!$	factorial of n
$\binom{m}{n}$	binomial coefficient
$\binom{m}{l_1,\cdots,l_n}$	multinomial coefficient
$\det(\boldsymbol{X})$	determinant of square matrix $\boldsymbol{X}$
$\mathrm{diag}(x_k)$	diagonal matrix with elements of x_k
$\mathrm{E}[\cdot]$	mathematical expectation
$\mathrm{erfc}(x)$	complementary error function
$\mathrm{etr}(\boldsymbol{X})$	exponent of the trace of matrix $\boldsymbol{X}$
$\exp(x)$	exponential function
${}_pF_q(\boldsymbol{a};\boldsymbol{b};x)$	generalized hypergeometric function
$\Phi(a,b,x)$	confluent hypergeometric function of the first kind
${}_1F_0(a,\boldsymbol{X})$	hypergeometric function with one matrix argument
$\Gamma(x)$	Gamma function
$\gamma(a,x)$	incomplete Gamma function
$\Gamma(a,x)$	complementary incomplete Gamma function
$\Gamma_p(n)$	complex multivariate Gamma function
$\Im(z)$	imaginary part of complex variable z
$I_m(x)$	mth order modified Bessel function of the first kind
$\boldsymbol{I}_n$	identity matrix of size $n \times n$
$\ln(x)$	natural logarithm, base e
$\log(x)$	logarithm, base 10

$\log_n(x)$	logarithm, base n
$\max\{x_1, \ldots, x_n\}$	maximum of the elements $x_1, \ldots, x_n$
$\min\{x_1, \ldots, x_n\}$	minimum of the elements of $x_1, \ldots, x_n$
$N(\mu, \sigma^2)$	normal distribution with mean μ and variance σ^2
$\tilde{N}(\mu, \sigma^2)$	complex normal distribution with mean μ and variance σ^2
$N_p^c(\boldsymbol{\mu}, \boldsymbol{\Sigma})$	complex p-variate normal distribution with mean $\boldsymbol{\mu}$ and covariance $\boldsymbol{\Sigma}$
$N_{p,n}^c(\boldsymbol{M}, \boldsymbol{\Sigma} \otimes \boldsymbol{\Psi})$	complex matrix variate normal distribution with mean $\boldsymbol{M}(p \times n)$ and covariance $\boldsymbol{\Sigma} \otimes \boldsymbol{\Psi}$
$\Pr(\mathcal{A})$	probability of an event $\mathcal{A}$
$Q(x)$	Q-function
$Q_m(a, b)$	mth order Marcum Q-function
$\Re(z)$	real part of complex variable z
$\mathrm{tr}(\boldsymbol{X})$	trace, i.e. sum of diagonal elements of $\boldsymbol{X}$
$\mathrm{vec}(\boldsymbol{X})$	vector with stacked columns of matrix $\boldsymbol{X}$
$W_p^c(n, \boldsymbol{\Sigma})$	central Wishart distribution with parameters $p, n, \boldsymbol{\Sigma}$
$W_p^c(n, \boldsymbol{M}, \boldsymbol{\Sigma})$	non-central Wishart distribution with parameters $p, n, \boldsymbol{M}$ and $\boldsymbol{\Sigma}$

Contents

List of Figures

List of Tables

Chapter 1

Introduction

Since the early 1980's, wireless technologies have been advancing at a tremendous pace. We have experienced the evolution of mobile cellular systems from the analogue age to digital era in the 1990's. Today, the third generation mobile systems are supporting multimedia transmissions, such as video and image, in addition to traditional voice communications. Other wireless technologies such as Bluetooth and wireless local area networks are also prevalent everywhere. While the spectrum of personal wireless communications has almost been exhausted, higher and higher data rates are required to support the ever demanding wireless services.

Suppose we have a system which comprises multiple antennas equipped at both the transmitter and the receiver, together with a wireless channel between the transmitter and the receiver. If we model the system as a black box with multiple inputs at the transmitter and multiple outputs at the receiver, such a system can be regarded as a *multiple-input multiple-output* (MIMO) system. Fig. 1.1 illustrates the structure of such a MIMO system.

For a single-antenna system, also called *single-input single-output* (SISO) system, its capacity is limited by the well-known Shannon capacity [19]. But when mul-

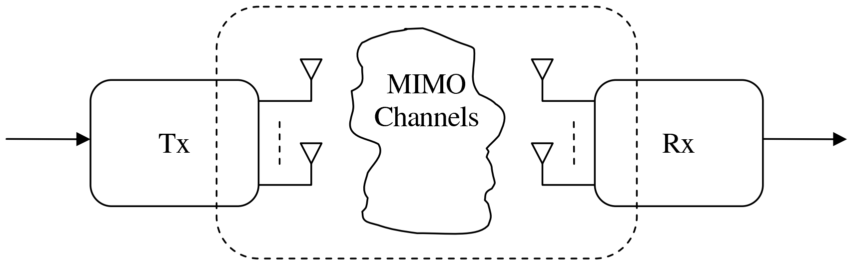

Figure 1.1: The structure of a MIMO system (Tx: Transmitter, Rx: Receiver).

tiple antennas are installed at the transmitting side, such as the base stations, it has been shown that the capacity and performance of wireless systems can be improved through the so-called beamforming techniques [55, 74, 81]. Under such a condition, the downlink, i.e., from the base station to mobile station, can be regarded as a *multiple-input single-output* (MISO) system whereas the uplink, i.e., mobile station to base station, can be treated as a *single-input multiple-output* (SIMO) system.

The earliest work on MIMO systems can be traced back to 1987, when Jack Winters at Bell Laboratories proposed a system that established communication between two mobiles, each with multiple antennas [33]. But the theoretical closed-form expression for the capacity of MIMO systems was first derived by Telatar in his pioneer paper [91]. The asymptotic analysis at the high signal-to-noise ratio (SNR) region has also shown that the capacity of such *multiple-input multiple-output* (MIMO) systems over an independent and identically distributed (i.i.d.) Rayleigh fading channel increases linearly with the number of transmit or receive antennas, whichever is the smaller [91]. Subsequently, Foschini proposed two types of Bell LAbs Space-Time architectures (BLAST), namely diagonal BLAST (D-BLAST) and vertical BLAST (V-BLAST), for MIMO systems [16, 17] which could achieve the capacity predicted in [91]. Laboratory experiments conducted in Bell Labs [97] have also revealed that spectral efficiencies of 20–40 bits per second per hertz

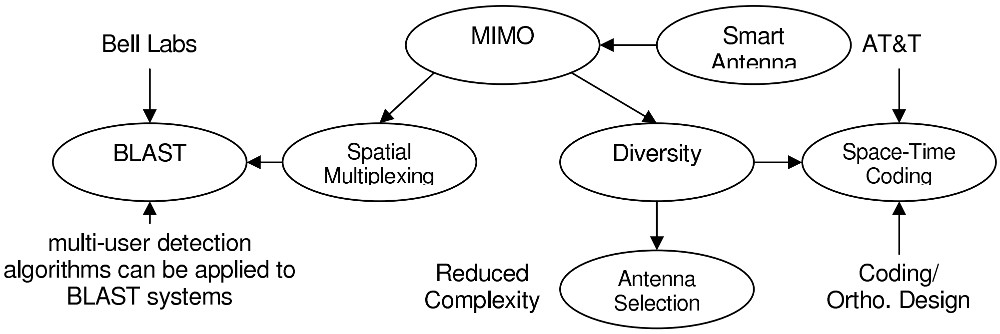

Figure 1.2: The two types of MIMO systems.

can be achieved with eight transmit antennas and twelve receive antennas in an indoor propagation environment at realistic SNRs and with acceptable error rates. Because of the works of Telatar and Foschini, the research of MIMO systems has become one of the most popular areas in wireless communications in recent years [27–30]. Generally speaking, MIMO systems can be broadly categorized into two main groups, namely spatial-multiplexing based and diversity based, as in Fig. 1.2, which will be described in the subsequent sections.

1.1 Spatial-Multiplexing-Based MIMO Systems

Fig. 1.3 shows the structure of a MIMO system using the spatial-multiplexing (SM) technique. In the SM-based system, the input data stream is first demultiplexed into a number of data sub-streams that equals the number of transmit antennas. After applying the mapping strategies, such as D-BLAST and V-BLAST, the data sub-streams are distributed to different antennas. At the receiver, the received signals are processed by a detector using various algorithms to estimate the transmitted data symbols. The algorithms applying to the detector include zero-forcing (ZF), minimum mean-square-error (MMSE), and V-BLAST, etc.

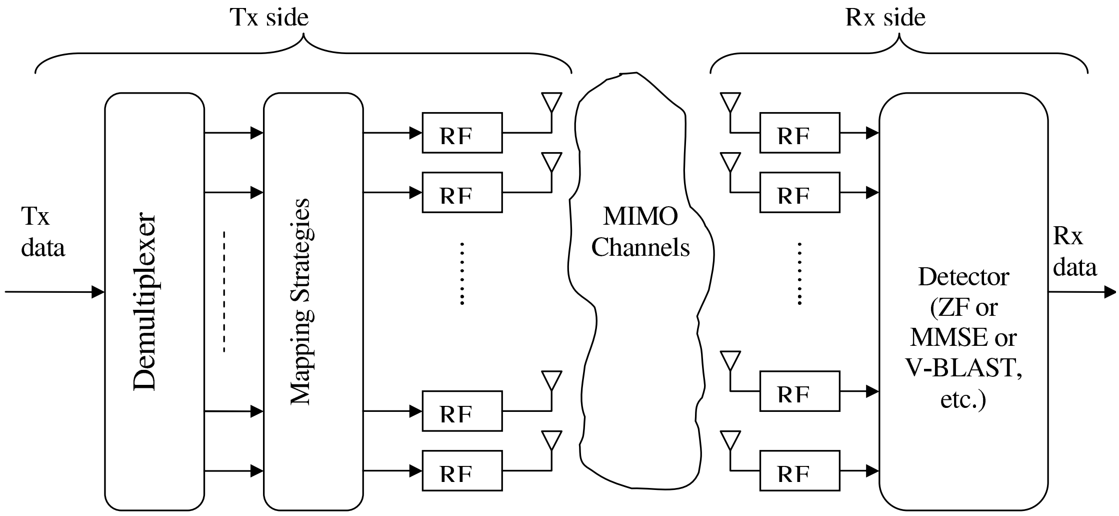

Figure 1.3: A spatial-multiplexing-based MIMO system (Tx: transmit, Rx: receive).

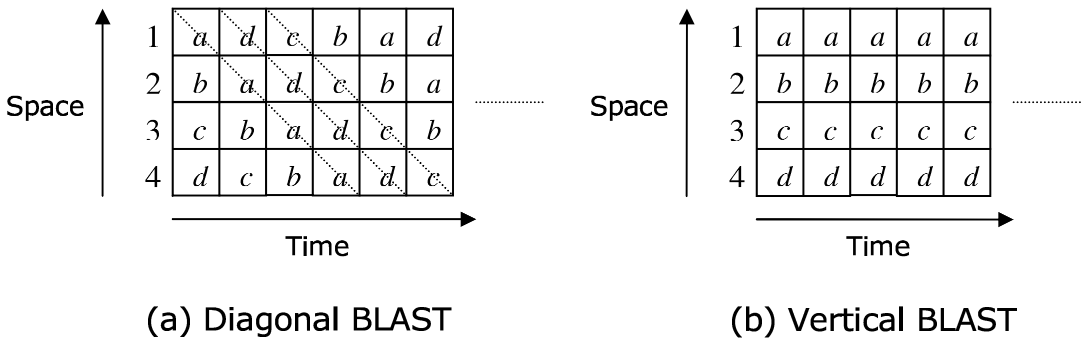

Figure 1.4: The mapping strategies of (a) D-BLAST and (b) V-BLAST systems.

1.1.1 D-BLAST Architecture

As mentioned earlier, Telatar derived only the theoretical capacity of MIMO systems [91] and it was Foschini who first proposed practical structures [16, 17], i.e., D-BLAST and V-BLAST, to achieve the predicted capacity [91]. In the BLAST structures, the incoming data stream is demultiplexed into a number of blocks that equals the number of transmit antennas. Different data blocks are sent through respective antennas that operate at the same carrier frequency. The receiver then separates and decodes the data streams using algorithms similar to multi-user detection [92].

The difference between the D-BLAST and V-BLAST lies in the way the data blocks are mapped to the respective antennas [16, 17]. Fig. 1.4 illustrates the mapping strategies for the two BLAST systems with four transmit antennas. In D-BLAST, the separates data blocks are circularly rotated and then transmitted among the antenna elements. Fig. 1.4(a) shows that in D-BLAST, the data blocks assigned to antennas 1–4 in the first burst are in the order $(a\ b\ c\ d)$, in the second burst $(d\ a\ b\ c)$, in the third burst $(c\ d\ a\ b)$ and in the fourth burst $(b\ c\ d\ a)$, and so on.

If we consider the transmit antennas individually in the space domain, the data from the same blocks in D-BLAST will be distributed diagonally. The rotation method can prevent the same data block from being transmitted over the same channel to provide spatial diversity. At the receiver, the D-BLAST detector decodes the data block from the same data stream diagonally in steps. The D-BLAST detecting algorithm includes joint detection, decoding, and interference cancellation process, in which the decoded sub-streams are used in succession to remove external interferences. For example, in Fig. 1.4(a), once the four data blocks denoted by " a " are obtained with joint detection, the interference from the sub-stream " a " will be removed for the following detection steps to decode d, c, b. Note that besides the D-BLAST detector, other linear detectors such as zero-forcing detector and minimum mean-square-error (MMSE) detector can be employed at the receiver. Such linear detectors are much simpler but with a degraded error performance.

1.1.2 V-BLAST Architecture

In V-BLAST, the data blocks are distributed among consecutive antennas. As shown in Fig. 1.4(b), the V-BLAST always assigns the data block " a " to antenna 1, " b " to antenna 2, " c " to antenna 3, and " d " to antenna 4. At the receiving end, when the V-BLAST detector is used, the data blocks with the maximum post-processing SNR are first decoded. Then the signals from the decoded data blocks are reconstructed and then subtracted from the original signals, thus reducing the interference to other data blocks. The decoding of the data block with the maximum post-processing SNR among the remaining data blocks and the interference cancellation process continue until all data blocks are decoded. Compared with the D-BLAST detector, the V-BLAST detector has a lower decoder complexity. Similar to the D-BLAST case, other linear detectors such as zero-forcing detector and MMSE detector can be used in the V-BLAST architecture but with a degraded error performance. Also, in [79], ZF and MMSE detections with successive interference cancellation based on the sorted QR-decomposition of the channel matrix have been proposed. In this scheme, only a fraction of the computational effort required by V-BLAST detector is required with a tradeoff of lower performance.

The capacity of D-BLAST and V-BLAST have been compared in detail in [18]. It has been concluded that the V-BLAST algorithm is a relatively simple algorithm to implement which can achieve a large part of the MIMO capacity. Furthermore, the V-BLAST capacity has been found to grow linearly with the increasing number of antennas and to give a large fraction (≈ 0.72 or more depending on SNR) of the capacity of the more complex D-BLAST architecture. However, in the V-BLAST architecture, the same data block is transmitted through the same channel and no spatial diversity presents. On the other hand, D-BLAST can provide both spatial and time diversity. Thus, D-BLAST always outperforms V-BLAST in terms of bit error rate [16].

1.1.3 Performance of Detectors

Multiple-input multiple-output systems have promised to provide high capacity for wireless communications over a multipath environment [16, 17, 91], and most of the researches and proposals in earlier works have been conducted under the assumption that the MIMO channels follow i.i.d. Rayleigh fading. In practical environments, correlation is present between sub-channels due to the limited number of scatters in the transmit paths, small angular spread at the transmitter or receiver, and the small separation between the antenna elements. In the presence of a purely specular or line-of-sight (LOS) path between the transmitter and the receiver, the MIMO channel is further modeled as Rician fading [15].

Moreover, the thesis considers the structure of SM-based MIMO systems. It can be observed that it is similar to that of a multi-user wireless communication system where multiple antennas have been installed at the base station. Thus, at the receiver of the MIMO system, if we regard the data sub-streams coming from the multiple transmit antennas as those sent by separate wireless users, multi-user detection algorithms can be directly applied to the SM-based MIMO system for decoding the data sub-streams. In the following, we will review the performance results of three types of detector, namely zero-forcing detector, MMSE detector and V-BLAST detector, over the aforementioned types of channels. Zero-forcing and MMSE detectors are simple linear detectors with lower error performances whereas the V-BLAST detector can provide better performance at the expense of a more complex decoding algorithm.

1.1.3.1 Zero-Forcing Detector

The linear zero-forcing (ZF) detector has been designed to eliminate the multi-stream interference (MSI) completely at the expense of noise enhancement [75].

The performance of MIMO ZF detector has been studied in [23, 40]. Given a certain transmit correlation matrix, the probability density function (p.d.f.) of the output SNR was derived as chi-square distributed. The average symbol error rate (SER) or bit error rate (BER) performance of MIMO systems over a correlated-Rayleigh fading channel using the ZF detector has been derived theoretically in [43]. It has further been found that the ZF detector can achieve a diversity order of $(r - t + 1)$ irrespective of the transmit or receive correlation, where r denotes the number of receive antennas and t represents the number of transmit antennas, respectively. Further, simulation results have shown that provided the signal power from the non-line-of-sight (fading) components remains the same, the performance of the MIMO system in a Rayleigh channel and a Rice channel will be the same [26].

1.1.3.2 MMSE Detector

The MMSE detector, on the other hand, is designed to minimize the mean-squared error (MSE) between the estimated data and the transmitted ones [75]. The MMSE technique can provide better estimations than the ZF algorithm at a similar computational cost. However, the MMSE algorithm requires an estimated value for SNR. The signal processing algorithm in the MMSE receiver for MIMO systems is the same as the optimum combining (OC) algorithm for multi-user communications. The exact analysis of OC can be found in literatures [20, 21, 51, 52, 64, 82, 83] and their references. These results can be used to calculate the performance of MIMO systems using MMSE receiver under spatially uncorrelated fading. The exact theoretical results for an arbitrarily correlated-Rayleigh fading channel can also be found in [41, 43]. However, the SER closed-form expressions with arbitrary numbers of transmit and receive antennas are lengthy and tedious. Fortunately, at high SNR, the performance of MMSE receiver converges to that of a ZF receiver. By making use of the average BER of ZF receiver as an upper BER bound of the MMSE receiver, we can conclude that the diversity order of MMSE receiver also equals $(r - t + 1)$.

1.1.3.3 V-BLAST Detector

In the above, we have reviewed the work on linear detectors, namely ZF and MMSE detectors, for SM-based MIMO systems. The iterative nulling and canceling scheme is a suboptimal algorithm that decodes the data streams in a sequential fashion. It is similar to the iterative interference cancellation schemes for multiuser detection [92] and has already been utilized in BLAST systems. When ZF or MMSE method is applied to mitigate the interferences from other undecoded data streams in each detection step, the performance of SM-based MIMO systems can be significantly improved [97]. Moreover, it has been found that when symbol cancellation is used, the order of detection becomes important to the overall performance of the system. It is because the data stream with the minimum post-processing SNR will dominate the error performance of the system. Further, the ordering based on post-detection signal-to-noise ratio (SNR) has been proven to be the optimal method [18, 97].

In the V-BLAST detector, the data stream with the maximum post-processing SNR is first decoded. Then the signal from the decoded data stream is reconstructed and substracted from the original signal received. The decoding of the data block with the maximum post-processing SNR among the remaining data blocks and the interference cancellation process is then continue until all data blocks are decoded. Since the detector ordering is based on the maximum post-detection SNR, it is the optimal ordering [18, 97]. Compared to the algorithm with fixed detection ordering, the optimal ordering algorithm requires a larger computational effort. In addition to the above symbol cancellation technique, other detection techniques such as V-BLAST based on minimum mean-squared-error (MMSE) reception with successive interference cancellation [99], and turbo-BLAST architecture using turbo principles [65] have been proposed for MIMO systems to obtain high spectral efficiency.

In [73], the exact average joint error probability (JEP) as well as symbol error probability (SEP) of MIMO ZF decision feedback detector with fixed ordering under an i.i.d. Rayleigh fading channel are derived under the assumption that errors propagate in consecutive detection steps. Asymptotic analysis has shown that the diversity order of average JEP or SEP is limited to $(r - t + 1)$ because of the error propagation [73]. Moreover, the theoretical performance of MMSE reception with successive cancellation and fixed detection ordering for MIMO systems has been studied in [99] for uncorrelated channels.

When optimal ordering is implemented, the only theoretical result has been given by Loyka for V-BLAST with two transmit antennas under an i.i.d. Rayleigh fading channel [59]. The closed-form expressions for outage probabilities and average BERs have been derived [59] based on the geometrical approach. It has further been concluded from both the analytical analysis and the numerical Monte-Carlo simulations that the effect of optimal ordering in a two-transmit-antenna system is equivalent to increasing the first step SNR by 3 dB, but not increasing the diversity order. For the correlated-Rayleigh fading and Rician fading channels, there are no published results in the literature.

1.1.4 Capacity

The capacity analysis of MIMO systems is another active research area that has been conducted in the past few years. The pioneer work by Telatar [91] has shown that much capacity gain can be achieved for MIMO systems under an i.i.d. flat Rayleigh fading environment.

But the capacity of MIMO systems is degraded whenever correlations exist among the sub-channels. For example, under the assumption that there is an exponential correlation among the sub-channels, an asymptotic analytical expression for the channel capacity has been derived in the high SNR region [56, 57]. The main conclusions were that the capacity decreased with the correlation coefficient and that correlation among the sub-channels produces the same effect as reducing the SNR. In [9], assuming arbitrary correlation among the transmit antennas or the receive antennas, closed-form expression for the characteristic function of MIMO system capacity has been found. Subsequently, the cumulative distribution function of the capacity is derived, allowing the evaluation of the mean capacity and outage capacity of the MIMO system. Based on the analysis, it is further concluded that under an exponential correlation model, the capacity reduction is minimal if the correlation coefficient between adjacent antennas is less than 0.5. A similar remark has also been made in [36] in which the capacity is evaluated by deriving first the moment generating function of and then the mean of the mutual information. In [68], assuming fading correlation at either the transmitting or receiving end, the asymptotic capacity per transmit antenna has been analyzed when the numbers of both transmitting and receiving antennas are increased at the same rate without bound. Results have shown that the growth rate of the asymptotic capacity per receive antenna is not affected by the fading correlation. Other independent works on the MIMO capacity over correlated-Rayleigh fading channels can be found further in [44–48, 77].

Some research work has also been performed on MIMO systems under a Rician channel [12, 34, 37, 53, 66, 67, 70, 78], which may be modeled approximately as the sum of a specular component and a scattered component [14]. In particular, the capacity found using the numerical integration method has verified that the line-of-sight signal component in the Rician channel reduces the MIMO channel capacity as a consequence of the lack of scattering [37]. Asymptotic analysis shows that the capacity for a MIMO system under a Rician channel decreases as the Rician factor increases and approaches the capacity of its scattered component when the antenna

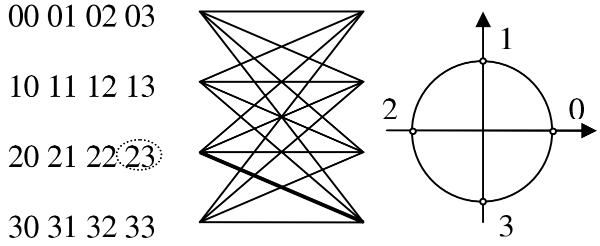

(a) Space-time trellis codes with 2 transmit antennas 4-PSK, 4-states, 2b/s/Hz

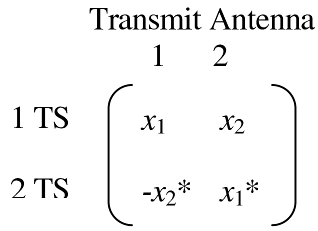

(b) Space-time block codes with 2 transmit antennas (TS: time slot)

Figure 1.5: The space-time codes.

numbers are large and the specular matrix has a unit rank [53]. However, the exact effect of the LOS path on the capacity loss of a Rician channel relative to an i.i.d. Rayleigh channel has not been given in closed-form expressions until now.

1.2 Diversity-Based MIMO Systems

In diversity-based MIMO systems, space-time codes (STC) and antenna selection are typical techniques used to accomplish diversity gain.

1.2.1 Space-Time Codes

In the STC scheme, the transmitter encodes the data stream through both space (different transmit antennas) and time domains (consecutive time symbols) to attain high diversity gain. In [89], Tarokh has proposed space-time trellis codes (STTCs) which can achieve both diversity and coding gains. The STTCs are based on the trellis used in convolutional codes and trellis coded modulation (TCM), whereas the labels of the trellis transition branch become vectors representing the signals transmitted on the multiple antennas. Fig. 1.5(a) displays an example of the STTCs with four states and quadrature-phase-shift-keying (QPSK) modulation using two transmit antennas. The labels on the left of each node represent the four trellis branches leading from that node, in the order from the top to the bottom. The four phase states of the QPSK constellation are denoted by the numbers "0" to "3". Because there are four branches diverging from each node, the transmitter encodes two bits of information in each trellis transition. For example, for the branch transition shown with a thicker line, "2" is sent to antenna 1 and "3" to antenna 2. Since the Viterbi algorithm is used to decode the STTC at the receiver [93], the complexity of the receiver will increase exponentially with the number of states of the trellis and the number of transmit antennas.

Space-time block coding (STBC) is another powerful STC scheme based on some well constructed transmit matrices [3,90]. Such transmit techniques can ensure that the data streams mapping to the different transmit antennas at consecutive time slots are orthogonal. Fig. 1.5(b) shows an example of STBC with two transmit antennas. In the first time slot, the data blocks x_1 and x_2 are transmitted by antenna 1 and 2, respectively. In the second time slot, $-x_1^*$ and x_2^* are distributed to antenna 1 and 2. Because of this transmission scheme, the receiver can use a very simple linear process to demodulate the data stream [3]. Therefore, the structure of STBC receiver is very simple. The disadvantage of STBC, however, is that there is no coding gain. For further discussion about space-time coding, interested readers can refer to the book written by Vucetic [94].

1.2.2 Antenna Selection

To reduce the cost and complexity of MIMO systems, antenna selection at the transmit or receive side, or at both sides has been proposed [69,80]. In practice, one of the main limitations of MIMO systems is the cost of RF chains and its relative

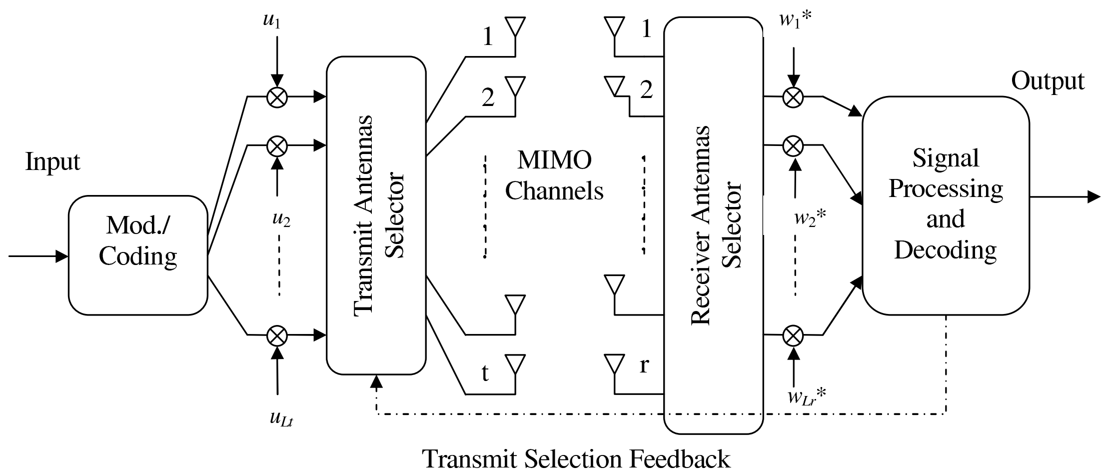

Figure 1.6: A generalized antenna selection MIMO system.

components. Antenna selection scheme, which selects a subset of transmit antennas and receive antennas to be active based on some criteria, can reduce the number of RF chains and then save the cost and power.

The structure of a generalized antenna selection MIMO system [69,80] is shown in Fig. 1.6. A bit stream, after being modulated and encoded, is replicated to L_t parallel streams. These data streams are multiplied by the coefficients $u_i(i = 1, 2, \cdots, L_t)$ to ensure that the receiver can distinguish the transmitted data from different antennas, which are sending the same data. Afterwards, the transmit antenna selector switches the modulated and encoded signals to the best L_t out of the t transmit antennas. At the receiver, the best L_r out of the r receive antennas are selected. The picked signals are weighted by the coefficients $w_j^*(j = 1, 2, \cdots, L_r)$ corresponding to the weighted method at the transmitter and then processed by the detector to obtain the estimated transmit data. If the transmitter has no knowledge of the channel, the information about transmit antenna selection must be fed back from the receiver.

It has been shown that antenna selection is an efficient scheme to improve the link quality of diversity-based MIMO systems according to the average BER [6,101]. Furthermore, this technique produces the same diversity order as the full complexity MIMO system, which refers to the systems that use all the RF chains at the transmit and receive side.

1.2.3 Performance of Antenna Selection

The performance of MIMO systems with antenna selection has been studied to some extent. The outage probability of a MIMO system with receive-antenna selection under an i.i.d. Rayleigh fading channel has been studied analytically [85], which shows that the diversity order of receive-antenna selection is the same as that of the full complexity system. The approximated SNR loss due to antenna selection has also been derived.

In [8], the authors have proposed a scheme combining transmit-antenna selection and receiver maximal-ratio-combining (MRC). The exact expressions of outage probability and average BER have been given for an i.i.d. Rayleigh fading channel. The simulation results have shown that the performance of the scheme outperforms some complex space-time codes with the same spectral efficiency. The performance of receive-antenna selection combining space-time coding has been investigated in [5]. The conclusion is that the proposed scheme can achieve the full diversity as the one using all available antenna elements.

For an arbitrary correlated-Rayleigh channel, Yang has studied the performance of the transmit-antenna selection scheme [98]. Further, a closed-form BER expression has been derived for the systems with two receive antennas. Later, Wang has derived accurate BER expressions of transmit-antenna selection over an arbitrarily correlated Nakagami-m fading channel [95,96]. The theoretical results are also validated with computer simulations. Unfortunately, the theoretical results derived for the arbitrarily correlated channels [95, 96, 98] are intricate and difficult for further analysis.

1.3 Objective and Organization of the Thesis

Our literature survey has indicated that evaluating the performance of MIMO systems over a Rician channel analytically remains one of the difficult tasks in the study of MIMO systems. In this thesis, we aim to evaluate the performance of MIMO systems analytically, especially over a Rician channel. We will show that the MIMO Rician model can be well approximated with correlated-Rayleigh channel models in statistics. In particular, we will evaluate thoroughly the performance of zero-forcing detector and $2 \times r$ V-BLAST detector over i.i.d. Rayleigh, correlated-Rayleigh, and Rician channels. Further, we will derive the capacity of MIMO systems over a Rician channel and compared its degradation with that over an i.i.d. Rayleigh channel. Finally, we will investigate MIMO systems with antenna selection over an intra-class correlated-Rayleigh fading channel. We will derive the exact bit error rates of the systems under three different diversity schemes, namely transmit-antenna selection, receive-antenna selection and full complexity schemes and we will compare the asymptotic performance of these three diversity schemes analytically. The rest of this thesis is organized as follows.

Chapter 2 is devoted to the analysis of spatial-multiplexing-based MIMO (SM-based) systems employing simple zero-forcing detectors at the receiver. Based on the distribution of the post-detection SNR of the ZF detector, we will derive the BER expressions for the MIMO system over three types of channels, namely independent and identically distributed (i.i.d.) Rayleigh channel, correlated-Rayleigh channel, and Rician channel. In particular, the exponential correlation matrix, which has been successfully used in many communication problems, will be used to model the correlated-Rayleigh channel. The SNR degradations of the correlated-Rayleigh channel and the Rician channel compared to an i.i.d. Rayleigh channel will also be determined in terms of the exponential correlation coefficient and Rician factor, respectively. Further, simulations will be performed to verify the analytical results.

In Chapter 3, we present a novel analytical approach to studying V-BLAST systems with two transmit antennas when optimal ordering is used. Based on the analytical tools and techniques developed in Chapter 2, we will derive the distributions of the post-detection SNRs of the V-BLAST detector. Closed-form analytical expressions of the BERs and the diversity orders for the $2 \times r$ V-BLAST systems employing optimal ordering will then be found when subject to i.i.d. Rayleigh fading, correlated-Rayleigh fading, and Rician fading, respectively. The effect of optimal ordering on SNR and the diversity order will also be discussed. Further, we investigate the SNR degradation of the detection steps for correlated-Rayleigh and Rician channels over an i.i.d. Rayleigh channel. Simulation results will also be used to validate our theoretical analysis.

Chapter 4 studies the capacity of MIMO systems over a Rician channel. We will first derive a close-form expression for the MIMO channel capacity. During the process, we will show that the capacity of a MIMO Rician channel can be well approximated by that of a MIMO correlated-Rayleigh channel. Based on the solution, the asymptotic capacities at low and high SNR regions will be analyzed. Also, the asymptotic capacity loss of the Rician channel relative to an i.i.d. Rayleigh channel will be derived. Further, the analytical findings will be presented together with the results found by simulations.

Chapter 5 presents our last set of results. In this chapter, we will investigate diversity-based MIMO systems with antenna selection over an intra-class correlated-Rayleigh fading channel. In our study, one single transmit or receive antenna with an aim to maximizing the total received signal-to-noise ratio will be selected for transmission or reception, while it is assumed that the other side will use all the available antennas. Using binary-phase-shift-keying (BPSK) modulation as an illustration, we will derive the exact bit error rates of the systems under three different diversity schemes, namely transmit-antenna selection, receive-antenna selection and full complexity schemes. Moreover, we will compare the asymptotic performance of these three diversity schemes analytically. The effect of correlation among the sub-channels on the SNR degradation will also be determined in terms of the correlation coefficient and the number of transmit/receive antennas.

In Chapter 6, we summarize the contributions in this thesis and provide some future research directions.

Chapter 2

Performance Analysis Of Zero Forcing Detectors

Although Rayleigh and Rice fading channels are the most popular models for wireless channels, much of the research work on the performance of MIMO systems has been focused on Rayleigh fading channels [6]. The performance of MIMO systems over a correlated-Rayleigh fading channel using the low complexity zero-forcing detector has been evaluated in [42,43]. The theoretical and simulated results have shown that the correlation between sub-branches can cause performance degradation. In [26], the bit error rate (BER) performance of MIMO systems using ZF detector in both Rayleigh and Rician fading channels has been evaluated by simulations. Results have shown that when the signal powers from the non-line-of-sight components remain the same, the performance of the MIMO system in Rayleigh and Rician fading channels is almost the same [26]. Yet, there is still a lack of theoretical results for the performance of MIMO systems over a Rician fading channel.

In this chapter, we start our formal investigations into MIMO systems. To begin with, we analyse the performance of spatial-multiplexing-based MIMO (SM-based) systems employing simple zero-forcing detectors at the receiver. Based on the distribution of the post-detection SNR of the ZF detector, we derive the BER expressions for the MIMO system over three types of channels, namely independent and identically distributed (i.i.d.) Rayleigh channel, correlated-Rayleigh channel, and Rician channel. In particular, the exponential correlation matrix, which has been successfully used in many communication problems, is used to model the correlated-Rayleigh channel. The SNR degradations of the correlated-Rayleigh channel and the Rician channel compared to an i.i.d. Rayleigh channel are also determined in terms of the exponential correlation coefficient and Rician factor, respectively. Further, simulations are performed to verify the analytical results.

The rest of this chapter is organized as follows. In Section 2.1, the SM-based MIMO system model is described and the symbols are defined. In Section 2.2, we derive the post-detection SNR distribution of MIMO systems with a ZF detector over fading channels. Moreover, the models for the i.i.d. Rayleigh channel, exponential correlated-Rayleigh channel, and Rician channel are given. The analytical BER performances of the MIMO system over these channels are also derived and compared. Finally, in Section 2.3, we show some analytical and simulation results.

2.1 System Model

We consider an SM-based MIMO system (t, r) where t and r denote the number of transmit and receive antennas, respectively. As shown in Fig. 2.1, the incoming data stream is first split into t data sub-streams with the same symbol rate. We assume that the same modulation scheme is used for each data sub-stream and all the transmitters (1 to t) are operating at the same carrier frequency. Also, data transmission is organized into bursts and the modulated signals are radiated through the respective antennas.

Consider the structure of the equivalent baseband system of a single-user link.

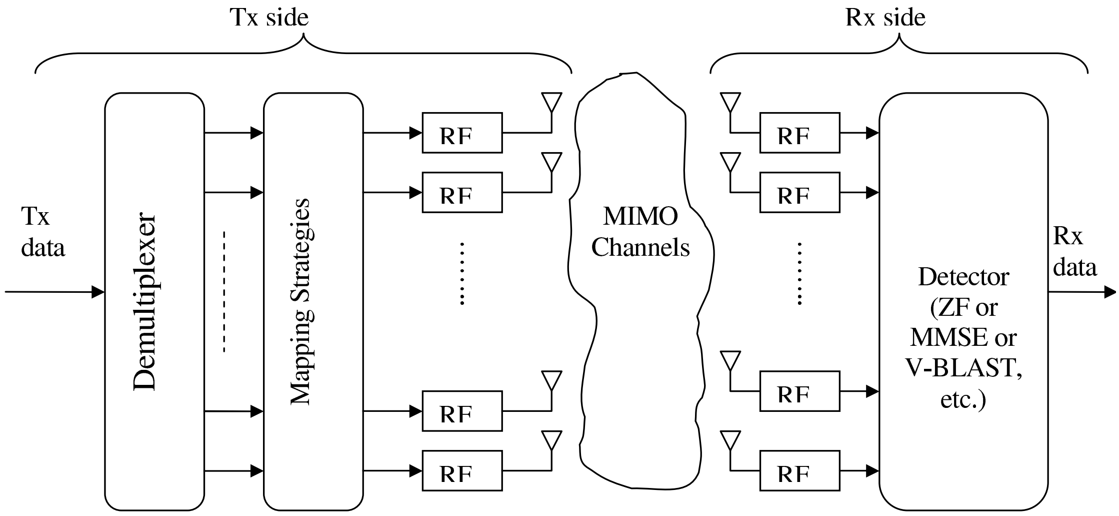

Figure 2.1: A spatial-multiplexing-based MIMO system (Tx: transmit, Rx: receive).

We assume that the transmitted signals encounter flat fading before reaching the receiving antennas. The impulse response of the channel between the jth ($j = 1, 2, \ldots, t$) transmit antenna and the ith ($i = 1, 2, \ldots, r$) receive antenna is denoted by $h_{i,j}$. The received signal can therefore be presented in the following complex baseband vector form

$$\boldsymbol{y} = \boldsymbol{H}\boldsymbol{d} + \boldsymbol{n} \tag{2.1}$$

where $\boldsymbol{y} = [y_1 \cdots y_r]^T$ is the received signal vector, $\boldsymbol{H}$ is a $r \times t$ channel matrix containing the elements $h_{i,j}$, $\boldsymbol{d} = [d_1 \cdots d_t]^T$ is the transmitted symbol vector, and $\boldsymbol{n} = [n_1 \cdots n_r]^T$ is the noise vector. The elements of $\boldsymbol{H}$ are assumed as circularly symmetric complex Gaussian (CSCG) random variables [75].

The received signal $\boldsymbol{y}$ will be processed by a detector whose aim is to determine the received data symbols. In our analysis, it is assumed that the channel matrix $\boldsymbol{H}$ is known at the receiver but not at the transmitter. We assume that the channel is random, quasi-static, frequency independent and the signal is corrupted by complex AWGN. Moreover, the elements of $\boldsymbol{n}$ are taken to be i.i.d. Gaussian random variables with zero mean and variance σ^2.

2.2 Performance Analysis

The zero-forcing detector is designed to completely eliminate the inter-stream interference (ISI), but at the expense of noise-level enhancement. Using the equivalent baseband MIMO system model, the estimated data vector can be obtained by simply multiplying the received signals with $\boldsymbol{H}^+$, the pseudo-inverse of the channel matrix [75]. In other words, the estimated data vector, denoted by $\hat{\boldsymbol{d}}$ is given by

$$\hat{\boldsymbol{d}} = \boldsymbol{H}^+(\boldsymbol{H}\boldsymbol{d} + \boldsymbol{n}) = \boldsymbol{d} + \boldsymbol{H}^+\boldsymbol{n}. \tag{2.2}$$

Using $\boldsymbol{H}^+ = (\boldsymbol{H}^H\boldsymbol{H})^{-1}\boldsymbol{H}^H$, the post-detection SNR with the ZF detector can be expressed as [23]

$$\gamma_k = \frac{\gamma_o}{[\boldsymbol{H}^H\boldsymbol{H}]^{-1}_{kk}},\ k = 1, \cdots, t \tag{2.3}$$

where γ_o is the normalized received SNR at each receive antenna and is defined as

$$\gamma_o = \frac{\mathrm{E}[|d_k|^2]}{\sigma^2}. \tag{2.4}$$

We assume that there is a large physical separation between the receive antennas, i.e., there is no correlation between any pair of receive antennas. This scenario corresponds to the uplink channel from the mobile terminal to the base station. In the case of mobile communications, using the Kronecker correlation model [38] and defining $\boldsymbol{\Sigma}$ as the covariance matrix of the channel at the transmitter side, $\boldsymbol{H}$ has a complex matrix variate normal distribution [22] denoted by $\boldsymbol{H} \sim N^c_{r,t}(\boldsymbol{M}, \boldsymbol{I}_r \otimes \boldsymbol{\Sigma})$, where $\boldsymbol{M}$ is the mean matrix of $\boldsymbol{H}$. Defining $\boldsymbol{Z} = \boldsymbol{H}^H\boldsymbol{H}$, $\boldsymbol{Z}$ then follows a complex Wishart distribution [22, 39] denoted by $\boldsymbol{Z} \sim W^c_t(r, \boldsymbol{M}, \boldsymbol{\Sigma})$. Depending upon $\boldsymbol{M} = \boldsymbol{0}$ or $\boldsymbol{M} \neq \boldsymbol{0}$, $\boldsymbol{0}$ being the all-zero matrix, the complex Wishart distribution is central or non-central, respectively. In the following, we will simply use *complex Wishart distribution* when referring to *central complex Wishart distribution*.

The p.d.f. of the non-central Wishart distribution (see (2.47) in Appendix 2A) includes the hypergeometric function with matrix arguments and is therefore difficult to analyze [10, 11]. However, the non-central complex Wishart distribution can be approximated by a complex Wishart distribution [88] by representing non-central complex Wishart matrix with normal vectors. Suppose we construct a complex Wishart distribution $\hat{\boldsymbol{Z}} \sim W_t^c(r, \hat{\boldsymbol{\Sigma}})$, where $\hat{\boldsymbol{\Sigma}} = \boldsymbol{\Sigma} + \frac{1}{r}\boldsymbol{M}^H\boldsymbol{M}$. Comparing $\boldsymbol{Z} \sim W_t^c(r, \boldsymbol{M}, \boldsymbol{\Sigma})$ and $\hat{\boldsymbol{Z}}$, it can be shown that the first order moments of $\boldsymbol{Z}$ and $\hat{\boldsymbol{Z}}$ are identical, whereas the second order moments $\mathrm{E}(\boldsymbol{Z}_{ij}\boldsymbol{Z}_{kl})$ and $\mathrm{E}(\hat{\boldsymbol{Z}}_{ij}\hat{\boldsymbol{Z}}_{kl})$ differs by $\frac{1}{r}[\boldsymbol{M}_{ik}(\boldsymbol{M}_{jl})^* + \boldsymbol{M}_{il}(\boldsymbol{M}_{jk})^*]$. This suggests that we can approximate the distribution of $\boldsymbol{Z}$ by a complex Wishart distribution with parameters r, t and $\boldsymbol{\Sigma} + \frac{1}{r}\boldsymbol{M}^H\boldsymbol{M}$, i.e., $\boldsymbol{Z} \sim W_t^c(r, \boldsymbol{\Sigma} + \frac{1}{r}\boldsymbol{M}^H\boldsymbol{M})$.

For the case where $\boldsymbol{Z}$ follows a complex Wishart distribution, the p.d.f. of γ_k is given by [23, 40]

$$f(\gamma_k) = \frac{\exp(-\gamma_k/\gamma_{o,k})}{\gamma_{o,k}\Gamma(r-t+1)} \left(\frac{\gamma_k}{\gamma_{o,k}}\right)^{r-t}, \; k = 1, \cdots, t \tag{2.5}$$

where

$$\gamma_{o,k} = \gamma_o / [\hat{\boldsymbol{\Sigma}}^{-1}]_{kk} \tag{2.6}$$

and $\Gamma(r-t+1)$ represents the Gamma function (see (2.32) in Appendix 2A). Also we can obtain the c.d.f. of γ_k as

$$F(\gamma_k) = \frac{\gamma(r-t+1, \gamma_k/\gamma_{o,k})}{\Gamma(r-t+1)} \tag{2.7}$$

where $\gamma(a, z)$ denotes the incomplete Gamma function (see (2.36) in Appendix 2A).

A unified approach to analyze the performance of digital communication systems over fading channels has been developed based on the moment-generating-function (MGF) method [87]. Once we have the p.d.f. of the post-detection SNR, i.e., $f(\gamma_k)$, we can obtain the MGF associated with γ_k using

$$M_{\gamma_k}(s) = \int_0^\infty f(\gamma_k) e^{s\gamma_k}\, d\gamma_k. \tag{2.8}$$

Then, the average SER or BER of the ZF detector can be found through the so-called *unified MGF-based approach* for almost all modulation schemes. As an example, we employ quadrature phase shift keying (QPSK) as the modulation/demodulation scheme throughout this chapter. We can subsequently obtain the average BER of the ZF detector as (see Appendix 2B for details)

$$P_k = \frac{1}{2} - \sqrt{\frac{\gamma_{o,k}}{\pi}} \times \frac{\Gamma(r-t+\frac{3}{2})}{\Gamma(r-t+1)} \times {}_2F_1\left(\frac{1}{2}, r-t+\frac{3}{2}; \frac{3}{2}; -\gamma_{o,k}\right) \tag{2.9}$$

where ${}_2F_1(a,b;c;z)$ is the hypergeometric function (see (2.53) in Appendix 2B). Alternatively, we can make use of (2.5) and (2.55) to obtain

$$P_k = J(r-t+1, 1, 2\gamma_{o,k}) \tag{2.10}$$

where $J(n,a,b)$ is defined in (2.57) in Appendix 2C. Both (2.9) and (2.10) can be used to calculate the average BER of the ZF detector. As for other modulation schemes (e.g., M-PSK, M-QAM etc.), the average BER or SER can be obtained using similar procedures and the corresponding conditional BER or SER expressions.

In the following, we derive the diversity order of the MIMO system under study. Diversity order has been defined as the absolute values of the slopes of the error probability curves plotted on a log-log scale at high SNR values [76], i.e.,

$$D_e \triangleq \lim_{\sigma^2 \to 0^+} \frac{\log(P_k)}{\log(\sigma^2)}. \tag{2.11}$$

Alternatively, based on (2.4), (2.11) can be expressed as

$$D_e = -\lim_{\gamma_o \to +\infty} \frac{\log(P_k)}{\log(\gamma_o)}. \tag{2.12}$$

Substituting (2.10) into (2.12) and making use of (2.61) in Appendix 2C, we arrive at

$$D_e = -\lim_{\gamma_o \to +\infty} \frac{\log(J(r-t+1, 1, 2\gamma_{o,k}))}{\log(\gamma_o)} = r - t + 1. \tag{2.13}$$

Hence, we conclude that ZF detector achieves a diversity order of $(r-t+1)$ regardless of the type of channel, which is consistent with the result reported in [23, 40, 100].

From (2.9), the average BER is dependent on $\gamma_{o,k}$, i.e., $\gamma_o/[\hat{\boldsymbol{\Sigma}}^{-1}]_{kk}$, for the given MIMO systems. When $\hat{\boldsymbol{\Sigma}} = \boldsymbol{I}_t$, the channel is uncorrelated and corresponds to an i.i.d. Rayleigh fading channel. $\hat{\boldsymbol{\Sigma}} \neq \boldsymbol{I}_t$ defines the correlated channel with correlation at the transmitter side. Therefore, the degradation in effective SNR due to transmit correlation can be best described with $[\hat{\boldsymbol{\Sigma}}^{-1}]_{kk}$. In the following, we focus on the diagonal elements of the inverse matrix $\hat{\boldsymbol{\Sigma}}^{-1}$ that are causing degradation in performance.

2.2.1 I.I.D. Rayleigh Fading Channel

The Rayleigh distribution is frequently used to model the multipath fading with no direct line-of-sight (LOS) path between the transmitter and receiver [32, 54, 76]. The channel coefficient of a Rayleigh fading channel is modeled as a zero mean circularly symmetric complex Gaussian (ZMCSCG) variable x. The distribution of x is denoted by $x \sim \tilde{N}(0, \xi^2)$ where ξ^2 represents the common variance of the real and imaginary parts of the channel response. Moreover, the envelope of the channel response follows a Rayleigh distribution. Defining $u = |x|$, the p.d.f. of u is given by

$$f_u(u) = \frac{u}{\xi^2} \exp\left(-\frac{u^2}{2\xi^2}\right), \quad u \geq 0. \tag{2.14}$$

Further, denoting the square u by v, i.e., $v = u^2$, v will follow an exponential distribution given by

$$f_v(v) = \frac{1}{2\xi^2} \exp\left(-\frac{v}{2\xi^2}\right), \quad v \geq 0. \tag{2.15}$$

The MIMO Rayleigh fading channel is a generalization of the univariate Rayleigh channel. Each element in the channel matrix $\boldsymbol{H}$ is now ZMCSCG distributed. When all the transmitted signals suffer from an i.i.d. Rayleigh fading, we have $\boldsymbol{\Sigma} = \boldsymbol{I}_t$ and $\boldsymbol{M} = \mathbf{0}$. As a consequence, $[\hat{\boldsymbol{\Sigma}}^{-1}]_{kk} = 1$ and $\gamma_{o,k} = \gamma_o$. The BER performance of the MIMO system can then be directly calculated from (2.9) or (2.10).

2.2.2 Rayleigh Fading Channel with Exponential Correlation Matrix

In a realistic environment, correlation may exist between the transmit antennas and the correlation coefficient $[\boldsymbol{\Sigma}]_{ij}$ decreases with increasing distance between the antenna elements. The exponential correlation matrix model, which has been successfully used in many communication problems, is a good candidate to model this scenario (for example, the unitary linear array). The elements of the exponential correlation matrix are given by [57]

$$[\boldsymbol{\Sigma}]_{ij} = \begin{cases} \rho^{j-i}, & \text{if} \quad i \leq j \\ (\rho^{i-j})^*, & \text{if} \quad i > j \end{cases} \quad |\rho| < 1 \tag{2.16}$$

where ρ is the (complex) correlation coefficient of neighboring antennas. In other words, $\mathbf{\Sigma}$ is represented by

$$\mathbf{\Sigma} = \begin{bmatrix} 1 & \rho & \rho^2 & \cdots & \cdots & \rho^{t-1} \\ \rho^* & 1 & \rho & \rho^2 & \cdots & \rho^{t-2} \\ \cdots & \cdots & \cdots & \cdots & \cdots & \cdots \\ (\rho^*)^{t-1} & (\rho^*)^{t-2} & \cdots & \cdots & \cdots & 1 \end{bmatrix}. \tag{2.17}$$

The determinant of $\mathbf{\Sigma}$ is readily shown equal to

$$\det(\mathbf{\Sigma}) = \det \begin{bmatrix} 1-|\rho|^2 & 0 & 0 & \cdots & \\ \rho^*(1-|\rho|^2) & 1-|\rho|^2 & 0 & \cdots & \\ \cdots & \cdots & \cdots & \cdots & \\ (\rho^*)^{t-1} & (\rho^*)^{t-2} & \cdots & 1 & \end{bmatrix} = (1-|\rho|^2)^{t-1}. \tag{2.18}$$

For the inverse of $\mathbf{\Sigma}$, i.e., $\mathbf{\Sigma}^{-1}$, we are only interested in the diagonal elements (refer to the paragraph before Section 2.2.1 for details), which can be shown equal to (see Appendix 2D for details)

$$[\mathbf{\Sigma}^{-1}]_{kk} = \begin{cases} 1/(1-|\rho|^2), & k = 1, t \\ (1+|\rho|^2)/(1-|\rho|^2), & k = 2, \ldots, t-1. \end{cases} \tag{2.19}$$

Combining the results in (2.9) and (2.19), the SNR degradation due to correlation at the transmitter side compared to an i.i.d. Rayleigh channel ($\mathbf{\Sigma} = \boldsymbol{I}_t$) is given by

$$\Delta\gamma_{k,\text{corr loss}} = [\mathbf{\Sigma}^{-1}]_{kk} = \begin{cases} 1/(1-|\rho|^2), & k = 1, t \\ (1+|\rho|^2)/(1-|\rho|^2), & k = 2, \ldots, t-1, \end{cases} \tag{2.20}$$

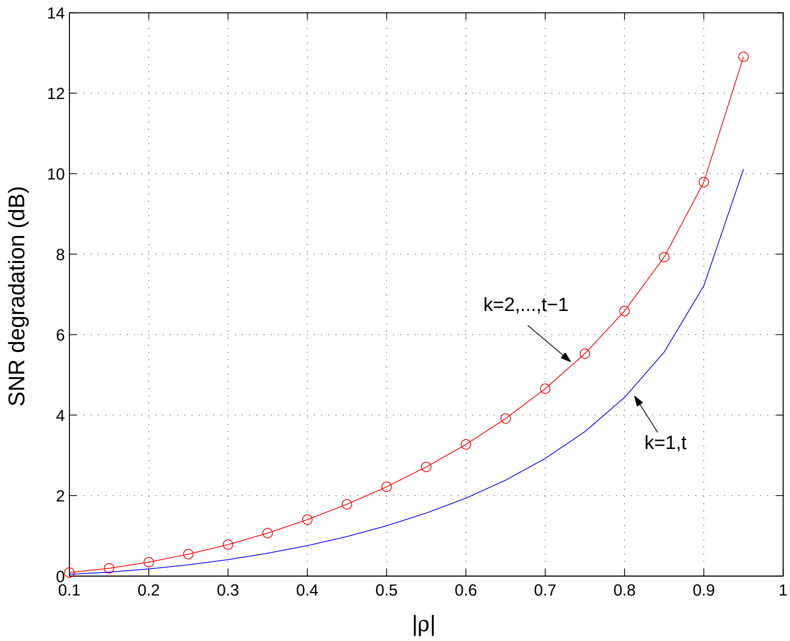

Figure 2.2: Analytical SNR degradation of MIMO systems with a ZF detector under exponential correlation matrix at the transmit side compared to an i.i.d. Rayleigh fading channel. $|\rho|$ is the absolute value of the correlation coefficient of neighboring antennas.

which is plotted in Fig. 2.2. It is apparent that an increase in the value of the correlation coefficient produces a larger SNR degradation. Based on the exponential correlation model, we observe that the symbols sent from the first and the last transmit antennas have smaller SNR degradations compared to the symbols sent from other transmit antennas.

2.2.3 Rician Fading Channel

In the presence of a purely specular signal or a line-of-sight (LOS) path between the transmitter and receiver, the channel is modeled as Rician [1] [32, 54, 76]. The Rician channel model contains two parts [15], namely a deterministic component corresponding to the LOS path and an uncorrelated fading component. Thus, the

[1]Rice channel, Ricean channel and Rician channel are exchangeable terms and they have the same meaning.

channel coefficient of a Rice channel is modeled by a non-zero mean CSCG variable x distributed as $x \sim \tilde{N}(\mu, \xi^2)$, where μ denotes the mean value of x and ξ^2 represents the variance of each of the real and imaginary components of x. Define the envelope of the channel response by u, i.e., $u = |x|$, and $|\mu|^2 = s^2$. We then have the p.d.f. of u following Rician distribution, i.e.,

$$g_u(u) = \frac{u}{\xi^2} \exp\left(-\frac{u^2+s^2}{2\xi^2}\right) I_0\left(\frac{us}{\xi^2}\right), \quad u \geq 0 \tag{2.21}$$

where $I_0(\cdot)$ is the modified Bessel function of the first kind. Note that when $s = 0$, the Rice distribution reduces to Rayleigh distribution. Define the Rician factor K as the ratio of the mean specular or LOS signal power to the mean diffused-scattered signal power and Ω as the average received power, the Rice distribution in (2.21) can then be rewritten as

$$g_u(u) = \frac{2u(1+K)e^{-K}}{\Omega} \exp\left(-\frac{(1+K)u^2}{\Omega}\right) I_0\left(2u\sqrt{\frac{K(1+K)}{\Omega}}\right), \quad u \geq 0. \tag{2.22}$$

The MIMO Rice channel, being a generalization of the scalar Rice channel, can be represented by [15]

$$\boldsymbol{H} = \sqrt{\frac{K}{1+K}}\boldsymbol{H}_1 + \sqrt{\frac{1}{1+K}}\boldsymbol{H}_2 \tag{2.23}$$

where

$$\sqrt{\frac{K}{1+K}}\boldsymbol{H}_1 = \mathrm{E}(\boldsymbol{H}) \tag{2.24}$$

denotes the fixed component and $\sqrt{1/(1+K)}\boldsymbol{H}_2$ represents the uncorrelated fading part containing i.i.d. ZMCSCG variables. Consequently, the distribution of the

MIMO Rice channel can be written as

$$\boldsymbol{H} \sim N^c_{r,t}\left(\sqrt{\frac{K}{1+K}}\boldsymbol{H}_1, \sqrt{\frac{1}{1+K}}\boldsymbol{I}_t\right). \tag{2.25}$$

Furthermore, using the first antennas at the receiver and transmitter as references, the LOS array responses at the receiver and transmitter, respectively, of a MIMO system with arbitrary antenna array topology can be written as

$$\boldsymbol{\alpha} = [1 \;\; \alpha_1 \;\; \cdots \;\; \alpha_{r-1}]^T, \quad |\alpha_i| = 1, \; i = 1, \ldots, r-1; \tag{2.26}$$

and

$$\boldsymbol{\beta} = [1 \;\; \beta_1 \;\; \cdots \;\; \beta_{t-1}]^T, \quad |\beta_j| = 1, \; j = 1, \ldots, t-1; \tag{2.27}$$

where the phases of α_i (β_j) depend on the angle of arrival (departure) and the antenna spacing in wavelength at the receiver (transmitter). Then, the fixed channel component can be represented by [15]

$$\boldsymbol{H}_1 = \boldsymbol{\alpha}\boldsymbol{\beta}^H \tag{2.28}$$

and the approximated covariance matrix $\hat{\boldsymbol{\Sigma}}$ for the MIMO Rician channel can be given as

$$\begin{aligned} \hat{\boldsymbol{\Sigma}} &= (1-\zeta)\boldsymbol{I}_t + \frac{\zeta}{r}\boldsymbol{\beta}\boldsymbol{\alpha}^H\boldsymbol{\alpha}\boldsymbol{\beta}^H \\ &= (1-\zeta)\boldsymbol{I}_t + \zeta\boldsymbol{\beta}\boldsymbol{\beta}^H \end{aligned} \tag{2.29}$$

where $\zeta = K/(1+K)$. Based on (2.29), we can conclude that $\hat{\boldsymbol{\Sigma}}$ is dependent on the parameters of the transmitter but is independent of the receiver parameters.

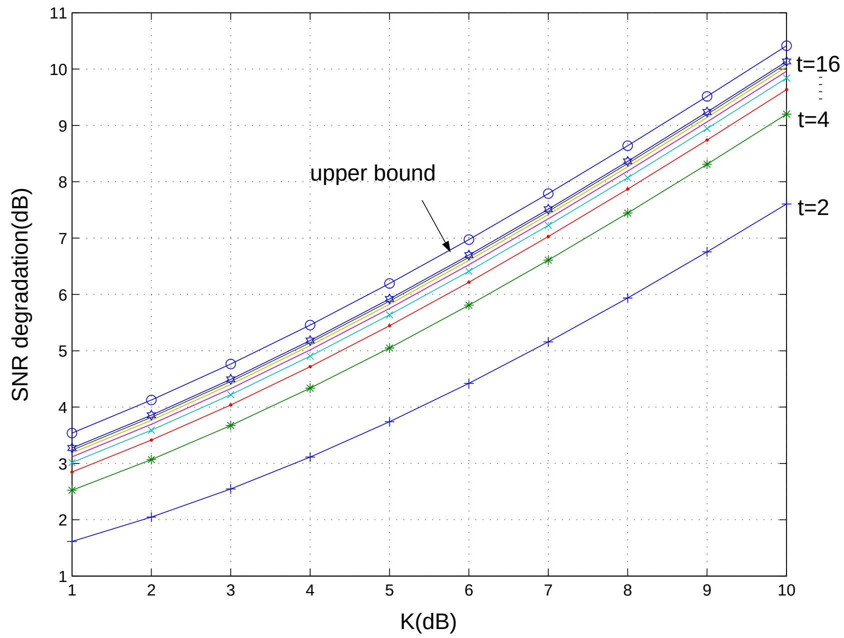

Figure 2.3: Analytical SNR degradation of a MIMO systems with ZF detector over a Rician fading channel compared to that over an i.i.d. Rayleigh fading channel. t is the number of transmit antennas.

Moreover, it can be shown that (see Appendix 2E for details)

$$[\hat{\mathbf{\Sigma}}^{-1}]_{kk} = \frac{(1+K)[1+K(t-1)]}{1+Kt}. \tag{2.30}$$

Therefore, the effective SNR degradation of the MIMO system over Rice fading as compared to that over i.i.d. Rayleigh fading equals

$$\begin{aligned} \Delta\gamma_{k,\text{Rice loss}} &= [\hat{\mathbf{\Sigma}}^{-1}]_{kk} \\ &= \frac{(1+K)[1+K(t-1)]}{1+Kt} < 1+K. \end{aligned} \tag{2.31}$$

When t becomes larger, $\Delta\gamma_{k,\text{Rice loss}}$ approaches its upper bound $(1+K)$. Note that here K is a decimal number (not in dB). In Fig. 2.3, the effective SNR degradation against K is plotted for different values of t.

In this section, we have found the post-detection SNR distribution of MIMO

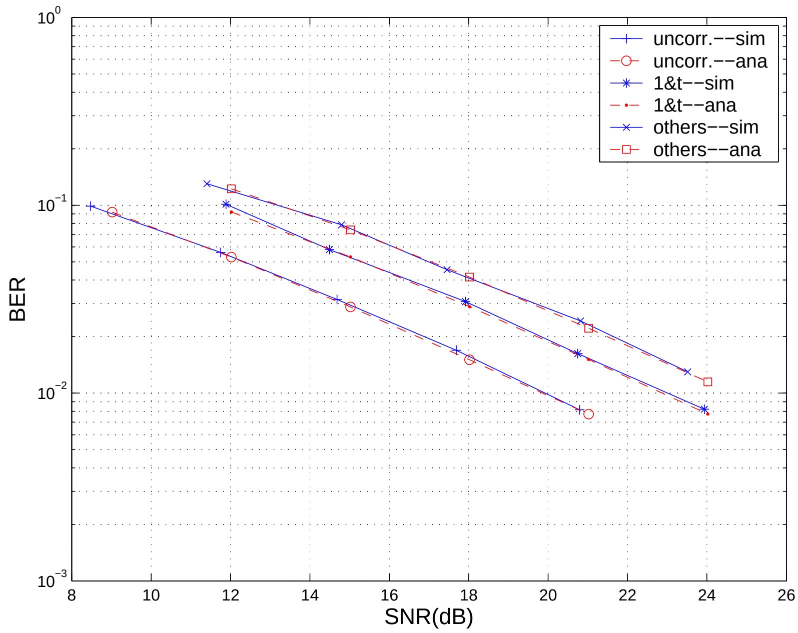

Figure 2.4: Analytical and simulated bit error rate performance of the MIMO systems over a Rayleigh fading channel. $t = 4$ and $r = 4$. $|\rho| = 0.707$. (uncorr: i.i.d. fading channel; $1\&t$: performance of data sent via the first and the last antennas; others: performance of data sent via other antennas except the first and the last ones; ana: analytical results; sim: simulation results.)

systems over fading channels using ZF detector. The degradation on the performance of MIMO systems under exponential correlation matrix is investigated. The effective SNR degradation of the systems over Rice fading as compared to that over an i.i.d. Rayleigh fading is also obtained. Moreover, the closed-form BER expression is given. In the next section, we will present the analytical and simulation findings.

2.3 Results and Discussion

Simulations are performed to evaluate the performance of the MIMO systems with ZF detector over the i.i.d. Rayleigh, correlated Rayleigh, and Rice fading channels. QPSK is employed for data modulation/demodulation.

Fig. 2.4 shows the BER results obtained under an exponential correlation ma-

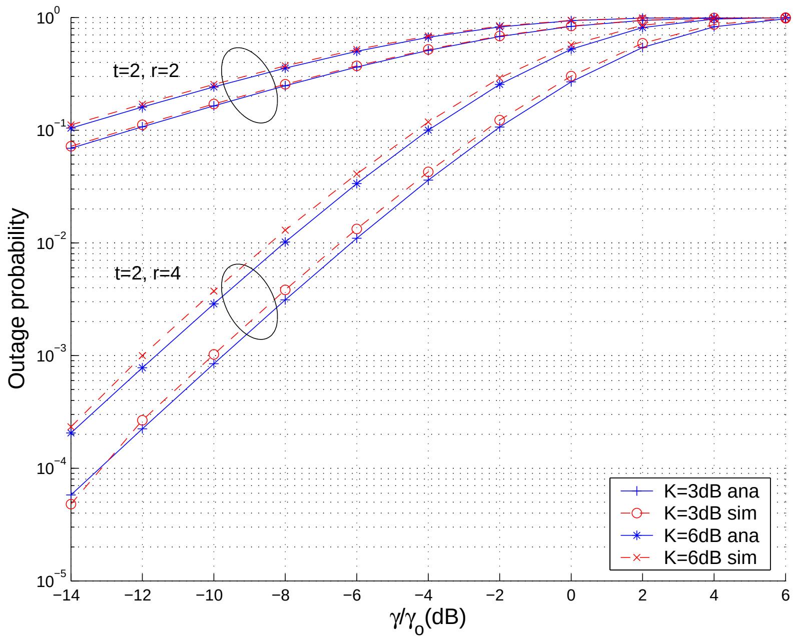

Figure 2.5: Analytical and simulated outage probabilities (cumulative distribution functions) of the MIMO systems over Rician fading channel with $K = 3$ dB and 6 dB. (ana: analytical results; sim: simulation results.)

trix with $t = 4$ and $r = 4$. The magnitude of the correlation coefficient between neighboring transmit elements is set to 0.707. The performance of MIMO systems over an i.i.d. Rayleigh fading channel is also plotted for comparison. The horizontal axis represents the spatially averaged SNR defined as $\frac{1}{r}\sum_{i=1}^{r} \mathrm{SNR}_i$, where SNR_i is the ratio of received signal power (from all t transmitters) to noise power at the ith receiver. It can be derived from the graphs that the SNR degradation between the uncorrelated-paths and correlated-paths cases is about 3 dB ($= 10 \log 2$) for symbol sequences sent from the first and last transmit antennas. For symbol sequences sent from other transmit antennas, the SNR degradation is about 4.77 dB ($= 10 \log 3$) compared to the uncorrelated cases. These results validate our theoretical analysis in Section 2.2.2.

Fig. 2.5 shows the analytical and simulated outage probabilities of the post-detection SNR (i.e., the probability that the post-detection SNR γ_k is less than a

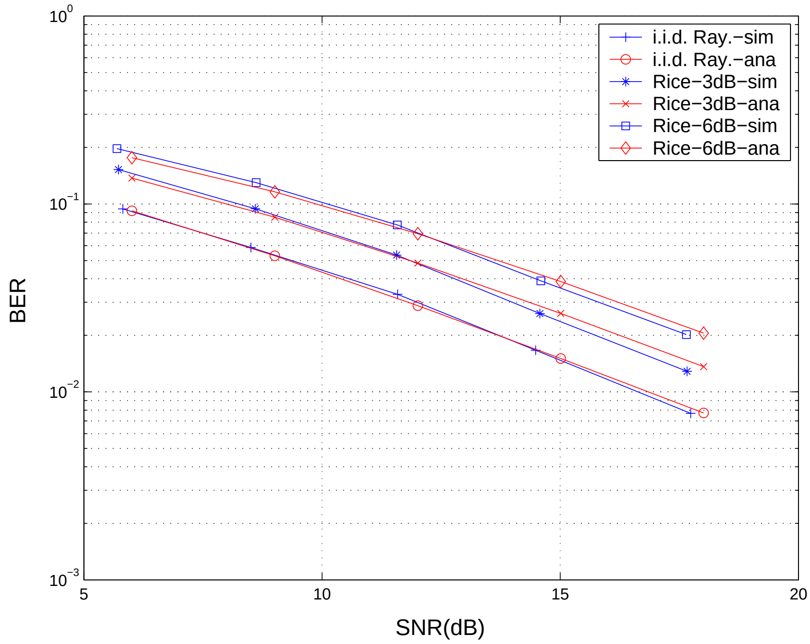

Figure 2.6: Analytical and simulated bit error rate performance of the MIMO systems over i.i.d. Rayleigh and Rician fading channels. $t = 2$ and $r = 2$. (ana: analytical results; sim: simulation results.)

certain value, or equivalently the c.d.f. of the post-detection SNR) for a Rice fading channel with ($t = 2$, $r = 2$) and ($t = 2$, $r = 4$), respectively. The horizontal axis represents the ratio of the post-detection SNR to the normalized received SNR (γ/γ_o). Results show that the analytical and simulation results are close to each other. We draw the conclusion that the approximation to the non-central complex Wishart distribution with complex Wishart distribution is strict. Moreover, when Ricean factor $K = 3$ dB, the outage probability is lower than that for $K = 6$ dB, implying that the signal at a lower Ricean factor has a higher probability of achieving a particular SNR, i.e., shows smaller SNR degradation.

Fig. 2.6 shows the analytical and simulated BER results over i.i.d. Rayleigh and Rice fading channels for the case ($t = 2$, $r = 2$). We observe that the analytical and simulation results are very close. Moreover, for $K = 3$ dB and 6 dB, respectively, the SNR degradations for the Rice channel over the i.i.d. Rayleigh channel are 2.5 dB

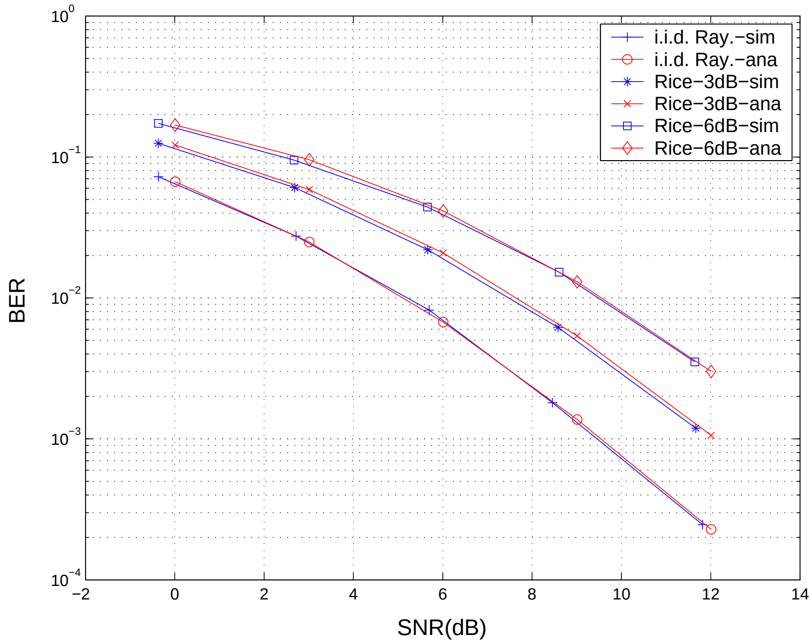

Figure 2.7: Analytical and simulated bit error rate performance of the MIMO systems over Rician and i.i.d. Rayleigh fading channels. $t = 2$ and $r = 4$. (ana: analytical results; sim: simulation results.)

and 4.4 dB. The results are very close to our analytical values plotted in Fig. 2.3.

Fig. 2.7 and Fig. 2.8 show the BER results over Rice fading channel for the cases $(t = 2, r = 4)$ and $(t = r = 4)$, respectively. Similar phenomenon can be seen from these graphs. Comparing Fig. 2.6 and Fig. 2.7, the SNR degradations between Rice fading and i.i.d. Rayleigh fading channels are identical for the same value of K. It is because the SNR degradation only depends on the Ricean factor and the number of transmit antennas, as judged from (2.30) and (2.31). In Fig. 2.8, the SNR degradation is 3.7 dB for $K = 3$ dB and is 5.8 dB for $K = 6$ dB. Under a fixed Ricean factor, the SNR degradation increases when the number of transmit antennas becomes larger.

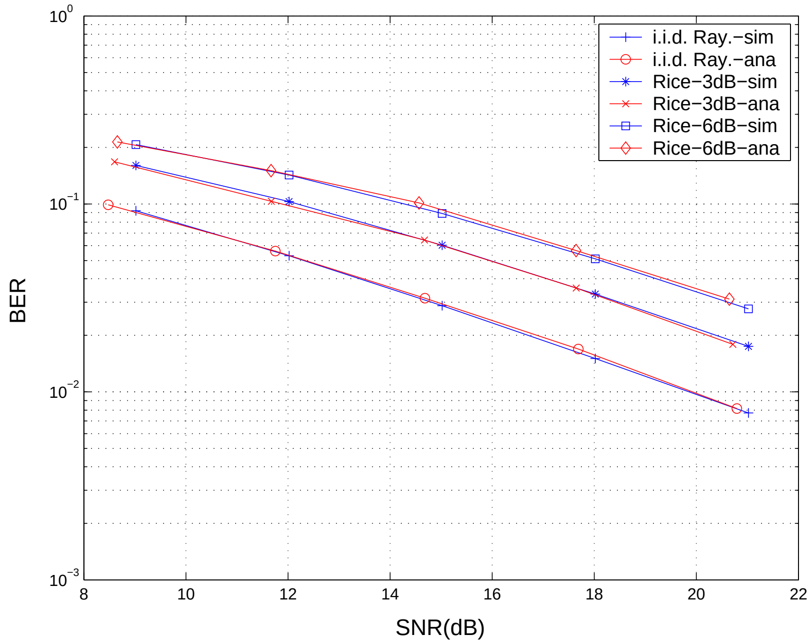

Figure 2.8: Analytical and simulated bit error rate performance of the MIMO systems over Rician and i.i.d. Rayleigh channels. $t = 4$ and $r = 4$. (ana: analytical results; sim: simulation results.)

2.4 Summary

In this chapter, we have studied the performance of the MIMO systems with zero-forcing detector over i.i.d. Rayleigh, correlated Rayleigh, and Rice fading channels. The closed-form expressions of the average bit error rates have been obtained. Simulations are then performed to verify the analytical findings. It has been concluded that the simulation results and the theoretical ones are similar.

Further, the degradation in the performance of MIMO systems with exponential correlation matrix at the transmit side have been investigated and analyzed. We observe that an increase in the value of the correlation coefficient produces a larger SNR degradation and that the symbols sent from the first and the last transmit antennas have smaller SNR degradations compared to the symbols sent from other transmit antennas.

In addition, the degradation of the systems over the Rice fading channel compared to the i.i.d. Rayleigh fading channel has been derived analytically. We find that the SNR degradation depends only on the Ricean factor and the number of transmit antennas. In general, a lower Ricean factor produces a higher probability of achieving a particular SNR, i.e., shows smaller SNR degradation, and that the SNR degradation increases with the number of transmit antennas.

In the next chapter, we will continue our study on SM-based MIMO systems. Instead of ZF detectors, more superior V-BLAST detection algorithm will be employed at the receiving end. In particular, we will evaluate thoroughly the performance of a two-transmit-antenna system when optimal ordering is used.

Appendix 2A: Mathematical Functions and Distributions

Definition 1. The Gamma function is defined by a definite integral as [2]

$$\Gamma(z) = \int_0^{\infty} t^{z-1} e^{-t}\, dt. \tag{2.32}$$

The Gamma function has the following property

$$\Gamma(z+1) = z\Gamma(z). \tag{2.33}$$

Also, for all natural numbers n,

$$\Gamma(n+1) = n\Gamma(n) = \cdots = n!\,. \tag{2.34}$$

Definition 2. Let x be a standard Gamma random variable denoted by $x \sim G(\alpha)$, where α is the shape parameter. The probability density function (p.d.f.) of x is given by [49]

$$f_x(x) = \frac{1}{\Gamma(\alpha)} x^{\alpha-1} e^{-x},\ x > 0,\ \alpha > 0. \tag{2.35}$$

Definition 3. The incomplete Gamma function[2] $\gamma(a, x)$ is defined by a definite integral as [2]

$$\gamma(a, x) = \int_0^x t^{a-1} e^{-t}\, dt. \tag{2.36}$$

The complementary incomplete Gamma function[3] $\Gamma(a, x)$ is defined similarly as [2]

$$\Gamma(a, x) = \int_x^\infty t^{a-1} e^{-t}\, dt. \tag{2.37}$$

From (2.32), (2.36) and (2.37), we have the relationship of $\gamma(a, x)$ and $\Gamma(a, x)$ as

$$\gamma(a, x) + \Gamma(a, x) = \Gamma(a). \tag{2.38}$$

Moreover, the cumulative distribution function (c.d.f.) of a Gamma random variable x with a shape parameter α can be expressed as

$$F_x(x) = \frac{\gamma(\alpha, x)}{\Gamma(\alpha)} = 1 - \frac{\Gamma(\alpha, x)}{\gamma(\alpha)}. \tag{2.39}$$

Definition 4. For a matrix $\boldsymbol{X}$ of size $m \times n$, $\mathrm{vec}(\boldsymbol{X})$ is defined as the $mn \times 1$ vector with stacked columns of $\boldsymbol{X}$ [60], i.e.,

$$\mathrm{vec}(\boldsymbol{X}) = \begin{pmatrix} \boldsymbol{x}_1 \\ \vdots \\ \boldsymbol{x}_n \end{pmatrix} \tag{2.40}$$

where $\boldsymbol{x}_i$, $i = 1, ..., n$ is the ith column of $\boldsymbol{X}$.

[2]In some literatures, it is called "lower incomplete gamma function".
[3]In some literatures, it is called "upper incomplete gamma function".

Definition 5. A scalar random variable x is said to have a Gaussian (normal) distribution, denoted by $x \sim N(\mu, \sigma^2)$, with mean value μ and variance σ^2, if its probability density function is given by [49]

$$f_x(x) = \frac{1}{\sqrt{2\pi\sigma^2}} \cdot \exp\left(-\frac{(x-\mu)^2}{2\sigma^2}\right). \tag{2.41}$$

Definition 6. A complex Gaussian random variable $z = z_r + jz_i$ is said to be circularly symmetric complex Gaussian (CSCG) distributed if z_r and z_i are independent real Gaussian random variables with equal variance. We write the distribution of z as $z \sim \tilde{N}(\mu, \sigma^2)$ with mean value μ and variance σ^2.

Definition 7. A random vector $\boldsymbol{x} = (x_1 \;\; x_2 \;\; \cdots \;\; x_p)^T$ is said to have a complex multivariate normal distribution, denoted by $\boldsymbol{x} \sim N_p^c(\boldsymbol{\mu}, \boldsymbol{\Sigma})$, with mean vector $\boldsymbol{\mu}$ and covariance matrix $\boldsymbol{\Sigma}$, if its joint p.d.f. is given by [4, 25, 71]

$$f_{\boldsymbol{x}}(\boldsymbol{x}) = \frac{\operatorname{etr}\left[-(\boldsymbol{x}-\boldsymbol{\mu})^H \boldsymbol{\Sigma}^{-1}(\boldsymbol{x}-\boldsymbol{\mu})\right]}{\pi^p \det(\boldsymbol{\Sigma})}. \tag{2.42}$$

Definition 8. For a complex random matrix $\boldsymbol{X}$ of size $p \times n$, if

$$\operatorname{vec}(\boldsymbol{X}^T) \sim N_{p,n}^c(\operatorname{vec}(\boldsymbol{M}^{\mathrm{T}}), \boldsymbol{\Sigma} \otimes \boldsymbol{\Psi}), \tag{2.43}$$

we say that $\boldsymbol{X}$ has a complex matrix variate normal distribution with mean $\boldsymbol{M}(p \times n)$ and covariance $\boldsymbol{\Sigma} \otimes \boldsymbol{\Psi}$, where $\boldsymbol{\Sigma}(p \times p) > 0$ and $\boldsymbol{\Psi}(n \times n) > 0$). Denote $\boldsymbol{X} \sim N_{p,n}^c(\boldsymbol{M}, \boldsymbol{\Sigma} \otimes \boldsymbol{\Psi})$, the joint p.d.f. of $\boldsymbol{X}$ is given by [4, 25, 71]

$$f_{\boldsymbol{X}}(\boldsymbol{X}) = \frac{\operatorname{etr}\left[-\boldsymbol{\Sigma}^{-1}(\boldsymbol{X}-\boldsymbol{M})\boldsymbol{\Psi}^{-1}(\boldsymbol{X}-\boldsymbol{M})^H\right]}{\pi^{np} \det(\boldsymbol{\Sigma})^n \det(\boldsymbol{\Psi})^p}. \tag{2.44}$$

Definition 9. Let $\boldsymbol{X} \sim N_{p,n}^c(\boldsymbol{0}, \boldsymbol{\Sigma} \otimes \boldsymbol{I}_n)$, with $p \leq n$. Then $\boldsymbol{S} = \boldsymbol{X}\boldsymbol{X}^H$ has a central complex Wishart distribution denoted as $\boldsymbol{S} \sim W_p^c(n, \boldsymbol{\Sigma})$. The joint p.d.f. of $\boldsymbol{S}$ is given by [4, 25, 71]

$$f_{\boldsymbol{S}}(\boldsymbol{S}) = \frac{\det(\boldsymbol{S})^{n-p}\mathrm{etr}(-\boldsymbol{\Sigma}^{-1}\boldsymbol{S})}{\Gamma_p(n)\det(\boldsymbol{\Sigma})^n} \tag{2.45}$$

where the complex multivariate Gamma function $\Gamma_p(n)$ is defined as

$$\Gamma_p(n) = \pi^{p(p-1)/2}\prod_{i=1}^{p}\Gamma(n-i+1). \tag{2.46}$$

Definition 10. Let $\boldsymbol{X} \sim N_{p,n}^c(\boldsymbol{M}, \boldsymbol{\Sigma} \otimes \boldsymbol{I}_n)$, with $p \leq n$. Then $\boldsymbol{S} = \boldsymbol{X}\boldsymbol{X}^H$ has a noncentral complex Wishart distribution denoted as $\boldsymbol{S} \sim W_p^c(n, \boldsymbol{M}, \boldsymbol{\Sigma})$. The joint p.d.f. of $\boldsymbol{S}$ is given by [4, 25, 71]

$$f_{\boldsymbol{S}}(\boldsymbol{S}) = \frac{\det(\boldsymbol{S})^{n-p}\,\mathrm{etr}(-\boldsymbol{\Sigma}^{-1}\boldsymbol{S})}{\Gamma_p(n)\det(\boldsymbol{\Sigma})^n} \times {}_0F_1(n; \boldsymbol{\Theta}\boldsymbol{\Sigma}^{-1}\boldsymbol{S}) \tag{2.47}$$

where $\boldsymbol{\Theta} = \boldsymbol{\Sigma}^{-1}\boldsymbol{M}\boldsymbol{M}^H$ and ${}_0F_1$ is the hypergeometric function with matrix arguments (Bessel function). The matrix $\boldsymbol{\Theta}$ is called the noncentrality parameter matrix. When $\boldsymbol{\Theta} = \boldsymbol{0}$, the noncentral Wishart distribution reduces to the central Wishart distribution.

Appendix 2B: Derivation of the Theoretical Bit Error Rate

Supposing QPSK is employed as the modulation/demodulation scheme, we can then express the conditional BER of the kth transmitted signal in terms of the received SNR γ_k [76], i.e.,

$$P(\gamma_k) = Q(\sqrt{2\gamma_k}) \tag{2.48}$$

where $Q(x)$ is the Q-function defined as [76, eq.(2-1-97)]

$$Q(x) = \frac{1}{\sqrt{2\pi}} \int_{x}^{\infty} \exp\left(-t^2/2\right) dt. \tag{2.49}$$

Alternatively, the Q-function can be written as

$$Q(x) = \frac{1}{2} - \frac{1}{2}\mathrm{erf}\left(\frac{x}{\sqrt{2}}\right) \tag{2.50}$$

where

$$\mathrm{erf}(x) = \frac{2}{\sqrt{\pi}} \int_{0}^{x} \exp(-t^2) dt \tag{2.51}$$

denotes the error function. Also, the error function can be expressed as [24]

$$\mathrm{erf}(x) = \frac{2x}{\sqrt{\pi}} \Phi\left(\frac{1}{2}, \frac{3}{2}, -x^2\right) \tag{2.52}$$

where $\Phi(a, b, z)$ is the confluent hypergeometric function of the first order, which is also denoted as ${}_1F_1(a; b; z)$ [24]. The generalized hypergeometric function is defined as

$${}_pF_q(\alpha_1, \cdots, \alpha_p; \beta_1, \cdots, \beta_q; z) = \sum_{k=0}^{\infty} \frac{(\alpha_1)_k \cdots (\alpha_p)_k}{(\beta_1)_k \cdots (\beta_q)_k} \frac{z^k}{k!} \tag{2.53}$$

where the Pochhammer's symbol $(a)_k$ is given by

$$(a)_k = a(a+1)\cdots(a+k-1) = \frac{\Gamma(a+k)}{\Gamma(a)}. \tag{2.54}$$

To obtain the error probabilities when γ_k is a random variable, we average $P(\gamma_k)$ over the p.d.f. of γ_k and the average BER of the kth transmitted signal is thus equal to

$$
\begin{aligned}
P_k &= \int_0^\infty P(\gamma_k) f(\gamma_k) d\gamma_k \\
&= \frac{1}{\gamma_{o,k}\Gamma(r-t+1)} \times \int_0^\infty Q(\sqrt{2\gamma_k}) \left[\exp\left(-\frac{\gamma_k}{\gamma_{o,k}}\right)\right] \left(\frac{\gamma_k}{\gamma_{o,k}}\right)^{r-t} \, d\gamma_k.
\end{aligned} \tag{2.55}
$$

Letting $\gamma_k = \gamma\gamma_{o,k}$ and substituting (2.50) and (2.52) into (2.55), we obtain

$$
\begin{aligned}
P_k &= \frac{1}{\Gamma(r-t+1)} \int_0^\infty Q(\sqrt{2\gamma\gamma_{o,k}}) \exp(-\gamma)\gamma^{r-t} \, d\gamma \\
&= \frac{1}{\Gamma(r-t+1)} \times \int_0^\infty \left[\frac{1}{2} - \frac{\sqrt{\gamma\gamma_{o,k}}}{\sqrt{\pi}} \, \Phi(\frac{1}{2}, \frac{3}{2}, -\gamma\gamma_{o,k})\right] \exp(-\gamma)\gamma^{r-t} \, d\gamma \\
&= \frac{1}{2} - \sqrt{\frac{\gamma_{o,k}}{\pi}} \times \frac{\Gamma(r-t+\frac{3}{2})}{\Gamma(r-t+1)} \times \, {}_2F_1\left(\frac{1}{2}, r-t+\frac{3}{2}; \frac{3}{2}; -\gamma_{o,k}\right)
\end{aligned} \tag{2.56}
$$

where the last equality is obtained by applying the integral in [24, eq.(7.621.4)].

Appendix 2C: Integration $J(n, a, b)$

In the study of average error rates in fading channels, the integral

$$
J(n, a, b) = \frac{a^n}{\Gamma(n)} \int_0^\infty e^{-at} t^{n-1} Q(\sqrt{bt}) \, dt \tag{2.57}
$$

frequently arises where $Q(x)$ is the Q-function defined in (2.49). In particular, it has been shown that the integral has the closed-form result [87, eq.(5A.2)]

$$
\begin{aligned}
J(n, a, b) = & \frac{\sqrt{c/\pi}}{2(1+c)^{n+1/2}} \times \frac{\Gamma(n+1/2)}{\Gamma(n+1)} \\
& \times \, {}_2F_1(1, n+\frac{1}{2}; n+1; \frac{1}{1+c}), \quad c = \frac{b}{2a},
\end{aligned} \tag{2.58}
$$

where ${}_2F_1(p, q; n, z)$ is the hypergeometric function (see Appendix 2B). When n is restricted to positive integral values, it has been shown that the integral has a closed-form result [76, eq.(14-4-15)]

$$J(n, a, b) = \frac{1}{2}\left[1 - \mu \sum_{k=0}^{n-1} \binom{2k}{k} \left(\frac{1-\mu^2}{4}\right)^k\right] \tag{2.59}$$

where $\mu \triangleq \sqrt{c/(1+c)}$ and $\binom{2k}{k}$ represents the binomial coefficient. For large b, $J(n, a, b)$ can be further approximated as [76, eq.(14-4-18)]

$$J(n, a, b) \approx \left(\frac{a}{4b}\right)^n \binom{2n-1}{n}. \tag{2.60}$$

Also, it can be readily shown that

$$\lim_{b \to +\infty} \frac{\log[J(n, a, b)]}{\log(b/(2a))} = -n. \tag{2.61}$$

Appendix 2D: Calculating $[\mathbf{\Sigma}^{-1}]_{kk}$ with Exponential Correlation Matrix

To calculate the kth ($k \neq 1, t$) diagonal element of $\mathbf{\Sigma}^{-1}$, firstly we compute the determinant of adjoint $[\bar{\mathbf{\Sigma}}]_{kk}$. After some equivalent transformations of the determinant (the kth row multiplied by $|\rho|^2$ is subtracted from the $(k-1)$th row, the other rows follow the same transformation as we compute the determinant of $\mathbf{\Sigma}$), we get the determinant of adjoint $\det[\bar{\mathbf{\Sigma}}]_{kk}$ in the same way as $\det(\mathbf{\Sigma})$, i.e.,

$$\det[\bar{\mathbf{\Sigma}}_{kk}] = \det \begin{array}{c} \begin{bmatrix} 1-|\rho|^2 & 0 & 0 & \cdots & \cdots & 0 \\ \cdots & \cdots & \cdots & \cdots & \cdots & \cdots \\ \cdots & \cdots & 1-|\rho|^4 & 0 & \cdots & 0 \\ \cdots & \cdots & \cdots & \cdots & \cdots & \cdots \\ \cdots & \cdots & \cdots & \cdots & \cdots & 1 \end{bmatrix} \end{array} \begin{array}{l} \\ \\ \dashrightarrow (k-1)\text{th row.} \\ \\ \\ \end{array} \tag{2.62}$$

It is then easily shown that

$$[\mathbf{\Sigma}^{-1}]_{kk} = \frac{\det[\bar{\mathbf{\Sigma}}_{kk}]}{\det(\mathbf{\Sigma})} = \frac{(1-|\rho|^4)(1-|\rho|^2)^{t-3}}{(1-|\rho|^2)^{t-1}} = \frac{1+|\rho|^2}{1-|\rho|^2}; \quad k = 2, ..., t-1. \quad (2.63)$$

Consequently, the diagonal elements of $\mathbf{\Sigma}^{-1}$ equal

$$[\mathbf{\Sigma}^{-1}]_{kk} = \begin{cases} 1/(1-|\rho|^2), & k = 1, t \\ (1+|\rho|^2)/(1-|\rho|^2), & \text{otherwise.} \end{cases} \quad (2.64)$$

Appendix 2E: Calculating $[\mathbf{\Sigma}^{-1}]_{kk}$ Under Rice Fading Channel

Here we derive the expression for the diagonal elements of the inverse matrix $\hat{\mathbf{\Sigma}}^{-1}$. First, we calculate the determinant of $\hat{\mathbf{\Sigma}}$. Without affecting the value of the determinant, the first column, after multiplying by β_{k-1}^*, is subtracted from the kth column for $k = 2, 3, \ldots, t$. Then the ith row is multiplied by β_{i-1}^* and added to the first row for $i = 2, 3, \ldots, t$. Hence we obtain a lower triangular matrix and

$$\det[\hat{\mathbf{\Sigma}}] = \det \begin{bmatrix} 1+\zeta(t-1) & 0 & 0 & 0 \\ \zeta\beta_1 & 1-\zeta & 0 & 0 \\ \vdots & \vdots & \vdots & \vdots \\ \zeta\beta_{t-1} & 0 & \cdots & 1-\zeta \end{bmatrix}. \quad (2.65)$$

The determinant of $\hat{\mathbf{\Sigma}}$ thus equals

$$\det[\hat{\mathbf{\Sigma}}] = (1-\zeta)^{t-1}[1+\zeta(t-1)]. \quad (2.66)$$

Also, it is readily shown that

$$
\begin{aligned}
[\hat{\boldsymbol{\Sigma}}^{-1}]_{kk} &= \frac{\det[\bar{\boldsymbol{\Sigma}}_{kk}]}{\det(\hat{\boldsymbol{\Sigma}})} \\
&= \frac{(1-\zeta)^{t-2}[1+\zeta(t-2)]}{(1-\zeta)^{t-1}[1+\zeta(t-1)]} \\
&= \frac{1+\zeta(t-2)}{(1-\zeta)[1+\zeta(t-1)]}
\end{aligned} \tag{2.67}
$$

where $[\bar{\boldsymbol{\Sigma}}_{kk}]$ is the adjoint matrix of $[\hat{\boldsymbol{\Sigma}}]_{kk}$. Finally, we substitute $\zeta = K/(K+1)$ into (2.67) and obtain

$$
[\hat{\boldsymbol{\Sigma}}^{-1}]_{kk} = \frac{(K+1)[1+K(t-1)]}{1+Kt}. \tag{2.68}
$$

Chapter 3

Performance Analysis of V-BLAST Algorithms For Two-Transmit-Antenna Systems

In the previous chapter, the performance of the zero-forcing (ZF) detector in spatial-multplexing-based (SM-based) MIMO systems, including Vertical Bell LAbs Layered Space-Time (V-BLAST) architecture and Diagonal-BLAST (D-BLAST) architecture, has been studied both analytically and by simulations over i.i.d. Rayleigh, correlated-Rayleigh and Rician channels. In this chapter, we focus on the performance of the V-BLAST architecture employing iterative nulling and canceling detection algorithm. Such an algorithm has been proposed as for use in the original V-BLAST detector [97]. Compared with the ZF detector, the V-BLAST detecting algorithm has a superior bit error rate performance. The V-BLAST algorithm, moreover, is a relatively simple algorithm to implement, compared with the diagonal-BLAST (D-BLAST) algorithm, that can achieve a large part of the MIMO capacity [97]. Since symbol cancellation is used in the V-BLAST detector, the order of detection becomes important to the overall performance of the system. In *fixed ordering*, the received data streams are decoded with a pre-defined sequence. To obtain the optimal performance, however, it has been proved that the order of detection should be determined based on the post-detection signal-to-noise ratio (SNR) [18, 97].

In [59], the V-BLAST detector performance has been investigated based on some geometrical ideas and equal gain combining. For a $t \times r$ system, where t and r, respectively, denotes the number of transmit and receive antennas, it has been shown that without optimal ordering, the diversity order at the ith processing step equals $r - t + i$ under an independent and identically distributed (i.i.d.) Rayleigh fading channel. In the case of a $2 \times r$ system, outage probabilities and average bit error rates (BERs) have also been derived when optimal ordering is implemented. It has further been concluded that implementing optimal ordering in a $2 \times r$ system will increase the first step SNR by 3 dB but will cause no effect to the diversity order.

In this chapter, we present a novel analytical approach to studying a $2 \times r$ V-BLAST system when optimal ordering is used. Three types of channel, namely i.i.d. Rayleigh channel, correlated-Rayleigh channel, and Rician channel, are considered. Based on the properties of Wishart matrices, we derive the distributions of the post-detection SNRs. Closed-form analytical expressions of the BERs and the diversity orders for optimal ordering are then found. The effect of optimal ordering on SNR and the diversity order are also discussed. Further, we investigate the SNR degradation of the detection steps for correlated-Rayleigh and Rician channels over an i.i.d. Rayleigh channel.

The rest of the chapter is organized as follows. In Section 3.1, we describe the system under investigation and the V-BLAST detector. In Section 3.2, Section 3.3 and Section 3.4, the performance of the V-BLAST detector is studied in detail over an i.i.d. Rayleigh channel, a correlated-Rayleigh channel, and a Rician channel, respectively. Analytical results together with simulations are also presented.

3.1 System Model and V-BLAST Detector

3.1.1 System Model

The system under investigation is the same as the one presented in Section 2.1 and is shown again in Fig. 3.1. In particular, we apply the V-BLAST mapping strategy, i.e., the incoming data stream is demultiplexed into a number of blocks and data from the same block is always transmitted via the same antenna. The definitions of the symbols are also identical to those in Section 2.1 and are reviewed as follows:

- $\boldsymbol{H}$: $r \times t$ channel matrix containing the elements $h_{i,j}$, which represents the impulse response of the channel between the jth ($j = 1, 2, \ldots, t$) transmit antenna and the ith ($i = 1, 2, \ldots, r$) receive antenna;
- $\boldsymbol{d} = [d_1 \cdots d_t]^T$: transmitted symbol vector;
- $\boldsymbol{n} = [n_1 \cdots n_r]^T$: noise vector with elements taken to be i.i.d. Gaussian random variables with zero mean and variance σ^2;
- $\boldsymbol{y} = [y_1 \cdots y_r]^T$: received signal vector and equals $\boldsymbol{Hd} + \boldsymbol{n}$.

3.1.2 V-BLAST Algorithm

The V-BLAST MIMO system was first proposed in [97] and subsequently analyzed in detail in [18]. In a V-BLAST detector, the received data streams can be decoded with a pre-defined sequence, also called *fixed ordering*. Alternatively, the data streams can be decoded according to the strengths of the post-detection SNRs. In *optimal ordering* [18, 97], the data stream with the maximum post-detection SNR is first detected, reconstructed and subtracted from the received signal. Then, the data stream with the maximum post-detection SNR among the remaining data streams

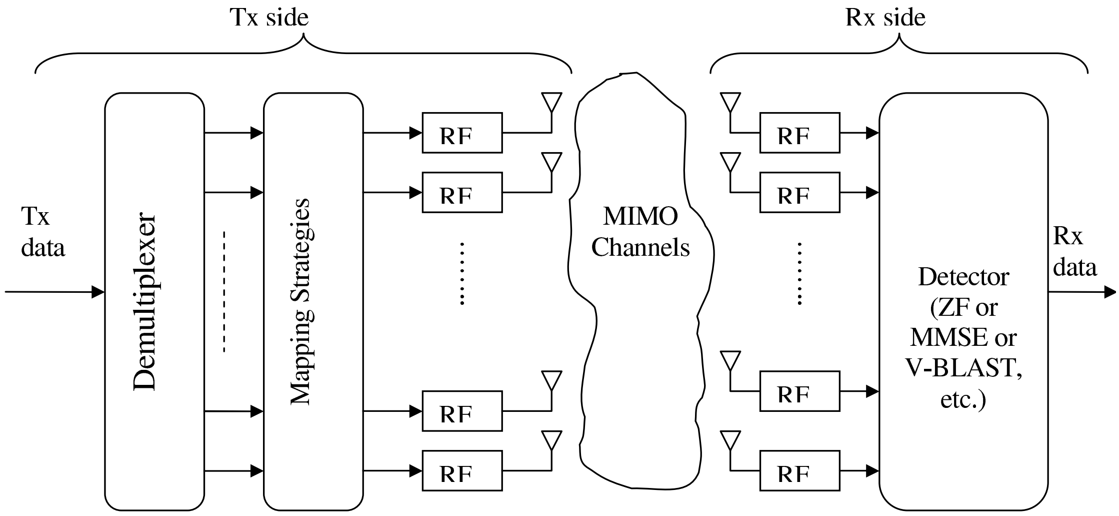

Figure 3.1: A spatial-multiplexing-based MIMO system (Tx: transmit, Rx: receive).

is detected, reconstructed and subtracted from the remaining signal. The same process is repeated until the last data stream is decoded. In the following, we make use of the zero-forcing-detector based V-BLAST detection algorithm to illustrate the major steps — initialization step and recursion step — used in the decoding process [97].

Initialization Step:

$$i = 1 \tag{3.1}$$

$$\boldsymbol{y}_i = \boldsymbol{y} \tag{3.2}$$

$$\boldsymbol{G}^{(i)} = \boldsymbol{H}^H \tag{3.3}$$

$$\boldsymbol{Z}^{(i)} = [\boldsymbol{H}^H \boldsymbol{H}]^{-1} \tag{3.4}$$

$$k_i = \begin{cases} i, & \text{for fixed ordering} \\ \arg\min_j \{\boldsymbol{Z}_{jj}^{(i)}\}, & \text{for optimal ordering.} \end{cases} \tag{3.5}$$

Recursion Step: During each recursion step, we decode the data stream with the maximum output SNR.

$$\boldsymbol{w}_{k_i} = (\boldsymbol{Z}^{(i)}\boldsymbol{G}^{(i)})_{k_i} \tag{3.6}$$

$$d_{k_i} = \boldsymbol{w}_{k_i}\boldsymbol{y}_i \tag{3.7}$$

$$\hat{a}_{k_i} = \mathrm{Quant}(d_{k_i}) \tag{3.8}$$

$$\boldsymbol{y}_{i+1}^T = \boldsymbol{y}_i^T - \hat{a}_{k_i}(\boldsymbol{H}^T)_{k_i} \tag{3.9}$$

$$\boldsymbol{F} = \Lambda(\boldsymbol{H}, k_i) \tag{3.10}$$

$$\boldsymbol{G}^{(i+1)} = \boldsymbol{F}^H \tag{3.11}$$

$$\boldsymbol{Z}^{(i+1)} = (\boldsymbol{F}^H\boldsymbol{F})^{-1} \tag{3.12}$$

$$k_{i+1} = \begin{cases} i+1, & \text{for fixed ordering} \\ \arg\min_{j \notin \{k_1,\ldots,k_i\}} (\boldsymbol{Z}_{jj}^{(i+1)}), & \text{for optimal ordering} \end{cases} \tag{3.13}$$

$$i = i+1 \quad \text{when} \quad i < t \tag{3.14}$$

where $(\boldsymbol{X})_{k_i}$ denotes the k_ith row of the matrix $\boldsymbol{X}$, $\Lambda(\boldsymbol{H}, k_i)$ represents a function that turns all elements in all the $k_1, \ldots, k_i$th columns in $\boldsymbol{X}$ into zeros. Also, in (3.8), $\mathrm{Quant}(\cdot)$ denotes the quantization operation, which is dependent on the modulation scheme used, and it produces the decoded symbol $\hat{a}_{k_i}$.

Our study focuses on the detector performance of V-BLAST with two transmit antennas. We consider the case when optimal detection ordering is used. In the receiver, the post-detection SNR with a linear zero-forcing detector is expressed as (see Section 2.2 for details)

$$\gamma_k = \frac{\gamma_o}{[\boldsymbol{H}^H\boldsymbol{H}]_{kk}^{-1}}, \; k = 1, 2 \tag{3.15}$$

where γ_o is the normalized received SNR at each receive antenna and is given by eq.(2.4). During the first step of the detection algorithm, the data symbol from the transmit antenna with a higher SNR will be chosen for decoding. Hence, the probability density function (p.d.f.) of the maximum value of γ_1 and γ_2 needs to be obtained first before proceeding to further analysis. In the following, we will analyse the performance of the V-BLAST detector under 3 different channel conditions, namely i.i.d. Rayleigh channel, correlated-Rayleigh channel, and Rician channel.

3.2 Performance over an I.I.D. Rayleigh Channel

3.2.1 Performance of the Data Symbol Stream from the Transmit Antenna with a Higher SNR

We define $\boldsymbol{Z} = \boldsymbol{H}^H\boldsymbol{H}$ and $\boldsymbol{W} = [\boldsymbol{H}^H\boldsymbol{H}]^{-1}$. For an i.i.d. Rayleigh channel, it has been shown in Section 2.2 that $\boldsymbol{Z}$ follows a complex Wishart distribution [22, 39] denoted by $\boldsymbol{Z} \sim W_t^c(r, \boldsymbol{\Sigma})$, where $\boldsymbol{\Sigma}$ is the covariance matrix of the row vectors in $\boldsymbol{H}$. Thus, $\boldsymbol{W}$ follows an inverted complex Wishart distribution denoted by $\boldsymbol{W} \sim IW_t^c(r, \boldsymbol{\Sigma})$ [62] and its p.d.f. is given by [62]

$$f_{\boldsymbol{W}}(\boldsymbol{W}) = \frac{(\det \boldsymbol{W}^{-1})^{r+t}}{\Gamma_t(r)\det(\boldsymbol{\Sigma})^r}\exp[-\mathrm{tr}(\boldsymbol{\Sigma}^{-1}\boldsymbol{W}^{-1})] \tag{3.16}$$

where $\Gamma_t(r)$ denotes the complex multivariate Gamma function (see Appendix 2A). Assume that the two transmit antennas have equal power. Normalizing each power to unity, the covariance matrix $\boldsymbol{\Sigma}$ equals an identity matrix of size 2×2, i.e., $\boldsymbol{\Sigma} = \boldsymbol{I}_2$. Under such a condition, we define

$$\boldsymbol{W} = \begin{pmatrix} w_{11} & w_{12} \\ w_{12}^* & w_{22} \end{pmatrix} \tag{3.17}$$

and substitute $\boldsymbol{W}$ and $\boldsymbol{\Sigma}$ into (3.16) to obtain the joint p.d.f. of $\boldsymbol{W}$, i.e.,

$$\begin{aligned} f_{\boldsymbol{W}}(\boldsymbol{W}) &= f(w_{11}, w_{12}, w_{22}) \\ &= \frac{(w_{11}w_{22} - |w_{12}|^2)^{-(r+2)}}{\pi\Gamma(r)\Gamma(r-1)} \times \exp\left[-\frac{w_{11}+w_{22}}{w_{11}w_{22} - |w_{12}|^2}\right]. \end{aligned} \tag{3.18}$$

We then map the complex variable w_{12} to the polar coordinates, i.e., $\Re(w_{12}) = \rho\cos(\theta)$ and $\Im(w_{12}) = \rho\sin(\theta)$, and substitute them into (3.18) to obtain

$$f_{w_{11},w_{22},\rho,\theta}(w_{11}, w_{22}, \rho, \theta) = \frac{(w_{11}w_{22} - \rho^2)^{-(r+2)}}{\pi\Gamma(r)\Gamma(r-1)} \times \exp\left[-\frac{w_{11}+w_{22}}{w_{11}w_{22} - \rho^2}\right] \times \rho. \tag{3.19}$$

Using the Cauchy-Schwarz inequality, we have $\rho^2 = |w_{12}|^2 \leq w_{11}w_{22}$. By integrating (3.19) in the ranges $0 < \rho \leq \sqrt{w_{11}w_{22}}$ and $0 \leq \theta < 2\pi$, we obtain the joint p.d.f. of w_{11} and w_{22}, i.e.,

$$f_{w_{11},w_{22}}(w_{11}, w_{22}) = \int_0^{2\pi}\int_0^{\sqrt{w_{11}w_{22}}} \frac{(w_{11}w_{22} - \rho^2)^{-(r+2)}}{\pi\Gamma(r)\Gamma(r-1)} \times \exp\left[-\frac{w_{11}+w_{22}}{w_{11}w_{22} - \rho^2}\right] \times \rho \, d\rho \ \ d\theta. \tag{3.20}$$

Denoting $\rho = \sqrt{w_{11}w_{22}}\sin(\phi)$, $0 < \phi \leq \pi/2$, we also have

$$\begin{aligned} f_{w_{11},w_{22}}(w_{11}, w_{22}) = & \frac{2(w_{11}w_{22})^{-(r+1)}}{\Gamma(r)\Gamma(r-1)} \\ & \times \int_0^{\pi/2} \sin\phi(\cos\phi)^{-(2r+3)} \exp\left[-\frac{1}{\cos^2\phi}(\frac{1}{w_{11}} + \frac{1}{w_{22}})\right] \ d\phi. \end{aligned} \tag{3.21}$$

By defining $x_1 = 1/w_{11}$ and $x_2 = 1/w_{22}$, the joint p.d.f. of x_1 and x_2 can be shown equal to

$$f_{x_1,x_2}(x_1, x_2) = \frac{2(x_1x_2)^{r-1}}{\Gamma(r)\Gamma(r-1)} \int_0^{\pi/2} \sin\phi(\cos\phi)^{-(2r+3)} \times \exp\left[-\frac{1}{\cos^2\phi}(x_1 + x_2)\right] \ d\phi. \tag{3.22}$$

Moreover, it can be readily shown that $\gamma_1 = \gamma_o x_1$ and $\gamma_2 = \gamma_o x_2$.

Define the c.d.f. of $\max(x_1, x_2)$ as $F_1(x)$, which is readily shown equal to

$$
\begin{aligned}
F_1(x) &= \Pr(\max(x_1, x_2) < x) = \Pr(x_1 < x, x_2 < x) \\
&= \int_0^x \int_0^x \left[\frac{2(x_1x_2)^{r-1}}{\Gamma(r)\Gamma(r-1)} \int_0^{\pi/2} \sin\phi(\cos\phi)^{-(2r+3)} \exp[-\frac{1}{\cos^2\phi}(x_1+x_2)]\, d\phi \right] \\
&\qquad dx_1 \ \ dx_2 \\
&= \frac{2}{\Gamma(r)\Gamma(r-1)} \int_0^{\pi/2} \gamma^2(r, \frac{x}{\cos^2\phi}) \sin\phi(\cos\phi)^{(2r-3)} \ \ d\phi
\end{aligned}
\tag{3.23}
$$

where $\gamma(r, z)$ denotes the incomplete Gamma function (see Appendix 2A). Letting $\cos^2\phi = 1/y$ and substituting it into (3.23), we obtain

$$
F_1(x) = \frac{1}{\Gamma(r)\Gamma(r-1)} \int_1^\infty y^{-r}\gamma^2(r, xy)\ dy. \tag{3.24}
$$

To obtain the p.d.f. of $\max(x_1, x_2)$, we differentiate $F_1(x)$ with respect to x. Also, by inter-changing the order of derivation and integration, we have

$$
\begin{aligned}
f_1(x) &= \frac{dF_1(x)}{dx} \\
&= \frac{2x^{r-1}}{\Gamma(r)\Gamma(r-1)} \int_1^\infty \exp(-xy)\cdot\gamma(r, xy)\ \ dy.
\end{aligned}
\tag{3.25}
$$

Moreover, for integral values of r, the incomplete Gamma function can be shown equal to [24, eq.(8.352.1)]

$$
\gamma(r, z) = (r-1)! \left[1 - \exp(-z) \sum_{m=0}^{r-1} \frac{z^m}{m!} \right]. \tag{3.26}
$$

Substituting (3.26) into (3.25), we arrive at the final expression of $f_1(x)$ as

$$
\begin{aligned}
f_1(x) &= \frac{2x^{r-1}}{\Gamma(r-1)} \int_1^\infty \exp(-xy) \left[1 - \exp(-xy) \sum_{m=0}^{r-1} \frac{(xy)^m}{m!} \right] \, dy \\
&= \frac{2x^{r-2}}{\Gamma(r-1)} \left[\exp(-x) - \sum_{m=0}^{r-1} \frac{\Gamma(m+1, 2x)}{m! 2^{m+1}} \right]
\end{aligned}
\tag{3.27}
$$

where $\Gamma(m, z)$ is the complementary incomplete Gamma function (see (2.37) in Appendix 2A. Using the fact that [24, eq(8.352.2)]

$$
\Gamma(n+1, z) = n! \exp(-z) \sum_{m=0}^{n} \frac{z^m}{m!}, \tag{3.28}
$$

n being an integer, we integrate $f_1(x)$ to obtain $F_1(x)$ as

$$
\begin{aligned}
F_1(x) &= \int_0^x f_1(x) \, dx \\
&= \frac{2\gamma(r-1, x)}{\Gamma(r-1)} - \frac{2^{2-2r}}{\Gamma(r-1)} \sum_{m=0}^{r-1} \frac{2^{r-m} - 1}{m!} \gamma(r+m-1, 2x).
\end{aligned}
\tag{3.29}
$$

Finally, the c.d.f. of the post-detection SNR in the first detection step is found by replacing x with γ/γ_o in (3.29).

Once we have the p.d.f. of the post-detection SNR, the average bit error rate or symbol error rate (SER) for different modulation schemes can be obtained easily [87]. Suppose quadrature phase shift keying (QPSK) is used. The average BER of the decoded data can be shown equal to [76]

$$
P_e = \int_0^\infty Q(\sqrt{2\hat{\gamma}_1}) f(\hat{\gamma}_1) \;\; d\hat{\gamma}_1 \tag{3.30}
$$

where $\hat{\gamma}_1$ is the post-detection SNR and $f(\hat{\gamma}_1)$ is its p.d.f. Substituting $\hat{\gamma}_1 = \gamma_o x$ and $f(\hat{\gamma}_1) \, d\hat{\gamma}_1 = f_1(x) \, dx$ into (3.30), the average BER of the data stream with a higher

SNR thus equals

$$P_{e1} = \int_0^\infty Q(\sqrt{2\gamma_o x}) f_1(x) \;\; dx. \tag{3.31}$$

Moreover, putting (3.27) into (3.31) and using the results in Appendices 2B and 2C, we have

$$\begin{aligned} P_{e1} &= 2J(r-1, 1, 2\gamma_o) \\ &\quad - \frac{2^{2-2r}}{\Gamma(r-1)} \sum_{m=0}^{r-1} \frac{2^{r-m}-1}{m!} \times \Gamma(r+m-1) \cdot J(r+m-1, 2, 2\gamma_o). \end{aligned} \tag{3.32}$$

3.2.2 Performance of the Data Symbol Stream from the Transmit Antenna with a Lower SNR

In the following, we derive the p.d.f. of the signal SNR at the second step after interference cancellation has been performed. We assume that the symbols have been correctly decoded during the first step, i.e., error propagation will not be considered. Denoting $\boldsymbol{Z} = \boldsymbol{H}^H \boldsymbol{H}$ as

$$\boldsymbol{Z} = \begin{pmatrix} z_{11} & z_{12} \\ z_{21} & z_{22} \end{pmatrix}, \tag{3.33}$$

we have $x_1 = 1/w_{11} = |\boldsymbol{Z}|/z_{22}$ and $x_2 = 1/w_{22} = |\boldsymbol{Z}|/z_{11}$. In the first step, the j-th data stream where $j = \arg\max_j \{z_{jj}\}$ has been decoded. Therefore, at the second step, the remaining data stream is decoded. It is obvious that the c.d.f. of SNR in the second step is proportional to the distribution of $\min(z_{11}, z_{22})$, i.e.,

$$\begin{aligned} F_2(x) &= \Pr(\min(z_{11}, z_{22}) < x) = 1 - \Pr(\min(z_{11}, z_{22}) > x) \\ &= 1 - \Pr(z_{11} > x) \cdot \Pr(z_{22} > x). \end{aligned} \tag{3.34}$$

It is also known that z_{11} and z_{22} are chi-squared distributed with $2r$ degrees of freedom[1], and are independent of each other. Hence, the p.d.f. of z_i can be shown equal to [76]

$$f_{z_i}(z) = \frac{z^{r-1}e^{-z}}{\Gamma(r)}. \tag{3.35}$$

Since

$$\Pr(z_i > x) = \int_x^{\infty} f_{z_i}(z)dz = \frac{\Gamma(r,x)}{\Gamma(r)}, \tag{3.36}$$

we substitute (3.36) into (3.34) to obtain

$$F_2(x) = 1 - \left[\frac{\Gamma(r,x)}{\Gamma(r)}\right]^2. \tag{3.37}$$

The p.d.f. of $\min(z_{11}, z_{22})$ is then given by

$$f_2(x) = \frac{dF_2(x)}{dx} = \frac{2}{\Gamma(r)}\exp(-2x)\sum_{m=0}^{r-1}\frac{x^{r+m-1}}{m!}. \tag{3.38}$$

Finally, we have the BER of the decoded data in the second step equal to

$$P_{e2} = \frac{2}{\Gamma(r)}\sum_{m=0}^{r-1}\frac{\Gamma(r+m)}{2^{r+m}m!} \times J(r+m, 2, 2\gamma_o). \tag{3.39}$$

The above results are obtained under the assumption of no error propagation. If error propagation has to be considered in the second step, we can derive the exact average BER based on the method in [73]. But the final analytical results are lengthy and tedious. Overall, the total probability of error (at least one error in the two steps), denoted by $\bar{P}_{e,tot}$, is tightly upper bounded by the sum of average BER in the first and second step [59], i.e., $\bar{P}_{e,tot} \leq P_{e1} + P_{e2}$.

[1]We can also say that z_{11} and z_{22} have Gamma distributions with shape parameter r.

3.2.3 Effect on SNR

At high SNR, the BER shown in (3.32) is denominated by the first term $2J(r-1,1,2\gamma_o)$ and the lowest order term in the summation sign. Under the same condition, the BER expression in (3.39) is denominated by the lowest order term in the summation sign. The BERs of the decoded data in the first and second steps can therefore be approximated, respectively, by

$$P_{e1} \approx 2J(r-1,1,2\gamma_o) - 2^{1-r}(2-2^{1-r})J(r-1,2,2\gamma_o) \tag{3.40}$$

and

$$P_{e2} \approx \frac{1}{2^{r-1}}J(r,2,2\gamma_o). \tag{3.41}$$

Let P_{e1}^f be the average BER of the first output using fixed ordering with average branch SNR γ_{o1} and P_{e2}^f be the one of the second output with average branch SNR γ_{o2}. Using the results in Section 2.2 ,i.e., (2.10), we have

$$P_{e1}^f = J(r-1,1,2\gamma_{o1}) \tag{3.42}$$

$$P_{e2}^f = J(r,1,2\gamma_{o2}). \tag{3.43}$$

Assuming $P_{e1} = P_{e1}^f$, $P_{e2} = P_{e2}^f$ and combining the results in (3.40), (3.41) and (2.60) in Appendix 2C, we have $\gamma_{o1} = 2\gamma_o$ and $\gamma_{o2} = 2^{-1/r}\gamma_o$. Therefore, at high SNR the effect of optimal ordering is to increase the SNR by 3 dB for the first step and decrease the SNR by $(3/r)$ dB for the second step.

3.2.4 Effect on Diversity Order

In Section 2.2, we have studied the diversity order of a ZF detector. For the V-BLAST detector under investigation, we apply (3.40) and (2.61) in Appendix 2C to the definition in (2.12). It can readily be shown that the diversity order for the data stream coming from the antenna with a higher SNR equals $(r-1)$. Similarly, the diversity order of the data stream coming from the other antenna can be found equal to r based on (3.41). Since it has been reported that without optimal ordering, the diversity order at the ith processing step equals $r-t+i$ for an i.i.d. Rayleigh fading channel [58, 59], we can, based on our analytical findings, conclude that optimal ordering has no effect on the diversity order in a $2\times r$ system. Such a conclusion is also consistent with that reported in [59].

3.2.5 Unbalanced Transmit Powers

Next, we study the performance of the detector in the case of unbalanced transmit powers. We define $\boldsymbol{\Lambda} = \mathrm{diag}[a\ b]$ as a diagonal matrix where a and b denote the transmit power from the first and second antennas, respectively. The total transmit power is fixed and has been normalized to 2 for simplicity, i.e., $a+b=2$. Consequently, we also have $0 < a, b < 2$. To include the unbalanced transmit power effect, we replace the $\boldsymbol{H}$ in Section 3.1 with $\hat{\boldsymbol{H}} = \boldsymbol{H}\boldsymbol{\Lambda}^{1/2}$. Thus, for the i.i.d. Rayleigh fading channel, we have a covariance matrix of the row vectors in $\hat{\boldsymbol{H}}$ equal to

$$\boldsymbol{\Sigma} = \begin{pmatrix} a & 0 \\ 0 & b \end{pmatrix}. \tag{3.44}$$

Substituting (3.44) into the joint p.d.f. of $\boldsymbol{W}$ shown in (3.16), we have

$$\begin{aligned} f_{w_{11},w_{12},w_{22}}(w_{11},w_{12},w_{22}) = {} & \frac{(w_{11}w_{22}-|w_{12}|^2)^{-(r+2)}}{\pi(ab)^r\Gamma(r)\Gamma(r-1)} \\ & \times \exp\left[-\frac{w_{11}/a+w_{22}/b}{w_{11}w_{22}-|w_{12}|^2}\right]. \end{aligned} \tag{3.45}$$

By defining $x_1 = 1/w_{11}$ and $x_2 = 1/w_{22}$ and using similar procedures as in Section 3.2.1, we can obtain the distribution of the $\max(x_1, x_2)$ as

$$\begin{aligned} F_3(x) &= \Pr(\max(x_1, x_2) < x) \\ &= \frac{1}{\Gamma(r)\Gamma(r-1)} \int_1^{\infty} y^{-r} \cdot \gamma(r, xy/a) \cdot \gamma(r, xy/b)\ \ dy. \end{aligned} \tag{3.46}$$

Then, the p.d.f. of $\max(x_1, x_2)$ is given by

$$f_3(x) = \frac{dF_3(x)}{dx} = I_1 + I_2 \tag{3.47}$$

where I_1 and I_2 have the following closed-form solutions:

$$\begin{aligned} I_1 &= \frac{x^{r-2}}{a^r\Gamma(r-1)} \cdot \frac{1}{\Gamma(r)} \int_x^{\infty} \exp(-t/a) \cdot \gamma(r, t/b)\ dt \\ &= \frac{1}{a^r\Gamma(r-1)} \left[ax^{r-2}e^{-x/a} - e^{-2x/(ab)} \sum_{m=0}^{r-1} \frac{x^{r+m-2}}{b^{m-1}m!} \frac{a/2 - (a/2)^{r-m+1}}{1 - a/2} \right] \end{aligned} \tag{3.48}$$

$$\begin{aligned} I_2 &= \frac{x^{r-2}}{b^r\Gamma(r-1)} \cdot \frac{1}{\Gamma(r)} \int_x^{\infty} \exp(-t/b) \cdot \gamma(r, t/a)\ dt \\ &= \frac{1}{b^r\Gamma(r-1)} \left[bx^{r-2}e^{-x/b} - e^{-2x/(ab)} \sum_{m=0}^{r-1} \frac{x^{r+m-2}}{a^{m-1}m!} \frac{b/2 - (b/2)^{r-m+1}}{1 - b/2} \right]. \end{aligned} \tag{3.49}$$

Again we integrate $f_3(x)$ to obtain the c.d.f. $F_3(x)$ as

$$\begin{aligned} F_3(x) = &\left[\frac{\gamma(r-1, x/a)}{\Gamma(r-1)} - \frac{(ab/4)^r}{\Gamma(r-1)} \sum_{m=0}^{r-1} \frac{(a/2)^{m-r} - 1}{(1 - a/2)m!} \gamma(r + m - 1, \frac{2x}{ab}) \right] \\ &+ \left[\frac{\gamma(r-1, x/b)}{\Gamma(r-1)} - \frac{(ab/4)^r}{\Gamma(r-1)} \sum_{m=0}^{r-1} \frac{(b/2)^{m-r} - 1}{(1 - b/2)m!} \gamma(r + m - 1, \frac{2x}{ab}) \right]. \end{aligned} \tag{3.50}$$

The BER of the decoded data stream coming from the antenna with a higher SNR can then be shown equal to

$$
\begin{aligned}
P_{e3} = {} & J(r-1, 1/a, 2\gamma_o) + J(r-1, 1/b, 2\gamma_o) \\
& - \frac{(b/2)^r}{\Gamma(r-1)} \sum_{m=0}^{r-1} \frac{(a/2)^m - (a/2)^r}{m!(1-a/2)} \times \Gamma(r+m-1) \times J(r+m-1, \frac{2}{ab}, 2\gamma_o) \\
& - \frac{(a/2)^r}{\Gamma(r-1)} \sum_{m=0}^{r-1} \frac{(b/2)^m - (b/2)^r}{m!(1-b/2)} \times \Gamma(r+m-1) \times J(r+m-1, \frac{2}{ab}, 2\gamma_o).
\end{aligned}
\tag{3.51}
$$

During the second step, after interference cancellation is performed, the c.d.f. of the SNR is related to the distribution of $\min(z_{11}, z_{22})$, which is given by

$$
F_4(x) = 1 - \Pr(z_{11} > x) \cdot \Pr(z_{22} > x). \tag{3.52}
$$

Following the procedures as in Section 3.2.2, we can obtain

$$
F_4(x) = 1 - \frac{\Gamma(r, x/a)}{\Gamma(r)} \cdot \frac{\Gamma(r, x/b)}{\Gamma(r)} \tag{3.53}
$$

and

$$
\begin{aligned}
f_4(x) &= \frac{1}{a^r} e^{-x/a} x^{r-1} \frac{\Gamma(r, x/b)}{\Gamma^2(r)} + \frac{1}{b^r} e^{-x/b} x^{r-1} \frac{\Gamma(r, x/a)}{\Gamma^2(r)} \\
&= \frac{e^{-2x/(ab)}}{a^r \Gamma(r)} \sum_{m=0}^{r-1} \frac{x^{r+m-1}}{b^m m!} + \frac{e^{-2x/(ab)}}{b^r \Gamma(r)} \sum_{m=0}^{r-1} \frac{x^{r+m-1}}{a^m m!}.
\end{aligned}
\tag{3.54}
$$

Therefore, the BER is readily shown equal to

$$
\begin{aligned}
P_{e4} = {} & \frac{(b/2)^r}{\Gamma(r)} \sum_{m=0}^{r-1} \frac{(a/2)^m \Gamma(r+m)}{m!} \cdot J(r+m, \frac{2}{ab}, 2\gamma_o) \\
& + \frac{(a/2)^r}{\Gamma(r)} \sum_{m=0}^{r-1} \frac{(b/2)^m \Gamma(r+m)}{m!} \cdot J(r+m, \frac{2}{ab}, 2\gamma_o).
\end{aligned}
\tag{3.55}
$$

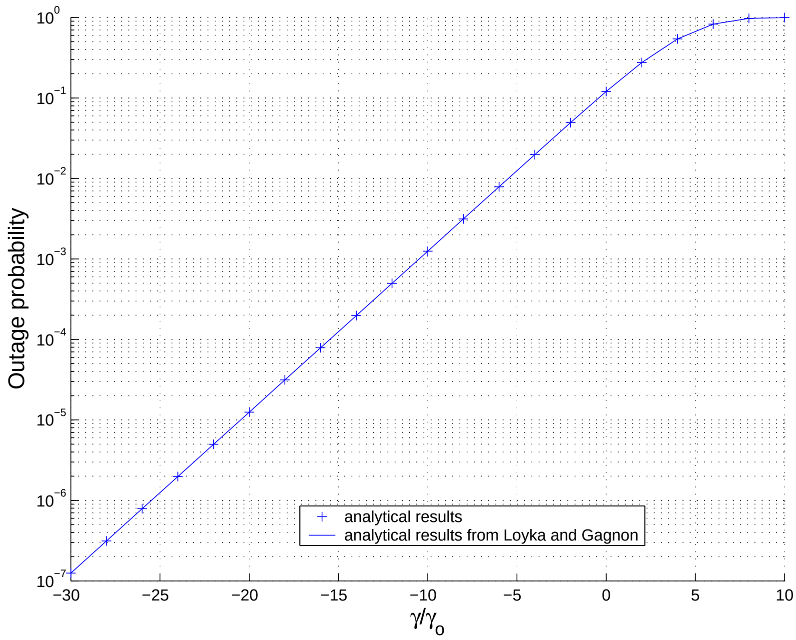

Figure 3.2: Analytical outage probability of the first detection step in the V-BLAST system with ($t = 2$, $r = 3$) over an i.i.d. Rayleigh fading channel.

3.2.6 Results and Discussion

Figure 3.2 plots the analytical outage probability of the first detection step (i.e., the probability that the post-detection SNR γ is less than a certain value, or equivalently the c.d.f. of the post-detection SNR) in the V-BLAST system with ($t = 2$, $r = 3$). Both results, namely (3.29) given in Section 3.2.1 and (30) in [59], are shown. It can be seen that our approach produces the same results reported by as Loyka and Gagnon [59].

Simulations are also performed to evaluate the performance of the V-BLAST system with two transmit antennas. Error propagation has not been considered in the simulations and QPSK is employed for data modulation/demodulation. Fig. 3.3 shows the analytical and simulated outage probability of the post-detection SNR with ($t = 2$, $r = 3$). The horizonal axis represents the ratio of the post-detection SNR to the normalized received SNR (γ/γ_o) in the first or the second detection step. The curves representing different diversity orders are also plotted using the

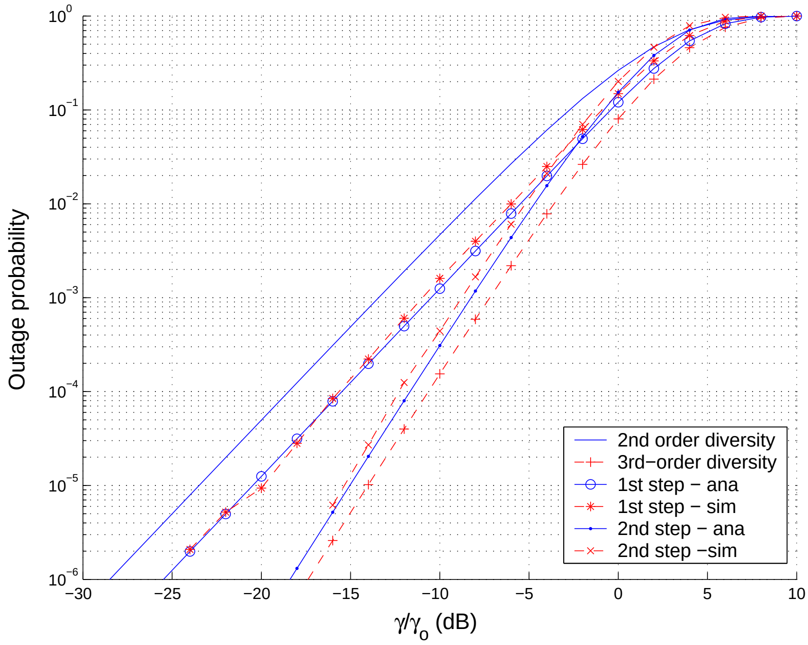

Figure 3.3: Analytical and simulated outage probabilities of the V-BLAST system with ($t = 2$, $r = 3$) over an i.i.d. Rayleigh fading channel. (ana:analytical results; sim: simulation results.)

normalized incomplete Gamma function $[\gamma(m,x)/\Gamma(m)]$. Results show that the analytical and simulation results are similar. Moreover, when γ/γ_o is small, the outage probability of the post-detection SNR at the first step is higher than that at the second step, implying that the signal at the first step has a lower probability of achieving the particular SNR. At high γ/γ_o, the reverse becomes true, i.e., the post-detection SNR at the second step has a lower probability of achieving the particular SNR.

Fig. 3.4 presents the BER performance of the V-BLAST system with ($t = 2$, $r = 3$). The horizontal axis represents the spatially averaged SNR defined as $\frac{1}{r}\sum_{i=1}^{r} \mathrm{SNR}_i$, where SNR_i is the ratio of received signal power (from all t transmitters) to noise power at the ith receiver. It can be observed that the simulation results and the analytical ones are similar. Also, the first detection step produces a better BER than the second step at low SNR. When the SNR increases, the BER at the second step will start outperforming that at the first step at a certain point. The

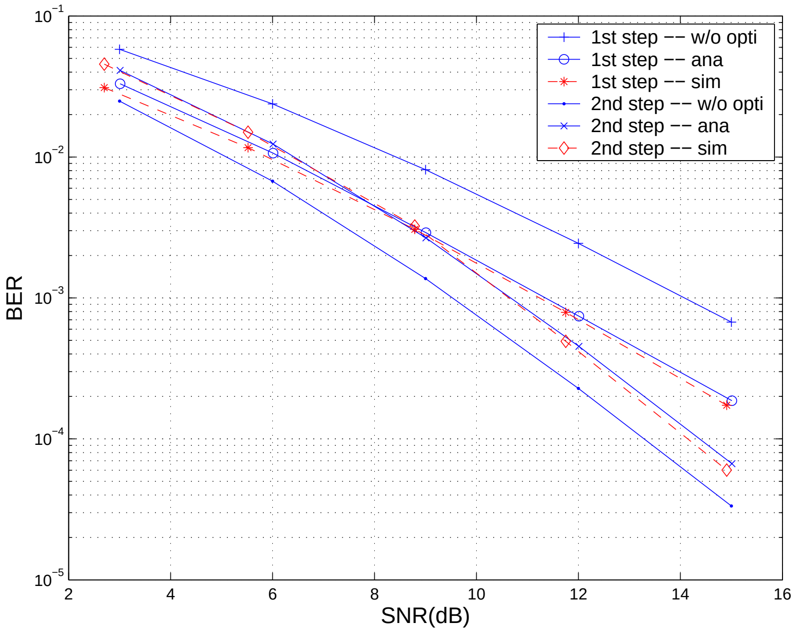

Figure 3.4: Analytical and simulated BERs of the V-BLAST system with ($t = 2$, $r = 3$) over an i.i.d. Rayleigh fading channel. (w/o opti: analytical results with fixed detection ordering; ana: analytical results with optimal detection ordering; sim: simulation results with optimal detection ordering.)

explanation can be found in (3.31). With an increase of γ_o, the slope of $Q(\sqrt{\gamma_o x})$ with high γ_o decreases sharply (see Fig. 3.5 for details). From (3.31), we can hence conclude that for high values of γ_o, the BER is dominated by the c.d.f. of x ($=\gamma/\gamma_o$) when x is small. Conversely, for low values of γ_o, the BER depends on the c.d.f. of x when x is large. Based on the c.d.f. curves shown in Fig. 3.3, the relative BER performance between the first and second steps is then clarified. Moreover, the asymptotic slope of the BER curve in the first or second steps with optimal ordering is the same as that with fixed detection ordering , i.e, the diversity order is the same as that with fixed detection ordering.

In Fig. 3.4, we also observe that at low BER levels, the SNR value of the first step with optimal ordering is about 3 dB lower than the one with fixed ordering. Correspondingly, the performance of the second step with optimal ordering is degraded by 1 dB ($= 3/r = 3/3$) comparing with fixed ordering. Both results verify

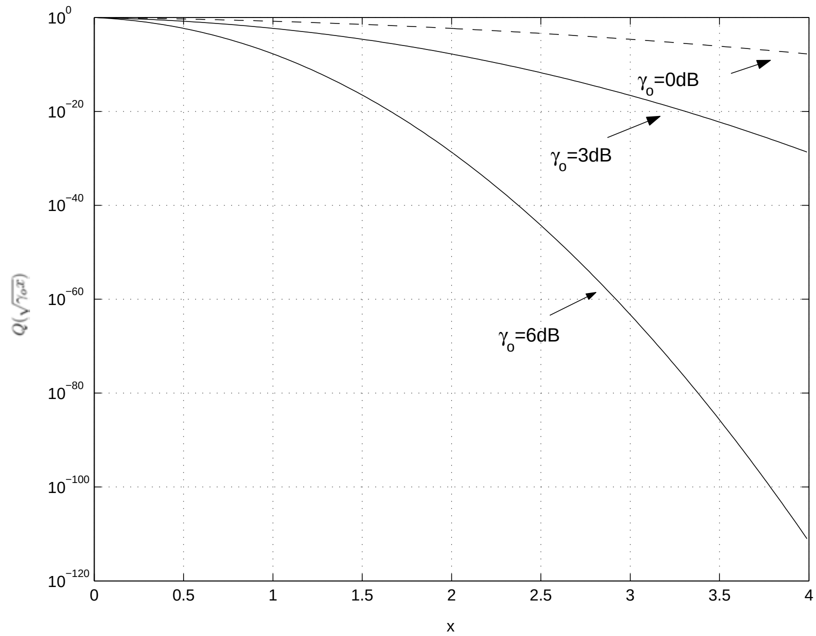

Figure 3.5: The value of Q-function with respect to different values of average received SNR.

our findings in Section 3.2.3. Further, in Fig. 3.6, we plot the BER results of V-BLAST systems with ($t = 2$, $r = 4$). Note that now the second step with optimal ordering suffers from a 0.75 dB ($= 3/r = 3/4$) SNR degradation relative to the one with fixed ordering.

In Fig. 3.7, we show the effect of unbalanced transmit powers on the BER performance with ($t = 2$, $r = 3$). No difference has been observed between the analytical and simulation results. Hence, only the analytical results are shown for all a/b values — the ratios of the two transmit powers. The vertical axis represents the combined average BER of the first and the second detection steps. In Fig. 3.7, the curves with $a/b > 0$ dB are not plotted because of the symmetry between a and b. It is found that equal transmit power produces the best BER performance. On the contrary, the degradation becomes significant when the ratio of the transmit powers between the two transmit branches is larger than 6 dB.

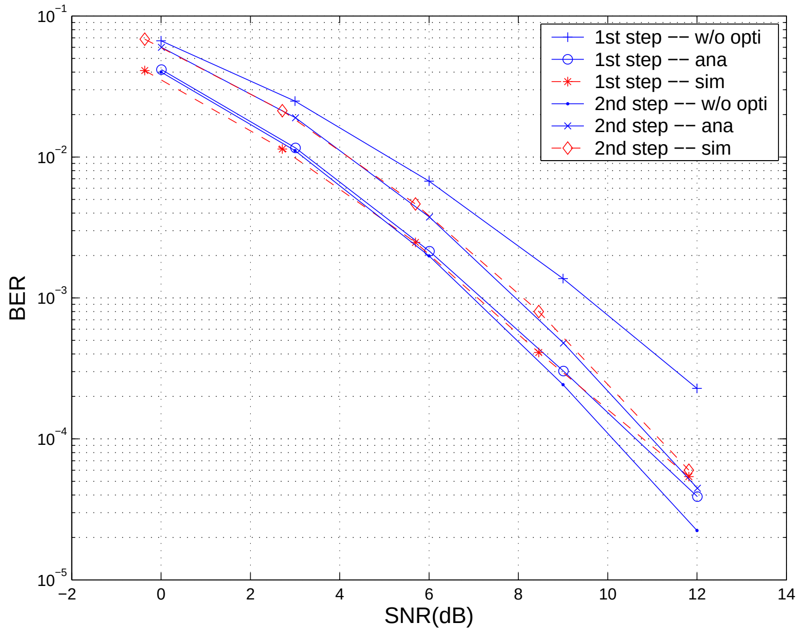

Figure 3.6: Analytical and simulated BERs of the V-BLAST system with ($t = 2$, $r = 4$) over an i.i.d. Rayleigh fading channel. (w/o opti: analytical results with fixed detection ordering; ana: analytical results with optimal detection ordering; sim: simulation results with optimal detection ordering.)

3.3 Performance over a Rayleigh Channel with Correlation at the Transmitter

In a realistic environment, correlation may exist between antenna elements due to the limited number of scatters, small angular spread, and small separation between the antenna elements. In this section, we study the performance of the V-BLAST algorithm when correlation exists at the transmitter. Denoting the correlation coefficient between the two transmit antennas by ζ, the covariance matrix of the row vectors in $\boldsymbol{H}$ then equals

$$\boldsymbol{\Sigma} = \begin{pmatrix} 1 & \zeta \\ \zeta^* & 1 \end{pmatrix} \tag{3.56}$$

where $|\zeta| < 1$.

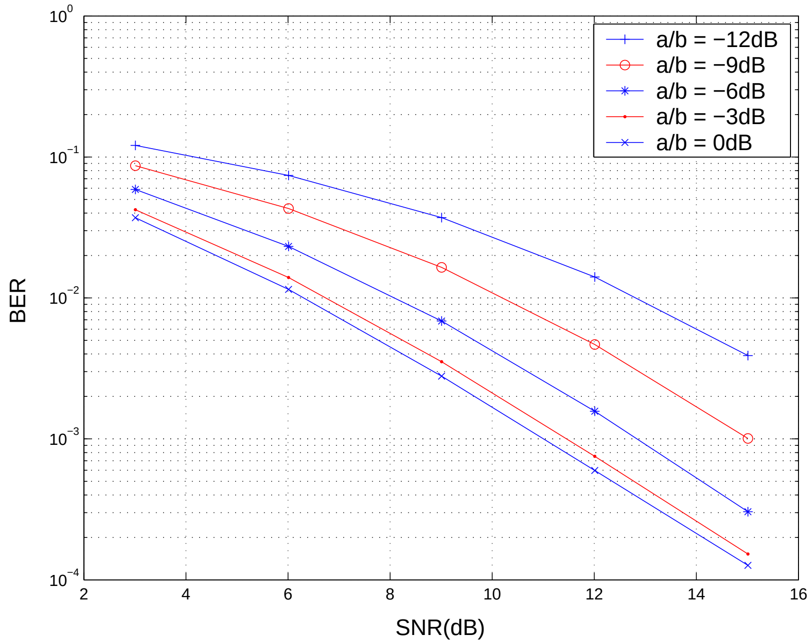

Figure 3.7: Analytical BER of the V-BLAST system with ($t = 2$, $r = 3$) for unbalanced transmit powers.

3.3.1 Performance of the Data Symbol Stream from the Transmit Antenna with a Higher SNR

We map the complex variable w_{12} and ζ to the polar coordinates as

$$w_{12} = \sqrt{w_{11}w_{22}}\rho e^{-\mathbf{i}\theta}, \qquad 0 \le \rho < 1; \tag{3.57}$$

$$\zeta = ae^{-\mathbf{i}b}, \qquad a = |\zeta| \text{ and } 0 \le a < 1 \tag{3.58}$$

where $\mathbf{i} = \sqrt{-1}$. Let $x_1 = 1/w_{11}$, $x_2 = 1/w_{22}$ and substitute them into (3.18). We obtain

$$\begin{aligned} f_{x_1,x_2,\rho,\theta}(x_1, x_2, \rho, \theta) = &\frac{(x_1x_2)^{r-1}\rho(1-\rho^2)^{-(r+2)}}{\pi(1-a^2)^r\Gamma(r)\Gamma(r-1)} \\ &\times \exp\left[-\frac{x_1 + x_2 + 2a\rho\sqrt{x_1x_2}\cos(\theta - b)}{(1-a^2)(1-\rho^2)}\right]. \end{aligned} \tag{3.59}$$

Integrating (3.59) with respect to θ in the range $0 \leq \theta < 2\pi$, we have

$$\begin{aligned} f_{x_1,x_2,\rho}(x_1,x_2,\rho) = & \frac{2(x_1x_2)^{r-1}\rho(1-\rho^2)^{-(r+2)}}{(1-a^2)^r\Gamma(r)\Gamma(r-1)} \\ & \times \exp\left[-\frac{x_1+x_2}{(1-a^2)(1-\rho^2)}\right] \times I_0\left(\frac{2a\rho\sqrt{x_1x_2}}{(1-a^2)(1-\rho^2)}\right) \end{aligned} \tag{3.60}$$

where $I_0(\cdot)$ is the zero-order modified Bessel function of the first kind [2] and has an infinite expansion representation given by [24, eq.(8.447.1)]

$$I_0(z) = \sum_{k=0}^{\infty} \frac{(z^2/4)^k}{(k!)^2}. \tag{3.61}$$

Substituting (3.61) into (3.60) and changing the variable $y = 1/(1-\rho^2)$, we have the expression of $\Pr(\max(x_1,x_2))$ conditioning on y as

$$\begin{aligned} F_{1,\mathrm{cor}}(x|y) &= \Pr(\max(x_1,x_2)|y) \\ &= \int_0^x \int_0^x f_1(x_1,x_2,\rho)\, dx_1dx_2 \\ &= \frac{(1-a^2)^r}{\Gamma(r)\Gamma(r-1)} \sum_{k=0}^{\infty} \frac{a^{2k}}{(k!)^2} \cdot y^{-(r+k)}(y-1)^k \cdot \gamma^2(r+k, \frac{xy}{1-a^2}). \end{aligned} \tag{3.62}$$

We differentiate $F_1(x)$ with respect to x, and integrate with respect to y to obtain the p.d.f. of x as

$$\begin{aligned} f_{1,\mathrm{cor}}(x) = & \frac{2x^{r-1}}{\Gamma(r)\Gamma(r-1)} \sum_{k=0}^{\infty} \frac{a^{2k}}{(k!)^2} \cdot \left(\frac{x}{1-a^2}\right)^k \\ & \times \int_1^{\infty} (y-1)^k \cdot \exp\left(-\frac{xy}{1-a^2}\right) \cdot \gamma\left(r+k, \frac{xy}{1-a^2}\right)\, dy. \end{aligned} \tag{3.63}$$

Defining $u = x/(1-a^2)$, we can derive the closed-form expression for the p.d.f. of u, i.e.,

$$\tilde{f}_{1,\mathrm{cor}}(u) = \frac{2(1-a^2)^r u^{r-2}}{\Gamma(r)\Gamma(r-1)} \sum_{k=0}^{\infty} \frac{a^{2k}}{(k!)^2} \cdot \Gamma(r+k) \sum_{p=0}^{k} \binom{k}{p} (-u)^{k-p} \cdot P(k,p,u) \tag{3.64}$$

where

$$
\begin{aligned}
P(k,p,u) &= \frac{1}{\Gamma(r+k)} \int_u^{\infty} y^p \cdot e^{-y} \gamma(r+k,y)\, dy \\
&= \Gamma(p+1,u) - \sum_{m=0}^{r+k-1} \frac{\Gamma(p+m+1,2u)}{m! 2^{p+m+1}} \\
&= (p!) \exp(-u) \sum_{m=0}^{p} \frac{u^m}{m!} - \frac{\exp(-2u)}{2^{p+1}} \sum_{m=0}^{r+k+p-1} a_{k,p,m} \cdot \frac{(2u)^m}{m!}
\end{aligned}
\tag{3.65}
$$

and

$$
a_{k,p,m} = \begin{cases} \sum_{n=0}^{r+k-1} \frac{(p+n)!}{n! 2^n}, & 0 \le m \le p \\ \sum_{n=m-p}^{r+k-1} \frac{(p+n)!}{n! 2^n}, & m > p. \end{cases} \tag{3.66}
$$

Integrating $\tilde{f}_{1,\mathrm{cor}}(u)$, we obtain the c.d.f. of u as

$$
\tilde{F}_{1,\mathrm{cor}}(u) = \frac{2(1-a^2)^r}{\Gamma(r)\Gamma(r-1)} \sum_{k=0}^{\infty} \frac{a^{2k}}{(k!)^2} \cdot \Gamma(r+k) \times \sum_{p=0}^{k} \binom{k}{p} (-1)^{k-p} (I_3 - I_4) \tag{3.67}
$$

where

$$
I_3 = \sum_{m=0}^{p} \frac{p!}{m!} \cdot \Gamma(r+k-p+m-1,u) \tag{3.68}
$$

$$
I_4 = \frac{1}{2^{r+k}} \sum_{m=0}^{r+k+p-1} \frac{a_{k,p,m}}{m!} \cdot \Gamma(r+k-p+m-1,2u). \tag{3.69}
$$

Finally, the c.d.f. of x can be obtained as

$$
F_{1,\mathrm{cor}}(x) = \tilde{F}_{1,\mathrm{cor}}\left(\frac{x}{1-a^2}\right). \tag{3.70}
$$

Based on the results above, when QPSK modulation is used, the expression for the average BER can be readily shown equal to

$$
P_{e1,\mathrm{cor}} = \frac{2(1-a^2)^r}{\Gamma(r)\Gamma(r-1)} \sum_{k=0}^{\infty} \frac{a^{2k}}{(k!)^2} \cdot \Gamma(r+k) \times \sum_{p=0}^{k} \binom{k}{p} (-1)^{k-p} (I_5 - I_6) \tag{3.71}
$$

where

$$I_5 = \sum_{m=0}^{p} \frac{p!\Gamma(r+k-p+m-1)}{m!} \cdot J(r+k-p+m-1, 1, 2\gamma_o(1-a^2)) \tag{3.72}$$

$$\begin{aligned} I_6 = \frac{1}{2^{r+k}} \sum_{m=0}^{r+k+p-1} \frac{a_{k,p,m}}{m!} \cdot \Gamma(r+k-p+m-1)) \\ \times J(r+k-p+m-1, 2, 2\gamma_o(1-a^2)). \end{aligned} \tag{3.73}$$

Further, by comparing (3.71) with (3.32), the SNR degradation (in decibel) due to transmit correlation can be approximated as

$$\begin{aligned} \Delta\gamma_{1,\mathrm{cor}}\ (\mathrm{dB}) = \frac{1}{r-1}(3r + 10\log(1-a^2)) + \frac{1}{r-1} \\ \times 10\log\left(\sum_{k=0}^{\infty}\binom{r+k-1}{k}a^{2k}\left[1-\frac{1}{2^{k+1}}\sum_{n=0}^{r+k-1}\binom{k+n}{n}\frac{1}{2^n}\right]\right). \end{aligned} \tag{3.74}$$

In Section 2.2.2, it has been found that when fixed ordering is used, the SNR loss due to transmit correlation equals $-10\log(1-a^2)$ dB. Combining with the results obtained in Section 3.2.3 for optimal ordering, we conclude that when transmit correlation exists, optimal ordering in the first step improves over fixed ordering at the low-BER region by

$$\Delta\gamma_{1,\mathrm{opti}}\ (\mathrm{dB}) = 3 - \Delta\gamma_{1,\mathrm{cor}} - 10\log(1-a^2). \tag{3.75}$$

3.3.2 Performance of the Data Symbol Stream from the Transmit Antenna with a Lower SNR

Using (3.33) and defining $z_1 = z_{11}$ and $z_2 = z_{22}$, the joint p.d.f. of z_1 and z_2 is given by [50, ch. 2.3]

$$f_{z_1,z_2}(z_1, z_2) = \left[\prod_{k=1}^{2} \frac{1}{\Gamma(r)} z_k^{r-1} \exp(-z_k)\right] \left\{1 + \sum_{j=1}^{\infty} a^j L_j^{(r-1)}(z_1) L_j^{(r-1)}(z_2)\right\} \quad (3.76)$$

where $L_j^{(r-1)}(x)$ is the Laguerre polynomial defined as

$$L_j^{(r-1)}(x) = \left[\frac{\Gamma(r)\Gamma(r+j)}{j!}\right]^{1/2} \sum_{k=0}^{j} (-1)^k \binom{j}{k} \frac{x^k}{\Gamma(r+k)}. \quad (3.77)$$

Define $F_{2,\mathrm{cor}}(x)$ as the c.d.f. of $\min(z_1, z_2)$. The expression of $F_{2,\mathrm{cor}}(x)$ thus equals

$$\begin{aligned} F_{2,\mathrm{cor}}(x) &= \Pr(\min(z_1, z_2) < x) = 1 - \Pr(z_1 > x, z_2 > x) \\ &= 1 - \left[\frac{\Gamma(r,x)}{\Gamma(r)}\right]^2 - \frac{1}{\Gamma(r)} \sum_{j=1}^{\infty} \frac{a^j \Gamma(r+j)}{j!} \left[\sum_{k=0}^{j} (-1)^k \binom{j}{k} \frac{\Gamma(r+k,x)}{\Gamma(r+k)}\right]^2. \end{aligned} \quad (3.78)$$

Then, we differentiate $F_{2,\mathrm{cor}}(x)$ with respect to x to obtain the p.d.f. of x as

$$\begin{aligned} f_{2,\mathrm{cor}}(x) &= \frac{2}{\Gamma(r)} e^{-2x} \sum_{k=0}^{r-1} \frac{x^{r+k-1}}{k!} + \frac{2}{\Gamma(r)} e^{-2x} \sum_{j=1}^{\infty} \frac{a^j \Gamma(r+j)}{j!} \\ &\quad \times \left[\sum_{k=0}^{j} (-1)^j \binom{j}{k} \frac{x^{r+k-1}}{\Gamma(r+k)}\right] \cdot \left[\sum_{p=1}^{j} b_{j,p} \cdot \frac{x^{r+p-1}}{\Gamma(r+p)}\right] \\ &= \frac{2}{\Gamma(r)} e^{-2x} \sum_{k=0}^{r-1} \frac{x^{r+k-1}}{k!} + \frac{2}{\Gamma(r)} e^{-2x} \sum_{j=1}^{\infty} \frac{a^j \Gamma(r+j)}{j!} \sum_{m=1}^{2j} c_{j,m} x^{2r+m-2} \end{aligned} \quad (3.79)$$

where

$$b_{j,p} = \sum_{n=p}^{j} (-1)^n \binom{j}{n} \quad (3.80)$$

and

$$c_{j,m} = \sum_{k=\max(0,m-j)}^{\min(m,j)} \frac{(-1)^k \binom{j}{k} b_{j,m-k}}{\Gamma(r+k)\Gamma(r+m-k)}. \tag{3.81}$$

Integrating $f_{2,\text{cor}}(x)$, we have the c.d.f. expression of $\min(x_1, x_2)$ as

$$\begin{aligned} F_{2,\text{cor}}(x) &= \frac{2}{\Gamma(r)} \sum_{k=0}^{r-1} \frac{\gamma(r+k, 2x)}{2^{r+k} k!} \\ &\quad + \frac{2}{\Gamma(r)} \sum_{j=1}^{\infty} \frac{a^j \Gamma(r+j)}{j!} \sum_{m=1}^{2j} \frac{c_{j,m}}{2^{2r+m-1}} \times \gamma(2r+m-1, 2x). \end{aligned} \tag{3.82}$$

Using similar procedures as in previous sections, the average BER using QPSK modulation can be obtained as

$$\begin{aligned} P_{e2,\text{cor}} &= \frac{2}{\Gamma(r)} \sum_{k=0}^{r-1} \frac{\Gamma(r+k)}{2^{r+k} k!} \cdot J(r+k, 2, 2\gamma_o) \\ &\quad + \frac{2}{\Gamma(r)^2} \sum_{j=1}^{\infty} \frac{a^j \Gamma(r+j)}{j!} \sum_{m=1}^{2j} \frac{c_{j,m} \Gamma(2r+m-1)}{2^{2r+m-1}} \cdot J(2r+m-1, 2, 2\gamma_o). \end{aligned} \tag{3.83}$$

At high SNR region, the average BER is dominated by the J-function with the lowest order. In (3.83), the lowest order of the J-function in the first summation equals r, while that in the second summation equals $2r$. Therefore, the second summation has a negligible contribution to the BER at high SNR region. Since the correlation coefficient a exists only in the second summation, we further conclude that transmit correlation has a negligible effect on the performance of the second detection step in the higher SNR areas. In fixed ordering, the output SNR of the second detection step is related only to the second column of $\boldsymbol{H}$ (for a $2 \times r$ system) and it has the same distribution whether correlation exists among the 2 transmit antennas or not. As a consequence, there is no SNR degradation for the second step due to correlation. Since transmit correlation has no effect on both optimal ordering

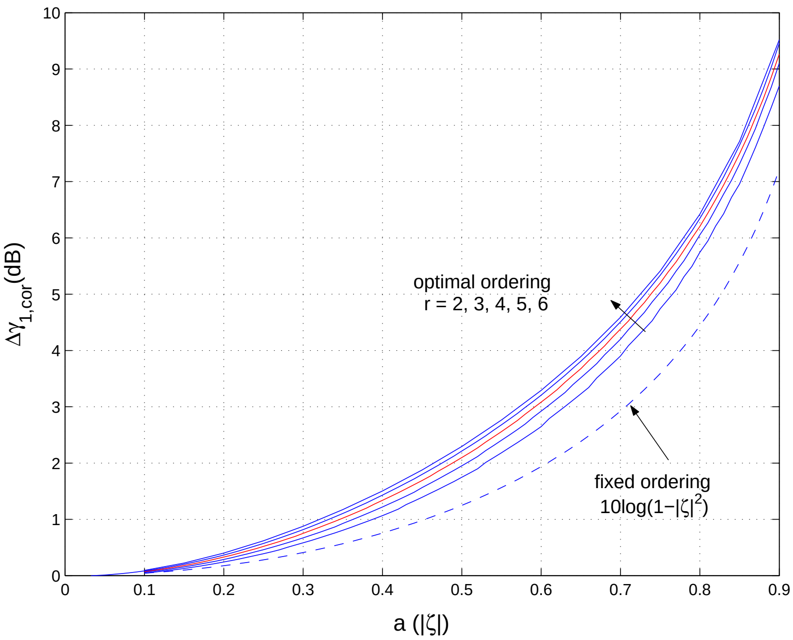

Figure 3.8: Analytical SNR degradation of the first step of the V-BLAST system due to correlation at the transmitter over a Rayleigh fading channel. $t = 2$.

and fixed ordering at high SNR region, we conclude that the SNR loss of the second step in optimal ordering remains at $(3/r)$ dB (see Section 3.2.3) compared with that in fixed ordering.

3.3.3 Results and Discussion

Fig. 3.8 displays the analytical results of (3.74), plotting the SNR loss of the first detection step for optimal ordering when transmit correlation exists. The corresponding SNR loss for fixed ordering is also shown for comparison. We observe that the SNR degradation due to transmit correlation increases with the correlation coefficient. Moreover, the degradation is higher for optimal ordering compared with fixed ordering. Thus, the advantage of optimal ordering over fixed ordering diminishes with the correlation coefficient. The same conclusion can also be drawn in Fig. 3.9, where the SNR gain of the first detection step in the V-BLAST system (Eq.(3.75)) with optimal ordering over that with fixed ordering is plotted.

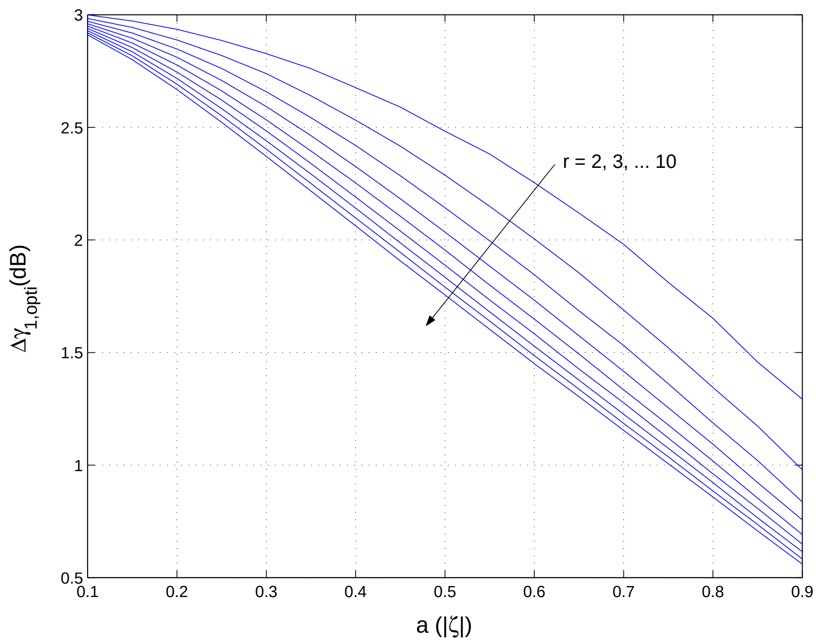

Figure 3.9: Analytical SNR improvement of the first step with optimal ordering over fixed ordering when correlation exists at the transmitter. $t = 2$.

Fig. 3.10 presents the outage probability of the post-detection SNR at the first step of optimal ordering for ($t = 2$, $r = 3$) with transmit correlation. For the analytical results of fixed ordering, they are calculated using (2.7). We observe that when the correlation coefficient increases, the outage probability increases, indicating higher SNR loss due to correlaton.

Fig. 3.11 presents the BER performance of the V-BLAST system for ($t = 2$, $r = 3$) with transmit correlation. We observe that the analytical and simulated results are close to each other. As has been predicted, the transmit correlation has no effect on the performance of the second step in optimal ordering. Also, the gain of optimal ordering in the first step decreases with the increase of correlation coefficient. The observation is consistent with the result in (3.75).

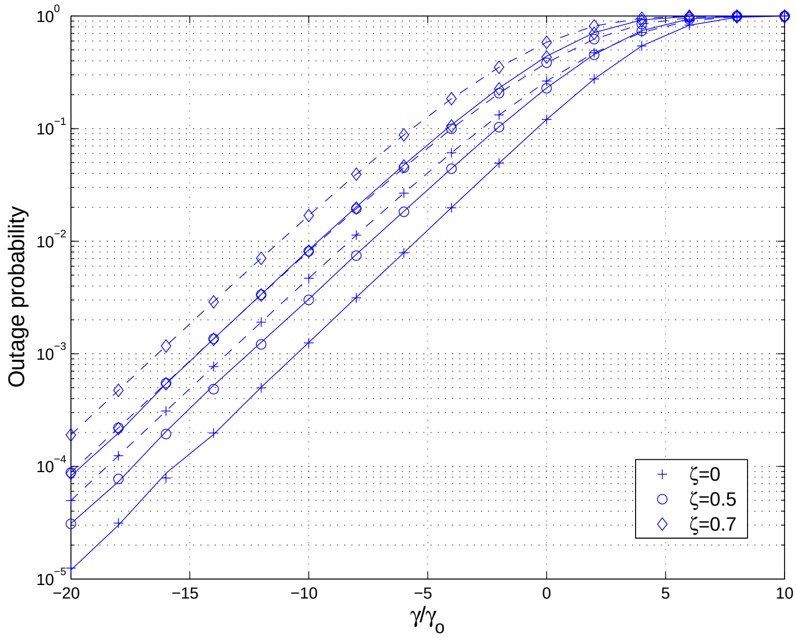

Figure 3.10: Analytical and simulated outage probabilities of the first step in the V-BLAST system for ($t = 2$, $r = 3$) over a Rayleigh fading channel with transmit correlation. (Simulated results of optimal ordering are represented by solid lines, analytical results of optimal ordering are shown with markers, and analytical results of fixed ordering are displayed with dashed line and markers.)

3.4 Performance Over A Rician Channel

For a Rician channel, it has been shown in Section 2.2.3 that $\boldsymbol{Z}$ follows a non-central complex Wishart distribution denoted by $\boldsymbol{Z} \sim W_t^c(r, \boldsymbol{M}, \boldsymbol{\Sigma})$ where

$$\boldsymbol{M} = \mathrm{E}(\boldsymbol{H}). \tag{3.84}$$

Moreover, the non-central complex Wishart distribution can be approximated by a complex Wishart distribution $\hat{\boldsymbol{Z}} \sim W_t^c(r, \hat{\boldsymbol{\Sigma}})$ with the covariance matrix given by

$$\hat{\boldsymbol{\Sigma}} = \boldsymbol{\Sigma} + \frac{1}{r}\boldsymbol{M}^H\boldsymbol{M}. \tag{3.85}$$

Based on the derivations in Section 2.2.3, the covariance matrix can be written

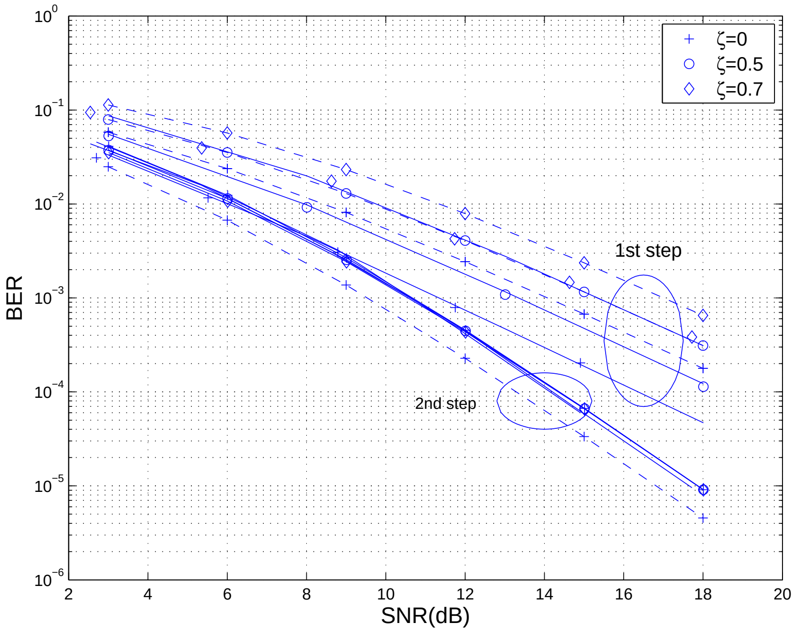

Figure 3.11: Analytical and simulated BERs of the V-BLAST system for ($t = 2$, $r = 3$) over a Rayleigh fading channel with transmit correlation. (Simulated results of optimal ordering are represented by solid lines, analytical results of optimal ordering are shown with markers, and analytical results of fixed ordering are displayed with dashed line and markers.)

as

$$\hat{\mathbf{\Sigma}} = \frac{1}{1+K}\boldsymbol{I}_t + \frac{K}{1+K}\boldsymbol{\beta}\boldsymbol{\beta}^H \tag{3.86}$$

where

$$\boldsymbol{\beta} = [1 \ \ \beta_1 \ \ \cdots \ \ \beta_{t-1}]^T, \quad |\beta_j| = 1, \ j = 1, \ldots, t-1; \tag{3.87}$$

is defined as the array response of transmit antennas and K is the Rician factor. For a system with 2 transmit antennas, (3.86) can be further reduced to

$$\begin{aligned} \hat{\mathbf{\Sigma}} &= \frac{1}{1+K}\begin{pmatrix} 1 & 0 \\ 0 & 1 \end{pmatrix} + \frac{K}{1+K}\begin{pmatrix} 1 & \beta_1^* \\ \beta_1 & 1 \end{pmatrix} \\ &= \begin{pmatrix} 1 & \frac{K}{1+K}\beta_1^* \\ \frac{K}{1+K}\beta_1 & 1 \end{pmatrix} \end{aligned} \tag{3.88}$$

with $|\beta_1| = 1$. Comparing $\hat{\mathbf{\Sigma}}$ in (3.88) with $\mathbf{\Sigma}$ in (3.56), we observe that the two covariance matrices are identical when

$$\zeta = \frac{K}{1+K}\,\beta_1^*. \tag{3.89}$$

In other words, the performance of the V-BLAST system over a Rice channel can be approximated by that over a correlated-Rayleigh channel with the substitution given in (3.89). Moreover, the analyses in Section 3.3 have shown that only the magnitude of ζ is required in characterising the system performance. Thus, for a given Rician factor K, the performance of a two-transmit-antenna MIMO system over a Rice fading channel can be obtained by modifying the $|\zeta|$ in the correlated-Rayleigh channel model in Section 3.3 to $|K\beta_1^*/(1+K)| = K/(1+K)$.

As K increases from $-\infty$ to ∞, $|\zeta|$ changes from 0 to 1. For example, K=$-\infty$ dB, 0 dB, 3 dB and 6 dB, corresponds to $|\zeta|$ =0, 0.5, 0.67 and 0.8, respectively. Therefore, based on the performance curves of the V-BLAST system over a correlated-Rayleigh channel, i.e., Fig. 3.8 to Fig. 3.11, we can deduce the performance of the V-BLAST system over a Rician channel. In fact, observations made for the correlated-Rayleigh channel are applicable to the Rician channel as $|\zeta|$ increases monotonically with K (so does K increase monotonically with $|\zeta|$).

For instance, from Fig. 3.8 and Fig. 3.9, we can conclude that for a Rician channel, (i) the SNR loss of the first detection step for optimal ordering increases with the Rician factor K; (ii) the degradation is higher for optimal ordering compared with fixed ordering; and (iii) the advantage of optimal ordering over fixed ordering diminishes with the Rician factor K. Also, Fig. 3.11 implies that the Rician factor has no effect on the performance of the second step in optimal ordering.

Finally, Fig. 3.12 compares the analytical and simulated outage probabilities of the post-detection SNR at the first step for ($t = 2$, $r = 3$) over a Rician channel. We

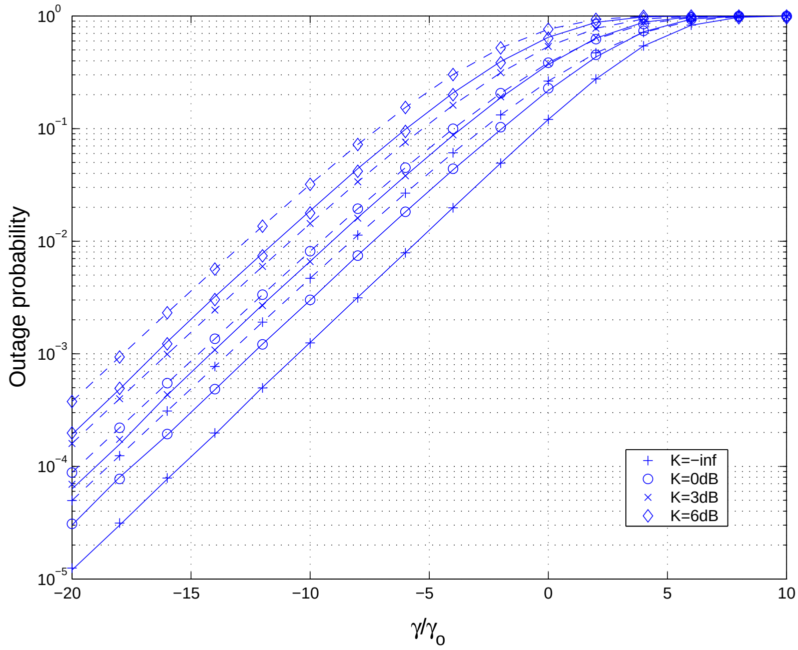

Figure 3.12: Analytical and simulated outage probabilities of the post-detection SNR at the first step in the V-BLAST system for ($t = 2$, $r = 3$) over a Rician fading channel. (Simulated results of optimal ordering are represented by solid lines, analytical results of optimal ordering are shown with markers, and analytical results of fixed ordering are displayed with dashed line and markers.)

can see that both results are very close, further verifying that the correlated-Rayleigh channel model is a good approximation of the Rician model.

3.5 Summary

In this chapter, we have studied thoroughly the performance of the V-BLAST system with two transmit antennas when optimal ordering is used. Three types of channel, namely i.i.d. Rayleigh channel, correlated-Rayleigh channel, and Rician channel, have been investigated. The exact SNR distributions of the system in the first and second detection steps have been derived and the closed-form expressions of the BERs have been obtained. Simulations have been performed and they are found to be very close to the theoretical ones.

For an i.i.d. Rayleigh channel, our study concludes that optimal ordering has no effect on the diversity order compared with fixed ordering. Also, at high SNR, we find that optimal ordering increases the SNR by 3 dB for the first step and decreases the SNR by $(3/r)$ dB for the second step as compared to fixed ordering. Further, we conclude that equal transmit power from the two antennas produces the best BER performance.

We have also approximated the performance of the V-BLAST system over a Rician channel by that over a correlated-Rayleigh channel. Simulation results have shown that the approximation is very accurate. As a consequence, observations made for both types of channels are very similar. We find that for the correlated-Rayleigh/Rician channel, the SNR loss of the first detection step for optimal ordering increases with the transmit-correlation coefficient/Rician factor. In addition, the degradation is higher for optimal ordering compared with fixed ordering and the advantage of optimal ordering over fixed ordering diminishes with the transmit-correlation coefficient/Rician factor. Finally, the transmit-correlation coefficient/Rician factor has been found to have no effect on the performance of the second step in optimal ordering.

Having evaluated the performance of MIMO systems in this and the previous chapters, we will switch to investigating the capacity of MIMO systems in the next chapter. In particular, we will study the asymptotic capacities at both low and high SNR regions and derive the asymptotic capacity loss of Rician channels relative to i.i.d. Rayleigh channels.

Chapter 4

Capacity Of MIMO Channels

In the last two chapters, the performances of the MIMO systems have been studied in terms of the bit error rate. In this chapter, we investigate the capacity of the MIMO systems over a Rician fading channel. Under an independent and identically distributed (i.i.d.) flat Rayleigh fading environment and in the high signal-to-noise ratio (SNR) regime, it has been shown that the capacity of MIMO systems increases almost linearly with the number of transmit antennas or the number of receive antennas, whichever the smaller [91]. However, the capacity diminishes over a Rician channel [12, 34, 37, 53, 66, 67, 70, 78].

In [37], based on the numerical integration method, it is found that the line-of-sight signal component in the Rician channel reduces the MIMO channel capacity as a consequence of the lack of scattering. Asymptotic analysis also shows that the capacity for a MIMO system over a Rician channel decreases with the Rician factor and approaches the capacity of its scattered component when the numbers of antennas are large and the specular matrix has a unit rank [53]. However, the exact capacity of a MIMO channel has not been derived as a closed-form expression, rendering the asymptotic analysis at low and high SNR regions not possible.

In this chapter, we evaluate the capacity of the MIMO Rician channel. First, in Section 4.1, we derive a close-form expression for the channel capacity. During the process, we show that the capacity of a MIMO Rician channel can be well approximated by that of a MIMO correlated-Rayleigh channel. Based on the solution, the asymptotic capacities at low and high SNR regions are analyzed in Section 4.2. Also, the asymptotic capacity loss of the Rician channel relative to an i.i.d. Rayleigh channel is derived. Finally, in Section 4.3, the analytical findings are presented together with the results found by simulations and by the numerical integration method.

4.1 Capacity of MIMO Rician Channels

In our analysis it is assumed that perfect channel information is known at the receiver but not at the transmitter. Under this scenario, we adopt the uniform power allocation scheme and the mutual information (MI) is then given by [17]

$$\mathcal{I} = \log_2 \left(\det \left(\boldsymbol{I}_r + \frac{\Omega}{t\sigma^2} \boldsymbol{H}\boldsymbol{H}^H \right) \right) \tag{4.1}$$

where Ω denotes the total transmitted power, σ^2 is the noise power, $\boldsymbol{H}$ is the channel matrix as defined in Section 2.1, t and r represent the number of transmit and receive antennas, respectively. It is readily shown that the MI can also be expressed as

$$\mathcal{I} = \log_2 \left(\det \left(\boldsymbol{I}_t + \frac{\Omega}{t\sigma^2} \boldsymbol{H}^H\boldsymbol{H} \right) \right). \tag{4.2}$$

The channel capacity, denoted by C and defined as the mean of mutual information, i.e., $C = \mathrm{E}(\mathcal{I})$, is critical in the performance evaluation of MIMO systems. In the following, we assume that $r \geq t$ and make use of (4.2) to evaluate the performance of MIMO under a Rician channel. In the reverse case where $r < t$, the procedures are similar but the starting point would be (4.1) instead.

It is clear that the probability density function (p.d.f.) of the channel matrix $\boldsymbol{H}$ determines the channel capacity. As for the elements of $\boldsymbol{H}$, they are always assumed to be circularly symmetric complex Gaussian random variables (ZMCSCG). Thus, the distribution of the channel matrix $\boldsymbol{H}$ can be modeled as a complex matrix variate normal distribution [25]. Same as in Section 2.2, we define

$$\boldsymbol{Z} = \boldsymbol{H}^H \boldsymbol{H} \tag{4.3}$$

and

$$\boldsymbol{M} = \mathrm{E}(\boldsymbol{H}). \tag{4.4}$$

If the row vectors of $\boldsymbol{H}$ are independent (no receive correlation) with identical covariance matrix $\boldsymbol{\Sigma}$, then $\boldsymbol{Z}$ follows a complex Wishart distribution denoted by $\boldsymbol{Z} \sim W_t^c(r, \boldsymbol{M}, \boldsymbol{\Sigma})$. It is known that a non-central complex Wishart distribution $\boldsymbol{Z} \sim W_t^c(r, \boldsymbol{M}, \boldsymbol{\Sigma})$ can be approximated by a complex Wishart distribution with covariance matrix (see Chapter 2 for details)

$$\hat{\boldsymbol{\Sigma}} = \boldsymbol{\Sigma} + \frac{1}{r} \boldsymbol{M}^H \boldsymbol{M}. \tag{4.5}$$

Based on the Rician channel model and the derivations in Section 2.2.3, we can approximate the distribution of $\boldsymbol{Z}$ by an approximated Wishart distribution with a covariance matrix equal to

$$\hat{\boldsymbol{\Sigma}} = (1 - \zeta)\boldsymbol{I}_t + \zeta \boldsymbol{\beta}\boldsymbol{\beta}^H \tag{4.6}$$

where

$$\boldsymbol{\beta} = [1 \;\; \beta_1 \;\; \cdots \;\; \beta_{t-1}]^T, \quad |\beta_j| = 1, \; j = 1, \ldots, t-1; \tag{4.7}$$

is defined as the array response of transmit antennas, and $\zeta = K/(1+K)$, K

being the Rician factor. In addition, it can be readily shown that the only non-zero eigenvalue of the matrix $\boldsymbol{\beta}\boldsymbol{\beta}^H$ equals t. Therefore, the eigenvalues of $\hat{\boldsymbol{\Sigma}}$, denoted by ϕ_k ($k = 1, 2, \ldots, t$), are given by

$$\phi_1 = \cdots = \phi_{t-1} = 1 - \zeta, \quad \phi_t = 1 + (t-1)\zeta. \tag{4.8}$$

In another study that investigates the capacity of MIMO correlated-Rayleigh channels with $r \geq t$ [36], it has been shown that if the covariance matrix equals

$$[\boldsymbol{\Phi}]_{i,j} = \begin{cases} 1, & \text{if} \quad i = j \\ \zeta, & \text{if} \quad i \neq j \end{cases} \tag{4.9}$$

with $0 < \zeta < 1$ being the correlation between any pair of transmit antenna elements, i.e., the correlation belongs to the intraclass correlation model[1], the eigenvalues of the matrix are the same as those in (4.8). We can therefore conclude that the covariance matrix of the approximated Wishart distribution corresponding to the MIMO Rician channel ($\hat{\boldsymbol{\Sigma}}$) and the covariance matrix of a MIMO Rayleigh channel under the intraclass correlation model ($\boldsymbol{\Phi}$) have the same eigenvalues.

It has been found in [9, 36] that for a correlated-Rayleigh fading channel, the channel capacity depends only on the eigenvalues of the covariance matrix. Thus, we conclude that the capacity of a MIMO Rician channel with Rician factor K is equivalent to that of a MIMO Rayleigh channel under the intraclass correlation model with a correlation coefficient $\zeta = K/(1 + K)$. Detailed derivations of the channel capacity of MIMO Rayleigh channels under intraclass correlation model can be found in [36]. Moreover, it is clear that the geometry of the antenna arrays has no effect on the MIMO Rician channel capacity. For the sake of completeness,

[1] This model can be used to approximate the case when the correlation between antenna elements are close to each other.

we will present the closed-form expression for the capacity of Rician channels in the following.

We define $P = \Omega/(\sigma^2 t)$ as the transmit SNR per branch, $a = 1 - \zeta$ and $b = 1 + (t-1)\zeta$. We further denote t different $t \times t$ matrices by $\mathbf{\Psi}(k),\ k = 1, \cdots, t$ with elements given by

$$
[\mathbf{\Psi}(k)]_{i,j}
= \begin{cases}
(-1)^{j-1} \int_0^\infty \ln(1+Py) y^{r-i+j-1} e^{-y/a}\, dy, & i = 1, \cdots, t;\ j = 1, \cdots, t-1 \text{ and } j = k \\
(-1)^{j-1} a^{r-i+j} \Gamma(r-i+j), & i = 1, \cdots, t;\ j = 1, \cdots, t-1 \text{ and } j \neq k \\
\int_0^\infty \ln(1+Py) y^{r-i} e^{-y/b}\, dy, & i = 1, \cdots, t;\ j = t \text{ and } k = t \\
b^{r-i+1} \Gamma(r-i+1) & i = 1, \cdots, t;\ j = t \text{ and } k \neq t.
\end{cases}
\tag{4.10}
$$

Note also that the integrals in (4.10) can be evaluated directly from the complementary incomplete gamma function and hence no numerical integrations are needed [35]. Finally, the capacity of the MIMO Rician channel can be shown equal to [36]

$$
C = \frac{\Gamma(t) \sum_{k=1}^{t} \det(\mathbf{\Psi}(k))}{\ln(2) a^{r(t-1)} b^r \left(\frac{1}{b} - \frac{1}{a}\right)^{t-1} \prod_{i=1}^{t} \Gamma(r-i+1)\Gamma(t-i+1)}. \tag{4.11}
$$

4.2 Asymptotic Capacity of Rician Channel

In this section, we analyze the asymptotic capacities of MIMO Rician channels. We first relate the SNR to the bit-energy-to-noise-spectral-density ratio at the receiver, i.e.,

$$
\frac{E_b}{N_0} = \frac{rtP}{C} \tag{4.12}
$$

where rtP relates to the total received SNR at the receiver and C represents the maximum information flow achieved.

4.2.1 Low SNR Region

The minimum E_b/N_0 required for a reliable communication can be obtained using [68]

$$\left(\frac{E_b}{N_0}\right)_{\min} = \lim_{P\to 0}\frac{rtP}{C} = rt\lim_{P\to 0}\frac{1}{\partial C/\partial P} = \ln(2) = -1.59 \text{ (dB)} \tag{4.13}$$

where the third equality is found based on (4.11). This result is consistent with the so-called lower bound E_b/N_0 for communication systems in AWGN channel explicated by Shannon capacity [84]. We also observe that the minimum E_b/N_0 is independent of the Rician factor K.

4.2.2 High SNR Region

As P approach infinity, the slope of the channel capacity with respect to SNR is found as

$$\lim_{P\to\infty}\frac{C}{10\log P} = \frac{t\log_2(10)}{10} = 0.33t \text{ (bps/Hz/dB)}, \tag{4.14}$$

where the first equality is obtained based on (4.11). The result indicates that every 3 dB increase in SNR can provide an extra t bps/Hz of capacity at the high SNR region. We therefore conclude that the capacity of MIMO Rician channels increases linearly with t in the high SNR region, irrespective of the Rician factor.

4.2.3 Capacity Loss of Rician Channels

Let C_{Ray} denote the capacity for i.i.d. Rayleigh channels ($K = 0$) and C_{Ric} denote the one for Rician channels. Applying

$$\int_0^\infty \ln(1+Py)y^{n-1}e^{-y/c}\,dy = c^n\int_0^\infty \ln(1+Pcy)y^{n-1}e^{-y}\,dy \tag{4.15}$$

and

$$\lim_{P\to\infty} \ln(1+Pcy) \approx \ln(Pcy) = \ln(P) + \ln(c) + \ln(y) \tag{4.16}$$

to (4.10), the capacity loss of Rician channels relative to i.i.d. Rayleigh channels at high SNR can be found as

$$C_{\text{loss}} = \lim_{P\to\infty}(C_{\text{Ray}} - C_{\text{Ric}}) = -\frac{(t-1)\ln(a)+\ln(b)}{\ln(2)} = t\log_2(1+K) - \log_2(1+tK) \tag{4.17}$$

where C_{Ray} has been calculated from [37, eq.(29)]. Clearly, the capacity loss is independent of the number of receive antennas. Defining the capacity loss of Rician channels per transmit antenna as $C_{\text{loss/Tx}}$, we have

$$C_{\text{loss/Tx}} = \log_2(1+K) - \frac{1}{t}\log_2(1+tK). \tag{4.18}$$

Fig. 4.1 and Fig. 4.2 plot the capacity loss of MIMO Rician channels per transmit antenna at high SNR values versus the Rician factor and the number of transmit antennas, respectively. It can be observed that the capacity loss compared to an i.i.d. Rayleigh channel increases with both the Rician factor K and the number of transmit antennas t. Also, the loss approaches the upper-bound $\log_2(1+K)$ as t goes to infinity. Note also that as K approaches infinity, the channel degenerates to a non-faded AWGN channel and the analyses in Section 4.2.2 and 4.2.3 do not hold anymore.

4.3 Results

Simulations are performed to verify our analytical method that evaluates the capacity of MIMO Rician channels. In Fig. 4.3, we plot the capacity for the case $(t = 3, r = 3)$ with different Rician factors. The results found using the numeri-

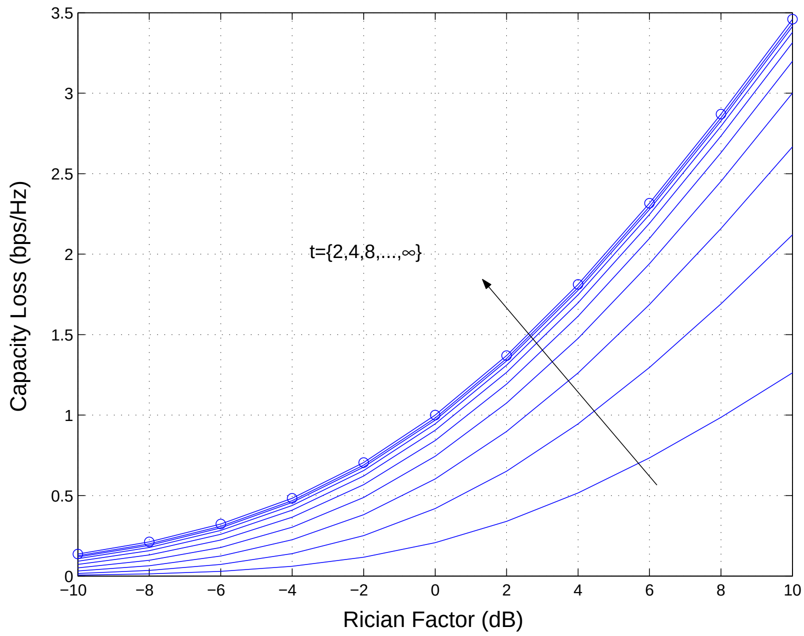

Figure 4.1: Loss of channel capacity per transmit antenna at high SNR values in MIMO Rician channels relative to i.i.d. Rayleigh channels. The upper bound of the loss is represented by circles.

cal integration method in [37] are also plotted for comparison. From the curves, it can be observed that the results produced by the three different methods are very similar. Thus, we conclude that the methods developed for computing the capacity of correlated MIMO Rayleigh channels (under intraclass correlation model) can be applied to evaluate the capacity of MIMO Rician channels. From the graphs, it is apparent that an increase in the Rician factor produces a larger capacity loss compared to the i.i.d. Rayleigh channels. But the slopes of the capacity curves with respect to normalized SNR are the same at high SNR values, irrespective of the Rician factor.

Fig. 4.4 plots the capacity of MIMO Rician channels with $K = 3$ dB. Again, the capacities found using our analytical method, simulations and the numerical integration method in [37] are very consistent. As expected, when the number of transmit or receive antennas increases, higher capacity gain is accomplished. More-

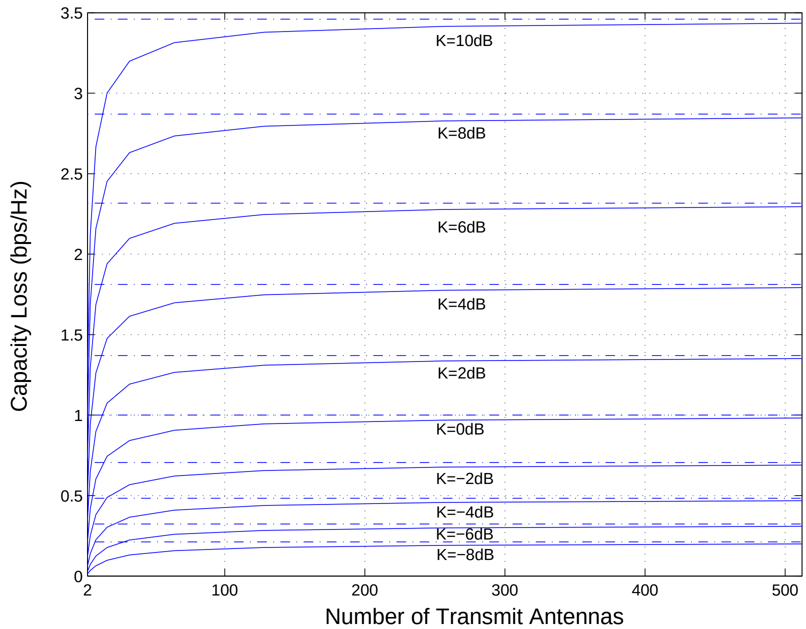

Figure 4.2: Loss of channel capacity per transmit antenna at high SNR values in MIMO Rician channels relative to i.i.d. Rayleigh channels. The upper bounds of the loss are displayed with dashed-dotted lines.

over, for a fixed number of transmit antennas ($t = 3$) and at high SNR values, the slopes of the curves corresponding to different number of receive antennas remain the same. This phenomenon is also consistent with the result found in (4.14).

4.4 Summary

In this chapter, we have shown that the capacity of MIMO Rician channels can be well approximated by that of correlated-Rayleigh MIMO channels under an intra-class correlated model. Based on the approximation, we have derived a closed-form expression for the MIMO Rician channel capacity. Moreover, the analytical results are found to be very close with those obtained using simulation.

In addition, based on the expression for the MIMO Rician channel capacity, we have been able to study the asymptotic behavior of the channel capacity. We find

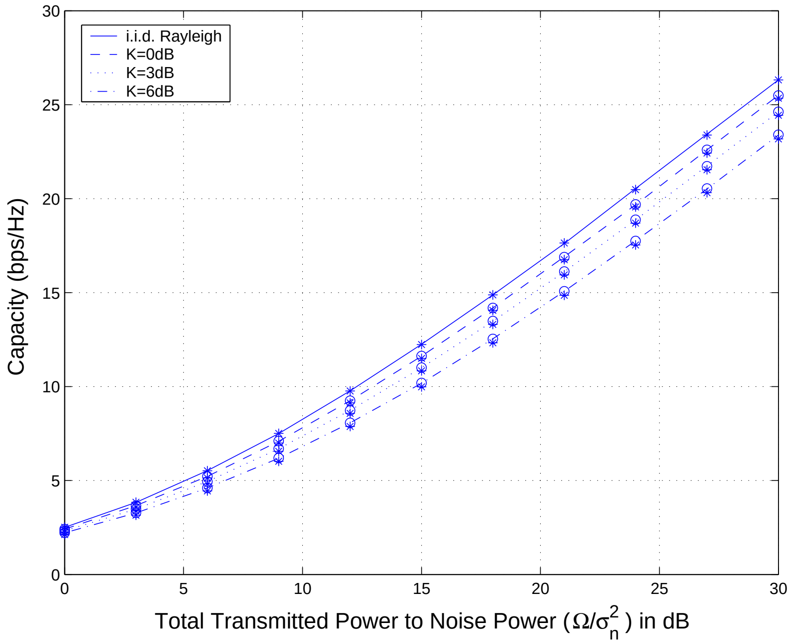

Figure 4.3: Capacity of MIMO Rician channels with ($t = 3$, $r = 3$). (Analytical results are shown with asterisks; simulated results are represented by lines; and the numerical integration results in [37] are displayed with circles.)

that at low SNR region, the minimum E_b/N_0 required for a reliable communication equals -1.59 dB and is independent of the Rician factor K. At the high SNR region, for every 3 dB increase in SNR, an extra t bps/Hz of capacity will be achieved. We can therefore conclude that the capacity of MIMO Rician channels increases linearly with t in the high SNR region, irrespective of the Rician factor. Finally, compared to an i.i.d. Rayleigh channel, the capacity loss of a MIMO Rician channel is found to increase with both the Rician factor K and the number of transmit antennas t. But the loss is upper-bounded by $\log_2(1 + K)$ as t goes to infinity.

This chapter concludes the study of spatial-multiplexing-based MIMO system. In the next chapter, we will look into the diversity-based MIMO systems. In particular, we will investigate thoroughly the performance of diversity-based MIMO systems with antenna selection over an intra-class correlated channel.

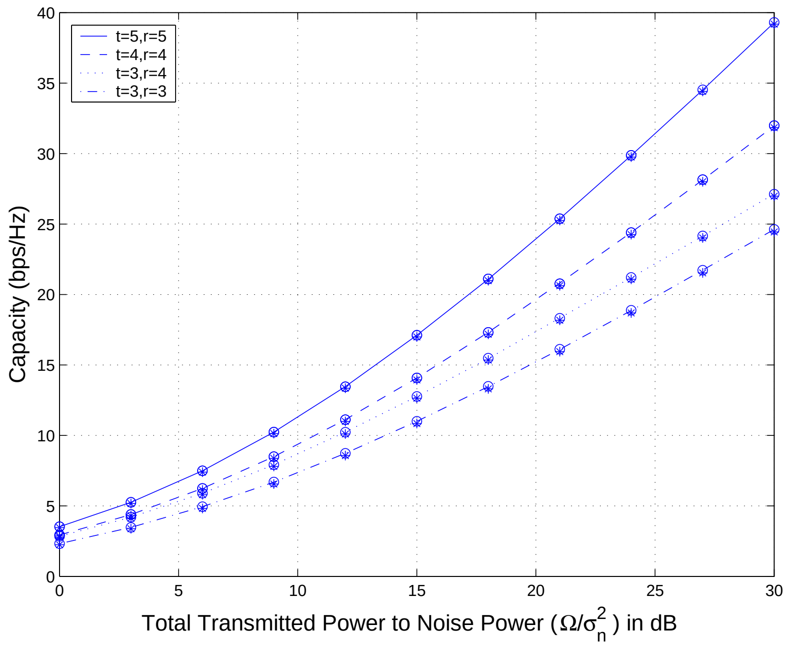

Figure 4.4: Capacity of MIMO Rician channels with $K = 3$ dB. (Analytical results are shown with asterisks; simulated results are represented by lines; and the numerical integration results in [37] are displayed with circles.)

Chapter 5

MIMO Diversity-Based Systems with Antenna Selection

In the last three chapters, we have studied the error performance and capacity of spatial-multiplexing MIMO systems. In this chapter, we aim to investigate thoroughly the performance of diversity-based MIMO systems with antenna selection over a specifically correlated Rayleigh fading channel, namely an intra-class correlated channel. In this model, the correlations between any pair of correlated antenna elements are equal. It is used to describe the scenario when the antenna elements are closely placed with correlations between any two elements almost identical.

In our study, for the transmit-antenna/receive-antenna selection (TAS/RAS) scheme, we assume that all the available receive/transmit antennas are used at the receive/transmit side, whereas only one single transmit/receive antenna will be selected for transmission/reception with an aim to maximizing the received SNR. We will derive the exact BERs of MIMO systems under an intra-class correlated Rayleigh channel with three different selection schemes, namely TAS, RAS and the full complexity (FC) schemes. Then, the asymptotic SNR degradations due to correlation are quantified in closed forms expressed in terms of the correlation coefficient and the number of antennas. We also compare the SNR requirements of the different selection schemes at low BER regions. Further, we evaluate the diversity orders of the three schemes and their relationships with the numbers of transmit and receive antennas. Finally, we verify and compare the theoretical BER performances of the three antenna selection schemes using computer simulations. We conclude that the TAS scheme, in which the transmit side is provided with a small amount of feedback information from the receiver, can achieve the best performance.

The rest of this chapter is organized as follows. We briefly describe the models of MIMO systems with antenna selection in Section 5.1. The analytical performances of the three different antenna selection schemes, namely TAS, RAS and FC, under an intra-class correlated Rayleigh fading channel are then derived and compared in Section 5.2. The diversity orders and the SNR degradations due to correlation are also investigated in the same section. Finally, in Section 5.3, we plot and discuss the analytical and simulation results.

5.1 System Model

Consider a MIMO diversity system with t transmit antennas and r receive antennas. We define $\boldsymbol{H}$ as the channel matrix with element h_{ij} representing the channel impulse response between the jth ($j = 1, \ldots, t$) transmit antenna and the i-th ($i = 1, 2, \ldots, r$) receive antenna. In our study, it is assumed that the channel matrix $\boldsymbol{H}$ is known at the receiver, but not at the transmitter. We also assume that the channel is random, quasi-static, frequency independent and that the transmitted signals are corrupted by complex additive white Gaussian noise. At the receiver side, the incoming signal will be processed with an aim to recovering the received data symbols. Denote the total transmit signal power by P and the channel noise

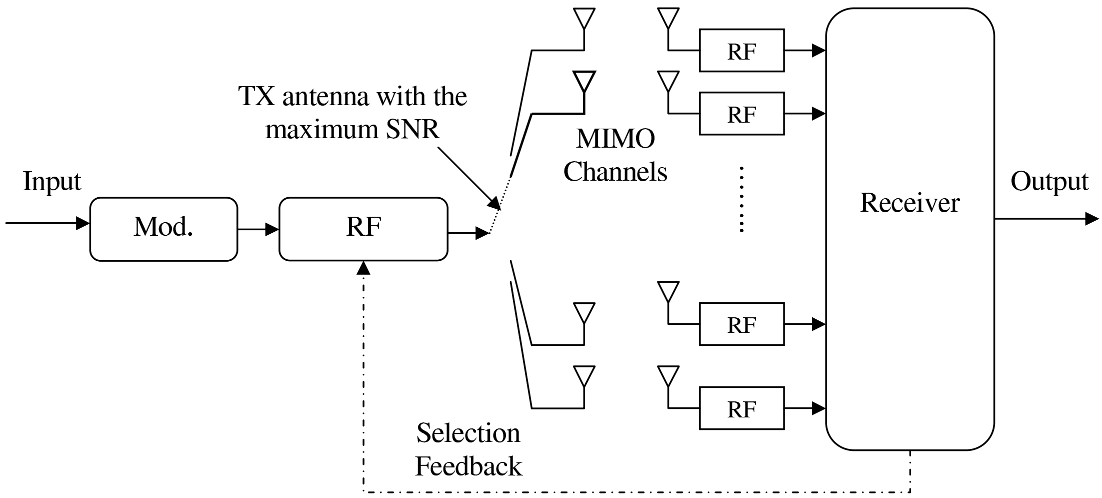

Figure 5.1: A MIMO system with transmit-antenna selection (RF: radio frequency components).

power by σ^2. We define

$$\lambda_o = \frac{P}{\sigma^2} \tag{5.1}$$

as the transmit signal-to-noise ratio (SNR). In the following, we briefly derive the output SNR at the receiver for each of the TAS, RAS and FC schemes.

5.1.1 Transmit-Antenna Selection (TAS)

Fig. 5.1 depicts the architecture of a MIMO system using TAS. In the TAS system, some information from the receiver side is feedback to the transmitter for selecting an appropriate RF chain at the transmit end. Here, we assume that there is no error or delay for the flow of such feedback information. Also, unlike RAS which requires orthogonality between signals from different transmit antennas, TAS does not have such a mandatory requirement because only one transmit antenna is active during data transmission. Corresponding to the jth ($j = 1, \ldots, t$) transmit antenna, we define

$$\boldsymbol{\nu}_j = \sum_{i=1}^{r} |h_{ij}|^2 \tag{5.2}$$

where $\boldsymbol{\nu}_j$ denotes the j-th element of $\boldsymbol{\nu}$. Then the transmit antenna that maximizes the received SNR is selected as the target in the TAS scheme. Alternatively, the kth transmit antenna will be chosen where

$$k = \arg\max_j \{\boldsymbol{\nu}_j\}. \tag{5.3}$$

Hence, for the TAS scheme, the (maximized) output SNR at the receiver is given by

$$\lambda_{\text{TAS}} = \lambda_o \boldsymbol{\nu}_k. \tag{5.4}$$

5.1.2 Receive-Antenna Selection (RAS)

Figure 5.2 shows the architecture of a MIMO system using RAS. In order to separate the signals radiated by different transmit antennas on the receiver side, a modulation approach with transmit diversity must be used. In general, modulations using orthogonal pulses for different transmit antennas are adopted because the orthogonality allows the receiver to separate the contributions of different antennas and to apply maximum ratio combining. Corresponding to the orthogonal signals, matched filters are used at the receiver. For example, in a code-division-multiple-access system, different orthogonal spreading sequences should be assigned for different transmit antennas. For the ith $(i = 1, \ldots, r)$ receive antenna, we define

$$\boldsymbol{\mu}_i = \sum_{j=1}^{t} |h_{ij}|^2 \tag{5.5}$$

where $\boldsymbol{\mu}_i$ denotes the i-th element of $\boldsymbol{\mu}$. In the RAS scheme, only the receive antenna with the maximum SNR is selected for use in the reception. In other words, the kth

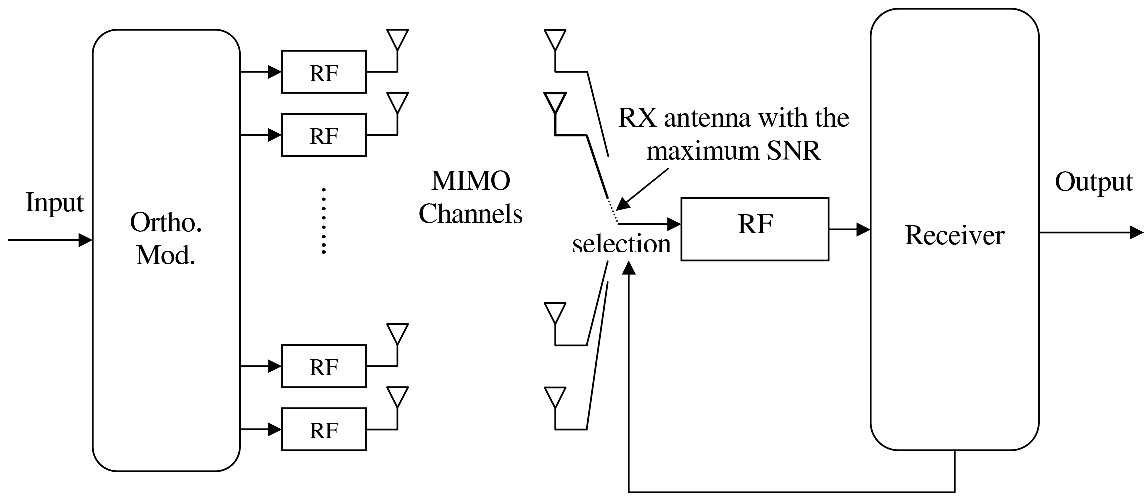

Figure 5.2: A MIMO system with receive-antenna selection (RF: radio frequency components).

receive antenna is chosen where

$$k = \arg\max_i \{\boldsymbol{\mu}_i\}. \tag{5.6}$$

Finally, for the RAS scheme, the (maximized) output SNR at the receiver is given by [1]

$$\lambda_{\text{RAS}} = \frac{\lambda_o}{t}\boldsymbol{\mu}_k. \tag{5.7}$$

5.1.3 Full Complexity (FC)

In the FC scheme, all available transmit antennas and receive antennas will be used. Moreover, the received signal powers from all sub-channels will be combined together. The post-processing SNR at the receiver is therefore given by

$$\lambda_{\text{FC}} = \frac{\lambda_o}{t}\sum_{j=1}^{t}\boldsymbol{\nu}_j = \frac{\lambda_o}{t}\sum_{j=1}^{t}\sum_{i=1}^{r}|h_{ij}|^2, \tag{5.8}$$

[1]The total transmit power P is equally distributed to the t transmit antennas. Thus the transmit SNR per branch equals λ_o/t.

or equivalently,

$$\lambda_{\mathrm{FC}} = \frac{\lambda_o}{t}\sum_{i=1}^{r}\boldsymbol{\mu}_i = \frac{\lambda_o}{t}\sum_{i=1}^{r}\sum_{j=1}^{t}|h_{ij}|^2. \tag{5.9}$$

5.2 Performance of MIMO systems with antenna selection

From the results in the previous section, it can be observed that the performances of the MIMO systems with antenna selection are determined by the distributions of the output SNRs, which in turn are governed by the characteristics of the channel matrix $\boldsymbol{H}$. In our study, we consider a MIMO correlated-Rayleigh channel, where correlation exists either at the transmitter or at the receiver, but not at both sides [31,86]. Moreover, we use the intra-class correlation model to describe the correlation at the transmit side or the receive side [87]. With such assumptions, we can denote the covariance matrix of $\boldsymbol{H}$ by $\boldsymbol{\Phi}$, in which the elements are readily shown equal to

$$[\boldsymbol{\Phi}]_{i,j} = \begin{cases} 1, & \text{if} \quad i = j \\ \rho, & \text{if} \quad i \neq j \end{cases} \tag{5.10}$$

where $\rho \in (0, 1)$ denotes the correlation coefficient between any pair of transmit antennas or receive antennas. In addition, based on the properties of complex normal variables, it can be shown that the elements of $\boldsymbol{\nu}$ and $\boldsymbol{\mu}$ follow multivariate Gamma distributions [50]. Incidentally, for a conventional diversity system over a Nakagami-m fading channel, the instantaneous SNRs of the branches are also found to be multivariate gamma variables. Thus, we can envisage that the analysis of MIMO systems with antenna selection over an intra-class correlated Rayleigh fading channel is similar to that of a diversity system over an equally correlated Nakagami-m fading channel (see Appendix 5 for details).

In the following, we will derive and compare the performance of FC, TAS and RAS schemes when correlation exists at the transmitter and receiver, respectively. We will also evaluate the diversity order for such systems. As an illustration, we apply BPSK as the modulation/demodulation technique. Systems using other modulation/demodulation can be easily evaluated following similar procedures.

5.2.1 Correlation at the Transmitter

Firstly, we consider the case where correlation exists at the transmit side. The performance of TAS, RAS and FC schemes will be investigated based on the system model in Section 5.1. Since the analysis of FC scheme can be used to provide a foundation for the study of TAS and RAS schemes, we begin with the performance evaluation of FC scheme.

5.2.1.1 Performance of FC Scheme

To calculate the probability density function (p.d.f.) of the output SNR for the FC scheme, we re-write (5.8), the FC output SNR, as

$$\lambda_{\text{FC-TxCor}} = \frac{\lambda_o}{t}\sum_{j=1}^{t}\boldsymbol{\nu}_j \triangleq \frac{\lambda_o(1-\rho)}{t}\,x. \tag{5.11}$$

Since the elements of $\boldsymbol{\nu}$ are correlated multivariate Gamma variables, we can apply (5.55) in Appendix 5, namely the result characterizing the output SNR of the maximal ratio combiner (MRC) for a diversity system over an equally correlated Nakagami-m fading channel, to determine the p.d.f. of x. It can be readily shown that the p.d.f. of x is equal to

$$f_{\text{FC-TxCor}}(x) = \left(\frac{1-\rho}{1+(t-1)\rho}\right)^{r}\sum_{k=0}^{\infty}\binom{r+k-1}{r-1}\left(\frac{t\rho}{1+(t-1)\rho}\right)^{k}\frac{x^{rt+k-1}e^{-x}}{\Gamma(rt+k)} \tag{5.12}$$

where $\Gamma(\cdot)$ represents the Gamma function.

Assuming QPSK modulation is used, the BER can be evaluated using [76, eq.(14-3-4)]

$$P_e = \int_0^\infty Q(\sqrt{2u}) f_\lambda(u)\, du \tag{5.13}$$

where $Q(x)$ is the Q-function defined as (2.49) in Appendix 2B, and $f_\lambda(u)$ denotes the p.d.f. of the output SNR. Using (5.11), (5.12) and the integration results in Appendix 2C, the BER expression in (5.13) can be re-written as

$$\begin{aligned} P_{e,\text{FC-TxCor}} = & \left(\frac{1-\rho}{1+(t-1)\rho}\right)^r \\ & \times \sum_{k=0}^{\infty} \binom{r+k-1}{r-1} \left(\frac{t\rho}{1+(t-1)\rho}\right)^k J(rt+k, 1, 2\lambda_o(1-\rho)/t) \end{aligned} \tag{5.14}$$

where $J(n, a, b)$ is defined in (2.59). In general, with the p.d.f. of the FC output SNR available, the BER or symbol error rate (SER) for different modulation schemes, e.g., M-ary PSK and QAM, can be readily obtained by modifying (5.13) and using the results in [87].

At high SNR region, the BER shown in (5.14) is dominated by the first term in the summation series, i.e., the term with $k = 0$. Under a such condition, the BER can be approximated by

$$P_{e,\text{ FC-TxCor}} \approx \left(\frac{1-\rho}{1+(t-1)\rho}\right)^r J(rt, 1, 2\lambda_o(1-\rho)/t). \tag{5.15}$$

Next, considering an independent and identically distributed (i.i.d.) Rayleigh fading channel, we denote the transmit SNR by $\lambda_{o,\text{ind}}$ and the corresponding BER of the FC scheme by $P_{e,\text{ FC-ind}}$. When SNR is large, we consider the case when the BERs for i.i.d. and correlated fading channels are identical, i.e.,

$$P_{e,\,\text{FC-ind}} = P_{e,\,\text{FC-TxCor}}. \tag{5.16}$$

Using the approximation in (2.60), we can show that at high SNR region, the asymptotic SNR degradation of FC scheme due to transmit correlation equals

$$\Delta\lambda_{o,\text{FC-TxCor}}\ (\text{dB}) = 10\log\left(\frac{\lambda_o}{\lambda_{o,\text{ind}}}\right) = 10\log\left(\frac{1}{1-\rho}\right) - \frac{1}{t}10\log\left(\frac{1-\rho+t\rho}{1-\rho}\right). \tag{5.17}$$

It can also be concluded that when the number of transmit antennas (t) is sufficiently large, the asymptotic SNR degradation converges to the upper bound given by $10\log(1/(1-\rho))$.

5.2.1.2 Performance of TAS Scheme

We re-write (5.4) as

$$\lambda_{\text{TAS-TxCor}} = \lambda_o \boldsymbol{\nu}_k \triangleq \lambda_o(1-\rho)\, x \tag{5.18}$$

where k is determined by (5.3). Since the elements of $\boldsymbol{\nu}$ are correlated multivariate Gamma variables, the performance of TAS scheme with transmit correlation can be obtained by referencing to that of a diversity system using a selective combiner (SC) under an equally correlated Nakagami-m fading, which is detailed in Appendix 5. Therefore, using (5.68), it can be shown that the p.d.f. of x equals

$$f_{\text{TAS-TxCor}}(x) = \left[\frac{1-\rho}{1+(t-1)\rho}\right]^r \frac{e^{-tx}}{\Gamma(r)} \sum_{k=0}^{\infty} x^{rt+k-1}[(rt+k)c_k(t,r,\rho) - tc_{k-1}(t,r,\rho)] \tag{5.19}$$

where $c_k(t,r,\rho)$ is defined as in (5.66) and (5.69) .

Combining (5.13), (5.18), (5.19) and (2.59), the analytical BER of TAS scheme with BPSK modulation can be found as

$$\begin{aligned}P_{e,\text{TAS-TxCor}} = &\left[\frac{1-\rho}{1+(t-1)\rho}\right]^r \frac{1}{\Gamma(r)} \sum_{k=0}^{\infty} [(rt+k)c_k(t,r,\rho) - tc_{k-1}(t,r,\rho)] \\ &\times \frac{\Gamma(rt+k)}{t^{rt+k}} J(rt+k, t, 2\lambda_o(1-\rho)).\end{aligned} \tag{5.20}$$

Moreover, at high SNR region, the BER is well approximated by the first term in the summation series in (5.20), i.e.,

$$P_{e,\text{TAS-TxCor}} \approx \left(\frac{1-\rho}{1+(t-1)\rho}\right)^r \frac{(rt)!}{t^{rt}(r!)^t} J(rt, t, 2\lambda_o(1-\rho)). \tag{5.21}$$

Applying (2.61) into (5.21) and following similar procedures as in the previous section, it can be readily shown that the SNR degradation of TAS due to transmit correlation equals

$$\Delta\lambda_{o,\text{TAS-TxCor}}\ (\text{dB}) = 10\log\left(\frac{1}{1-\rho}\right) - \frac{1}{t} 10\log\left(\frac{1-\rho+t\rho}{1-\rho}\right), \tag{5.22}$$

which is identical to that of the FC scheme, as shown in (5.17).

Next, we compare the asymptotic performance of TAS and FC when the channels are intra-class correlated. Assume that the correlation coefficients for both schemes are identical and that $\lambda_{o,\text{TAS}}$ and $\lambda_{o,\text{FC}}$ are the transmit SNRs required to obtain the same BERs for TAS and FC, respectively. Comparing the results in (5.15) and (5.21), it can be seen that at low BER region, TAS outperforms FC by

$$\Delta\lambda_{o,\text{TAS}-\text{FC}}\ (\text{dB}) = 10\log\left(\frac{\lambda_{o,\text{FC}}}{\lambda_{o,\text{TAS}}}\right) = 10\log t + \frac{1}{r}10\log(r!) - \frac{1}{rt}10\log(rt)!\ . \tag{5.23}$$

5.2.1.3 Performance of RAS Scheme

We define

$$\lambda_i = \frac{\lambda_o}{t}\boldsymbol{\mu}_i, \quad i = 1, \ldots, r \tag{5.24}$$

which is the received SNR at the ith receive antenna. Since correlation exists only at the transmit side, the received SNRs at the receive antennas are i.i.d. variables. For each λ_i, its distribution is equivalent to that of the FC scheme with one receive antenna. Further defining

$$\lambda_i = \frac{\lambda_o(1-\rho)}{t}\, z \tag{5.25}$$

and using the results in (5.12), the p.d.f. of z is readily shown equal to

$$f(z) = \left(\frac{1-\rho}{1+(t-1)\rho}\right) e^{-z} \sum_{k=0}^{\infty} \left(\frac{t\rho}{1+(t-1)\rho}\right)^k \frac{z^{t+k-1}}{\Gamma(t+k)}. \tag{5.26}$$

Integrating (5.26), the cumulative distribution function (c.d.f.) of z can be found as

$$F(z) = \left(\frac{1-\rho}{1+(t-1)\rho}\right) \sum_{k=0}^{\infty} \left(\frac{t\rho}{1+(t-1)\rho}\right)^k \frac{\gamma(t+k, z)}{\Gamma(t+k)} \tag{5.27}$$

where $\gamma(\cdot,\cdot)$ denotes the incomplete Gamma function (see Appendix 2A). Since both t and k are non-negative integers, we can substitute the expression of the incomplete Gamma function shown in (5.59) into (5.27) and obtain

$$F(z) = e^{-z} \sum_{k=0}^{\infty} \frac{z^{t+k}}{(t+k)!} \left[1 - \left(\frac{t\rho}{1+t\rho-\rho}\right)^{k+1}\right]. \tag{5.28}$$

Re-write the output SNR for the RAS scheme, i.e., (5.7), as

$$\lambda_{\text{RAS-TxCor}} = \frac{\lambda_o}{t}\boldsymbol{\mu}_k \triangleq \frac{\lambda_o(1-\rho)}{t}\, x \tag{5.29}$$

where k is determined by (5.6). Then applying the knowledge of order statistics

[13], the c.d.f. of the output SNR for the RAS scheme is found to be

$$F(\lambda_{\text{RAS-TxCor}}) = [F(\lambda_i)]^r \tag{5.30}$$

where $F(\lambda_i)$ denotes the c.d.f. of λ_i. Combining (5.25), (5.28), (5.29) and (5.30), the c.d.f. of x can be readily shown equal to

$$F(x) = e^{-rx} \sum_{k=0}^{\infty} a_k(r,t,\rho) x^{rt+k} \tag{5.31}$$

where

$$a_k(r,t,\rho) = \sum_{\substack{(i_1,\cdots,i_r) \\ 0 \leq i_1 \cdots \leq i_r \leq k \\ i_1+\cdots+i_r=k}} \binom{r}{l_1,\ldots,l_q} \prod_{j=1}^{r} \frac{1-\left(\frac{t\rho}{1+t\rho-\rho}\right)^{i_j+1}}{(t+i_j)!} \tag{5.32}$$

with $(l_1,\ldots,l_q)$ representing the number of equal elements in $(i_1,\ldots,i_L)$ (see Appendix 5 for an example). The p.d.f. of x can then be obtained using

$$f(x) = \frac{dF(x)}{dx} = e^{-rx} \sum_{k=0}^{\infty} ((rt+k)a_k(r,t,\rho) - ra_{k-1}(r,t,\rho)) x^{rt+k-1} \tag{5.33}$$

with $a_{-1}(r,t,\rho) = 0$. Finally, using (5.13), (5.29) and (5.33), the analytical BER of the RAS scheme with BPSK modulation can be readily shown equal to

$$P_{e,\text{RAS-TxCor}} = \sum_{k=0}^{\infty} \frac{\Gamma(rt+k)}{r^{rt+k}} ((rt+k)a_k(r,t,\rho) - ra_{k-1}(r,t,\rho)) J(rt+k, r, 2\lambda_o(1-\rho)/t). \tag{5.34}$$

Furthermore, at high SNR region, the BER can be approximated by the first term in (5.34), i.e.,

$$P_{e,\text{RAS-TxCor}} \approx \left(\frac{1-\rho}{1-(t-1)\rho}\right)^r \frac{(rt)!}{r^{rt}(t!)^r} J(rt, r, 2\lambda_o(1-\rho)/t) \tag{5.35}$$

in which we have made the following substitution

$$a_0(r,t,\rho) = \left(\frac{1-\rho}{1-(t-1)\rho}\right)^r \frac{1}{(t!)^r}. \tag{5.36}$$

Following similar procedures as used in the FC and TAS schemes, it is readily shown that the SNR degradation of RAS due to correlation is equal to

$$\Delta\lambda_{o,\text{RAS-TxCor}}\ (\text{dB}) = 10\log\left(\frac{1}{1-\rho}\right) - \frac{1}{t}10\log\left(\frac{1-\rho+t\rho}{1-\rho}\right). \tag{5.37}$$

Comparing (5.37) with the results for the FC and TAS schemes, we conclude that the asymptotic SNR degradations due to correlation at the transmit side are identical for FC, TAS and RAS schemes.

We further compare (5.35) and (5.15), and observe that at low BER region, FC outperforms RAS by

$$\Delta\lambda_{o,\mathrm{FC-RAS}}\ (\text{dB}) = \frac{1}{rt}10\log(rt!) - \frac{1}{t}10\log(t!). \tag{5.38}$$

Also, for a finite r and a very large t, applying Stirling's formula $n! \approx \sqrt{2\pi}e^{-n}n^{n+1/2}$ [61, eq.(1.11)] shows that (5.38) is upper-bounded by $10\log r$.

5.2.2 Correlation at the Receiver

Based on the results in the previous section where correlation exists at the transmit side, we can easily deduce the performances of FC, TAS and RAS schemes when correlation exists at the receive side. In this section, we will simply present the results without giving too much detail on the derivations.

5.2.2.1 Performance of FC Scheme

We make use of (5.9) to calculate the output SNR of FC scheme. In (5.9), the elements of $\boldsymbol{\mu}$ follow correlated multivariate Gamma distribution. Following the procedures as in Section 5.2.1.1, a BER expression similar to (5.14) will be obtained, except that the roles of r and t need to be exchanged and that λ_o has to be replaced by $r\lambda_o/t$. In other words, the BER expression becomes

$$\begin{aligned} P_{e,\text{FC-RxCor}} = &\left(\frac{1-\rho}{1+(r-1)\rho}\right)^t \\ &\times \sum_{k=0}^{\infty} \binom{t+k-1}{t-1} \left(\frac{r\rho}{1+(r-1)\rho}\right)^k J(tr+k, 1, 2\lambda_o(1-\rho)/t). \end{aligned} \tag{5.39}$$

Moreover, at high SNR region, the analytical BER can be approximated as

$$P_{e,\text{ FC-RxCor}} \approx \left(\frac{1-\rho}{1+(r-1)\rho}\right)^t J(tr, 1, 2\lambda_o(1-\rho)/t) \tag{5.40}$$

and the asymptotic SNR loss due to receive correlation can be readily derived as

$$\Delta\lambda_{o,\text{FC-RxCor}}\ (\text{dB}) = 10\log\left(\frac{1}{1-\rho}\right) - \frac{1}{r}10\log\left(\frac{1-\rho+r\rho}{1-\rho}\right). \tag{5.41}$$

5.2.2.2 Performance of TAS Scheme

The analysis in this case is similar to that in Section 5.2.1.3, except that the roles of t and r are exchanged and that λ_o is replaced by $r\lambda_o$. Thus the BER can be shown equal to

$$P_{e,\text{TAS-RxCor}} = \sum_{k=0}^{\infty} \frac{\Gamma(tr+k)}{t^{tr+k}}((tr+k)a_k(t,r,\rho) - ta_{k-1}(t,r,\rho))J(tr+k, t, 2\lambda_o(1-\rho)). \tag{5.42}$$

Further, at high SNR region, the analytical BER can be approximated as

$$P_{e,\text{TAS-RxCor}} \approx \left(\frac{1-\rho}{1-(r-1)\rho}\right)^t \frac{(tr)!}{t^{tr}(r!)^t} J(tr, t, 2\lambda_o(1-\rho)) \tag{5.43}$$

and the SNR degradation due to receive correlation can be shown to be the same as that for the FC scheme, i.e., the expression given by (5.41). Judging from the results in (5.43) and (5.40), it can also be deduced that at low BER region, TAS outperforms FC by the expression shown in (5.23). In other words, TAS outperforms FC with the same value when correlation exists at either the transmit end or the receive end.

5.2.2.3 Performance of RAS Scheme

The analysis of RAS scheme when correlation exists at the receive side is similar to that of TAS scheme with transmit correlation. All we need are to exchange the role of r and t, and to replace λ_o with λ_o/t. Therefore, making the aforementioned changes to (5.20), the analytical BER of RAS scheme can be obtained as

$$\begin{aligned} P_{e,\text{RAS-RxCor}} &= \left[\frac{1-\rho}{1+(r-1)\rho}\right]^t \frac{1}{\Gamma(t)} \\ &\times \sum_{k=0}^{\infty} [(tr+k)c_k(r,t,\rho) - rc_{k-1}(r,t,\rho)] \frac{\Gamma(tr+k)}{r^{tr+k}} J(tr+k, r, 2\lambda_o(1-\rho)/t). \end{aligned} \tag{5.44}$$

Moreover, at high SNR region, the BER expression can be approximated as

$$P_{e,\text{RAS-RxCor}} \approx \left(\frac{1-\rho}{1+(r-1)\rho}\right)^t \frac{(tr)!}{r^{tr}(t!)^r} J(tr, r, 2\lambda_o(1-\rho)/t) \tag{5.45}$$

and the SNR degradation due to receive correlation is found to be the same expression given in (5.41). We therefore conclude that with receive correlation, the asymptotic SNR degradations are the same for FC, TAS and RAS schemes. Furthermore, when we compare the results in (5.45) and (5.40), we observe that at low BER region, FC is superior to RAS with the same value as that shown (5.38). Alternatively, we can conclude that FC outperforms RAS with the same value when correlation exists at either the transmit end or the receive end.

5.2.3 Diversity Order

In this section, we investigate the diversity order of the MIMO systems employing FC, TAS and RAS schemes. The diversity order, denoted by D_e, is defined as the absolute value of the slope of the error probability curve plotted on a log-log scale at high SNR region [76], i.e.,

$$D_e \triangleq - \lim_{\lambda_o \to +\infty} \frac{\log(P_e)}{\log(\lambda_o)}. \tag{5.46}$$

Substituting the approximated BERs obtained at the high SNR region in the previous sections into (5.46) and by applying (2.61), we find that the diversity orders for all cases are identical and are equal to tr. The results conclude that the diversity orders of MIMO systems employing FC, TAS and RAS schemes are the same and are not affected by the correlation among the transmit antennas, or the correlation among the receive antennas.

5.3 Results and Discussions

5.3.1 Asymptotic SNR Degradation

Recall that when transmit correlation exists, the asymptotic SNR degradations of FC, TAS and RAS schemes are identical (refer to (5.17), (5.22) and (5.37)) and the

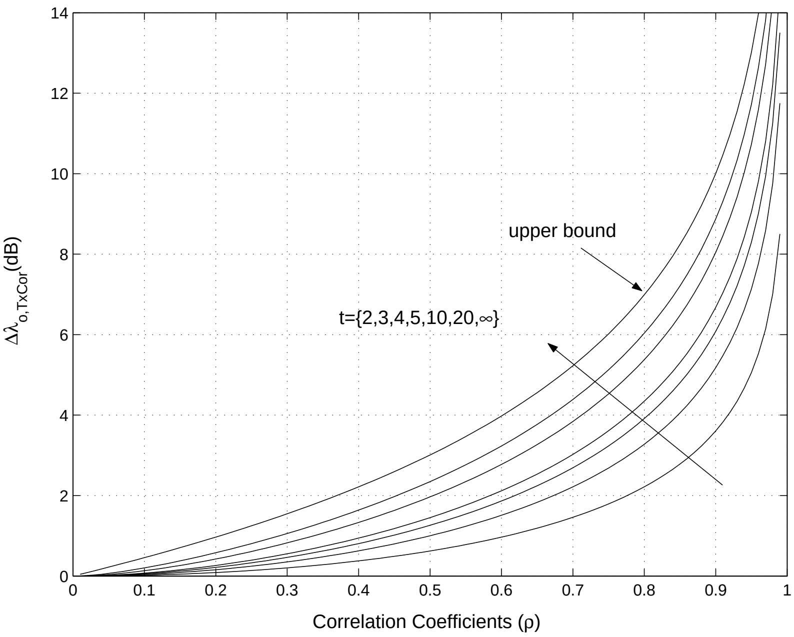

Figure 5.3: The asymptotic SNR degradation of FC, TAS and RAS schemes over an intra-class correlated Rayleigh fading channel. Correlation exists at the transmit side.

degradation is given by

$$\Delta\lambda_{o,\mathrm{TxCor}}\ (\mathrm{dB}) = 10\log\left(\frac{1}{1-\rho}\right) - \frac{1}{t}10\log\left(\frac{1-\rho+t\rho}{1-\rho}\right). \tag{5.47}$$

In Fig. 5.3, we plot the degradation versus the correlation coefficient for different number of transmit antennas (t). The curves indicate that the SNR loss increases with the number of correlated (transmit) antennas and the correlation coefficient (ρ). But the SNR degradation is not affected by the number of uncorrelated (receive) antennas. When the correlation coefficient is small, say less than 0.5, the asymptotic SNR degradation is within 3 dB compared to the case when the channels are independent (correlation coefficient equals 0). However, when ρ is larger than 0.9, a small increase in ρ will cause a large increase in SNR degradation.

Similarly, when receive correlation exists, the SNR degradations for all antenna

Table 5.1: Asymptotic SNR Losses of TAS, RAS and FC Schemes Due to Transmit or Receive Correlation

Condition	$\rho = 0.5$	$\rho = 0.7$	$\rho = 0.9$
$t = 2, r = 3$ with transmit correlation	0.62 dB	1.46 dB	3.60 dB
$t = 2, r = 3$ with receive correlation	1.00 dB	2.22 dB	5.18 dB
$t = 3, r = 2$ with transmit correlation	1.00 dB	2.22 dB	5.18 dB
$t = 3, r = 2$ with receive correlation	0.62 dB	1.46 dB	3.60 dB

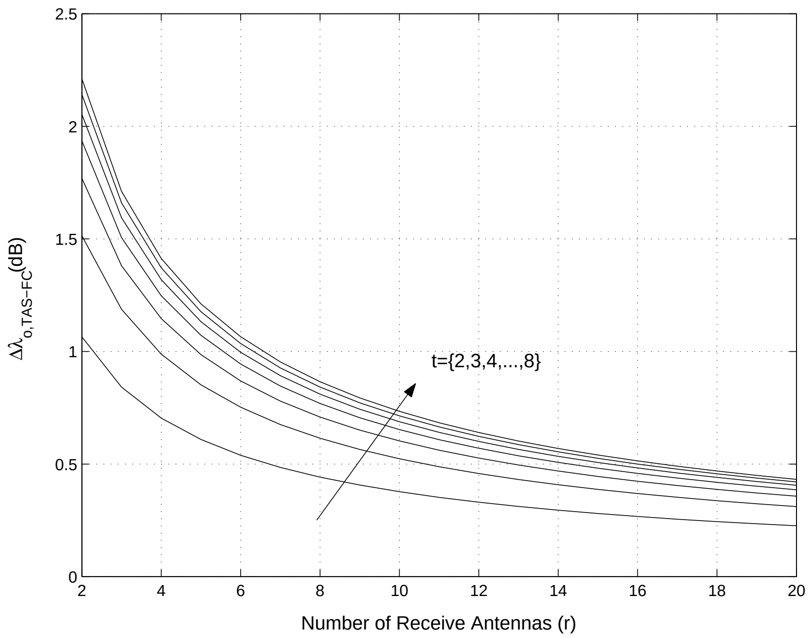

Figure 5.4: Difference in SNR value between TAS and FC over an intra-class correlated Rayleigh fading channel at low BER values. Correlation exists at the transmit side or the receive side.

selection schemes have been shown equal to

$$\Delta\lambda_{o,\mathrm{RxCor}} = 10\log\left(\frac{1}{1-\rho}\right) - \frac{1}{r}10\log\left(\frac{1-\rho+r\rho}{1-\rho}\right). \tag{5.48}$$

Because the only difference between (5.47) and (5.48) is that t has been replaced by r, arguments valid in the transmit-correlation case are applicable here. In Table 5.1, some values of the SNR losses due to transmit or receive correlation are presented.

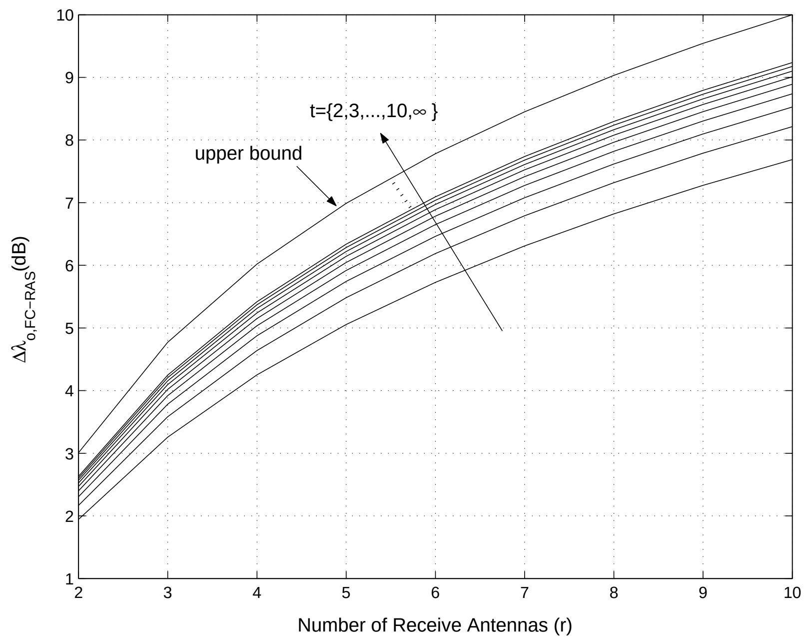

Figure 5.5: Difference in SNR value between FC and RAS over an intra-class correlated Rayleigh fading channel at low BER values. Correlation exists at the transmit side or the receive side.

Table 5.2: SNR Performance Difference Between TAS and FC, and Between FC and RAS at Low BER Values

Condition	$\Delta\lambda_{o,\text{TAS-FC}}$	$\Delta\lambda_{o,\text{FC-RAS}}$
$t = 2, r = 3$ with transmit correlation	0.84 dB	3.26 dB
$t = 2, r = 3$ with receive correlation	0.84 dB	3.26 dB
$t = 3, r = 2$ with transmit correlation	1.51 dB	2.17 dB
$t = 3, r = 2$ with receive correlation	1.51 dB	2.17 dB

5.3.2 Performance Comparison Between FC, TAS and RAS Schemes

As shown in (5.23), (5.38) and Section 5.2.2, when the BER is low, the differences in SNR performance between FC, TAS and RAS schemes are not related to the transmit/receive correlation coefficient, but dependent upon the number of transmit antennas (t) and the number of receive antennas (r). In Fig. 5.4, we plot (5.23), the SNR value by which TAS outperforms FC at low BER values over an intra-class correlated Rayleigh channel, versus the number of receive antennas (r) for different number of transmit antennas (t). The results indicate that TAS outperforms FC all the time, and the discrepancy is increasing with the number of transmit antennas and is decreasing with the number of receive antennas. In Fig. 5.5, we further plot the SNR difference between FC and RAS at low BER values. Results show that FC always outperforms RAS. The discrepancy also increases with the number of transmit antennas and the number of receive antennas. In Table 5.2, some SNR differences between TAS and FC, and between FC and RAS are given. In fact, we observe that TAS always outperforms FC which in turn outperforms RAS over all transmit SNR values. The reasons of which will be presented in the next section.

5.3.3 BER Curves

We have performed computer simulations to evaluate the BERs of MIMO systems with antenna selection over an intra-class correlated Rayleigh fading channel. Moreover, we calculate the analytical BER results derived in Section 5.2 using truncated series with a relative error tolerance of 0.02. Both simulated and analytical BERs are then plotted in Fig. 5.6 and Fig. 5.7 for $(t = 2, r = 3)$ and $(t = 3, r = 2)$, respectively. The results corresponding to the i.i.d. Rayleigh fading channel are also plotted for reference.

First, we observe that in all cases, the analytical BERs are very close to the simulation results, indicating that our analyses can accurately predict the BER performances of the MIMO systems with antenna selection. Second, correlation at the transmit end or receive end is found to degrade the BER performance of the systems under study, which is consistent with our understanding that higher correlation leads to lower diversity and poorer performance.

Also, among the antenna selection schemes under study and over all SNR values, the TAS scheme achieves the best performance, whereas RAS scheme is the worst. The reasons are as follows. In contrast to RAS and FC scheme without feedback information where the transmit power is equally distributed to all the transmit antennas, the TAS scheme supplies all the transmit power to a single transmit antenna which has been selected because of its best channel response. Hence, in the TAS scheme, no power has been wasted in transmitting signals over less favorable channels, making TAS superior to both FC and RAS. In FC, all the receive antennas are used to capture the transmitted signal as compared to RAS which only selects one receive antenna for reception. Thus, FC can achieves a larger receive SNR and thus better performance than RAS.

Furthermore, at low BER regions, the asymptotic SNR degradations due to correlation are found to be close to the theoretical values. For example, in Fig. 5.6(a), at a BER of 10^{-8}, the SNR degradation for $\rho = 0.7$ is approximately 1.4 dB, regardless of the antenna selection schemes being used. This value is close to the theoretical value shown in Table 5.1. Note that the same degradation can be seen in Fig. 5.7(b) at a BER of 10^{-8}. Also, in Fig. 5.6(b) and Fig. 5.7(a), an asymptotic SNR degradation of about 2.2 dB is observed for $\rho = 0.7$, which is close to the theoretical value shown in Table 5.1.

In Fig. 5.6, for the same value of ρ and at a BER of 10^{-8}, when we compare the transmit SNRs for different antenna selection schemes, we observe that TAS outperforms FC by about 0.8 dB while FC has a 3.3 dB advantage over RAS. These values are close to the asymptotic differences shown in Table 5.2. Finally, when we measure the slopes of the curves in Fig. 5.6 and Fig. 5.7 at low BER regions, they all produce

$$\text{slope} \triangleq -\frac{\log(P_e)}{10\log(\lambda_o)} = 0.6, \tag{5.49}$$

which equals $tr/10$ and fits exactly into our derivations in Section 5.2.3.

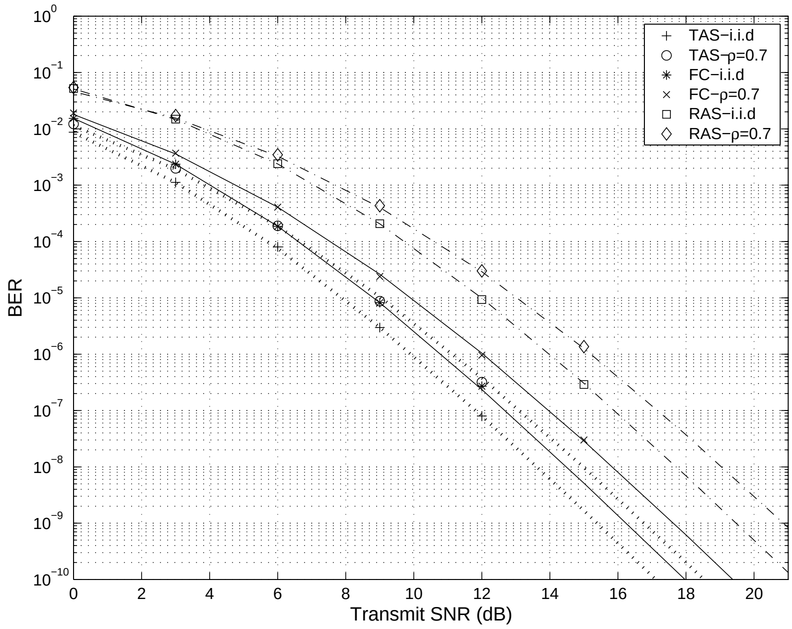

(a)

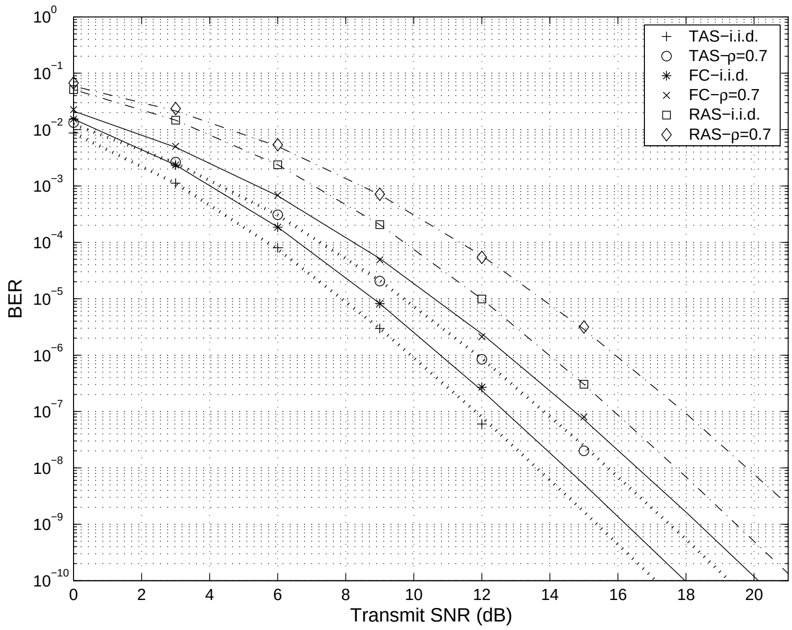

(b)

Figure 5.6: Simulated and analytical BERs of MIMO diversity systems using TAS, RAS and FC schemes with equal correlation and ($t = 2, r = 3$). Results under an independent and identically distributed (i.i.d.) Rayleigh fading channel are also plotted for comparison. Simulated results are represented by markers and analytical results are shown with lines (FC: solid lines; TAS: dotted lines; RAS: dashed-dotted lines). Correlation at (a) transmit side; and (b) receive side.

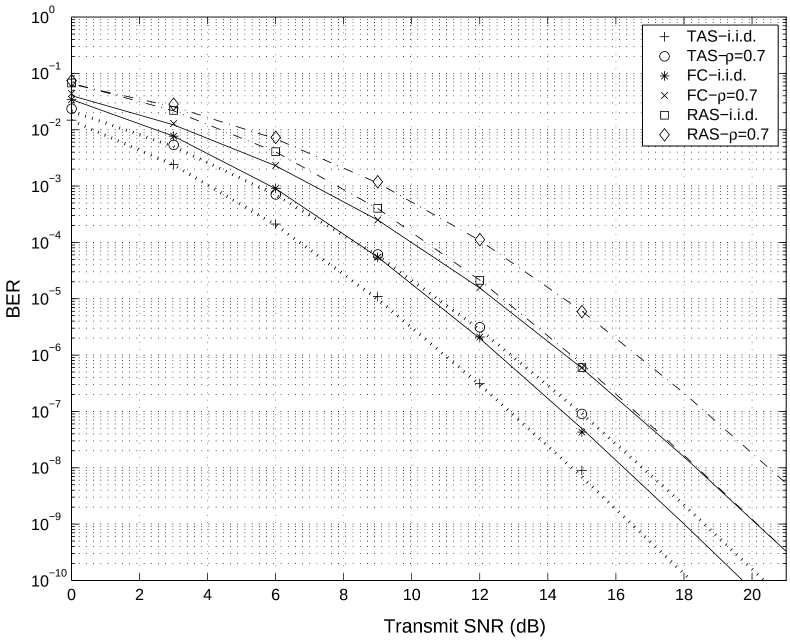

(a)

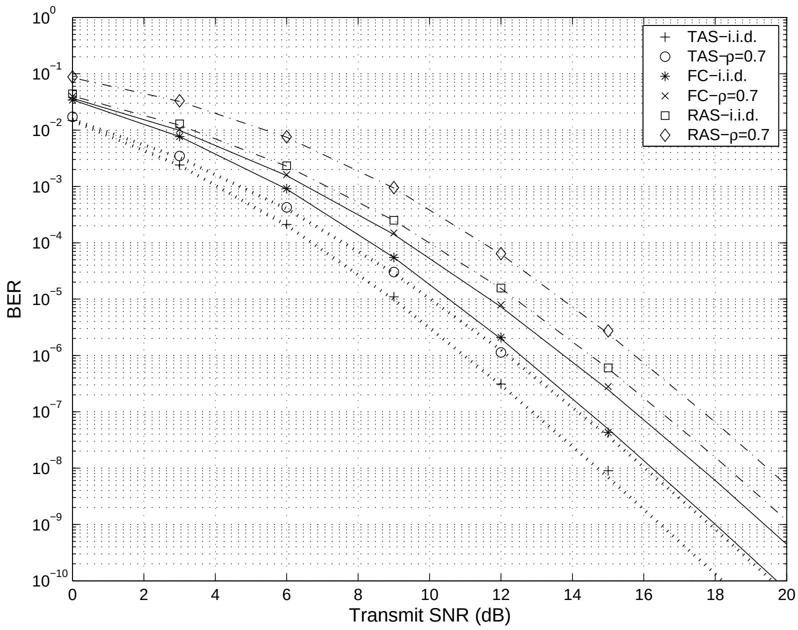

(b)

Figure 5.7: Simulated and analytical BERs of MIMO diversity systems using TAS, RAS and FC schemes with equal correlation and $(t = 3, r = 2)$. Results under an independent and identically distributed (i.i.d.) Rayleigh fading channel are also plotted for comparison. Simulated results are represented by markers and analytical results are shown with lines (FC: solid lines; TAS: dotted lines; RAS: dashed-dotted lines). Correlation at (a) transmit side; and (b) receive side.

5.4 Summary

In this chapter, we have studied the performances of MIMO diversity systems using antenna selection over an intra-class correlated Rayleigh fading channel. The bit error rate (BER) expressions of 3 antenna selection schemes, namely transmit-antenna selection (TAS), receive-antenna selection (RAS) and full complexity (FC) schemes, for correlation at the transmit side or receive side have been derived analytically. The analytical BERs are found to be very close to the simulation results, indicating that our analyses can accurately predict the BER performances of the MIMO systems with antenna selection.

In addition, the asymptotic performances of the three schemes have been evaluated and compared. We find that the diversity orders of MIMO systems employing FC, TAS and RAS schemes are identical (equal to tr) and are not affected by the correlation among the transmit antennas, or the correlation among the receive antennas. When correlation exists at the transmit (or receive) side, the asymptotic SNR degradations of FC, TAS and RAS schemes are also the same. Further, the SNR loss increases with the number of correlated (transmit or receive) antennas and the correlation coefficient (ρ), but is not affected by the number of uncorrelated (receive or transmit) antennas.

Among the 3 antenna selection schemes, TAS has been found to provide the best performance over all transmit SNR values, followed by FC, while RAS always performs worst. Moreover, at the low BER region, the differences in SNR performance between FC, TAS and RAS schemes are not related to the transmit/receive correlation coefficient, but dependent only upon the number of transmit antennas (t) and the number of receive antennas (r). In particular, the discrepancy in performance between TAS and FC has been found to increase with the number of transmit antennas and decrease with the number of receive antennas. But between FC and

RAS, the discrepancy increases with both the number of transmit antennas and the number of receive antennas.

Appendix 5: Diversity Systems over Nakagami-m Fading

We consider a diversity system (L, m) where L denotes the number of diversity branches and m the fading parameter of the Nakagami-m channel. We assume that m is an integer. Suppose the transmitted signal undergoes a flat, quasi-static fading before reaching the receiver side. For the kth diversity branch, the equivalent complex baseband signal sampled at the nth interval equals

$$y_k(n) = h_k(n)e^{-j\phi_k(n)}d(n) + n_k(n), \quad k = 1, \ldots, L. \tag{5.50}$$

Here, $h_k(n)$ and $\phi_k(n)$, respectively, denote the random channel gain and the phase shift due to multipath effect; $d(n)$ is the transmitted symbol with an average energy $2E_s$, and $n_k(n)$ is a zero-mean complex white Gaussian random processes with two-sided power spectral density $2N_0$. Moreover, the channel gains $h_1(n), \ldots, h_L(n)$ are assumed to be equally correlated Nakagami-m random variables with the same fading parameter m, whereas the noise samples $n_1(n), \ldots, n_L(n)$ are taken to be independent and identically distributed (i.i.d.) Gaussian random variables. Such an equally correlated model is always used to approximate the correlation between branches for closely placed antenna arrays [7, 63].

The received signals $y_1(n), y_2(n), \ldots, y_L(n)$ will be processed to determine the transmitted symbol. For simplicity, we remove the sample index n from this point forward. Define

$$\lambda_k = h_k^2 \frac{E_s}{N_0} \tag{5.51}$$

as the instantaneous SNR at the kth branch. The p.d.f. of λ_k is then given by [72]

$$f_{\lambda_k}(\lambda_k) = \frac{1}{\Gamma(m)} \left(\frac{m}{\bar{\lambda}_{ok}}\right)^m \lambda_k^{m-1} \exp\left(-\frac{m\lambda_k}{\bar{\lambda}_{ok}}\right), \ \lambda_k \geq 0, \tag{5.52}$$

where $\Gamma(\cdot)$ represents the Gamma function, and $\bar{\lambda}_{ok} = \mathrm{E}(\lambda_k) = \mathrm{E}(h_k^2)\frac{E_s}{N_0}$ is the average SNR of the kth branch with $\mathrm{E}(\cdot)$ denoting the expectation operator. Then, $\lambda_k(k = 1, \ldots, L)$ are multivariate Gamma distributed [50]. Since the Nakagami-m channels are assumed to be equally correlated, we can denote the common correlation coefficient between any pair of λ_k and λ_l $(k \neq l)$ by ρ_λ.

Maximal-Ratio Combiner

Furthermore, when maximal-ratio combiner is used at the receiver, the output SNR equals

$$\lambda_{\mathrm{MRC}} = \sum_{k=1}^{L} \lambda_k. \tag{5.53}$$

Define

$$\lambda_{\mathrm{MRC}} \triangleq \frac{\bar{\lambda}_o(1-\rho)}{m}\, u \tag{5.54}$$

where ρ denotes the square root of correlation coefficient, i.e., $\rho = \sqrt{\rho_\lambda}$, and $\bar{\lambda}_o$ represents the average SNR of all the L branches, i.e., $\bar{\lambda}_o = \bar{\lambda}_{ok}$ $(k = 1, \ldots, L)$. Then, the p.d.f. of the variable u can be shown equal to [1, eq.(12)]

$$f_{\mathrm{MRC}}(u) = \left(\frac{1-\rho}{1+(L-1)\rho}\right)^m \sum_{k=0}^{\infty} \binom{m+k-1}{m-1} \left(\frac{L\rho}{1+(L-1)\rho}\right)^k \frac{u^{mL+k-1}e^{-u}}{\Gamma(mL+k)}. \tag{5.55}$$

Selective Combiner

The cumulative distribution function (c.d.f.) of the selective combiner (SC) output with L diversity branches in an equally correlated Nakagami-m fading channel with identical average branch SNR can be shown as [7]

$$F_{\lambda_{sc}}(x) = \frac{1}{\Gamma(m)} \int_0^\infty \left[1 - Q_m\left(\sqrt{\frac{2\rho z}{1-\rho}}, \sqrt{\frac{2mx}{\bar{\lambda}_o(1-\rho)}}\right)\right]^L z^{m-1} e^{-z}\, dz \tag{5.56}$$

where Q_m is the mth order Marcum Q-function defined as [87, eq.(4.33)]

$$Q_m(\alpha, \beta) = \frac{1}{\alpha^{m-1}} \int_{\beta}^{\infty} y^m \exp\left(-\frac{y^2 + \alpha^2}{2}\right) I_{m-1}(\alpha y)\, dy \tag{5.57}$$

and $I_m(\cdot)$ is the mth order modified Bessel function of the first kind. Although a closed-form expression, in terms of an infinite incomplete Gamma function series, has been obtained for $F_{\lambda_{sc}}(x)$ in [7, eq.(29)], it is still difficult to obtain an explicit closed-form solution for the average symbol error rate. In the following, we attempt to derive the p.d.f. of the SC output based on (5.56).

Replacing $I_m(\cdot)$ by an infinite series [24, eq.(8.445)], and using the property $Q_m(a, \infty) = 1$, we re-write (5.56) as

$$F_{\lambda_{sc}}(x) = \frac{(1-\rho)^m}{\Gamma(m)} \int_0^{\infty} z^{m-1} \exp(-[1 + (L-1)\rho]z) \left[\sum_{k=0}^{\infty} \frac{z^k \rho^k}{k!} \frac{\gamma(m+k, \frac{mx}{\overline{\lambda}_o(1-\rho)})}{\Gamma(m+k)} \right]^L dz \tag{5.58}$$

where $\gamma(a, z)$ denotes the incomplete Gamma function (see Appendix 2A). Moreover, for integral values of n, the incomplete Gamma function can be shown equal to [24, eq.(8.352.1)]

$$\gamma(n, z) = (n-1)! \left[1 - \exp(-z) \sum_{i=0}^{n-1} \frac{z^i}{i!} \right]. \tag{5.59}$$

Substituting (5.59) into (5.58) and letting

$$u \triangleq \frac{m}{\overline{\lambda}_o(1-\rho)}\, x, \tag{5.60}$$

we obtain the c.d.f. of u as

$$F_{\lambda_{sc}}(u) = \frac{(1-\rho)^m}{\Gamma(m)} \int_0^{\infty} z^{m-1} \exp(-[1 + (L-1)\rho]z) e^{-Lu} \left[\sum_{k=0}^{\infty} \frac{u^{k+m}}{(k+m)!} e_k(\rho z) \right]^L dz \tag{5.61}$$

where the exponential sum function $e_k(v)$ is defined as

$$e_k(v) = \sum_{q=0}^{k} \frac{v^q}{q!}. \tag{5.62}$$

The power sequence in the integral of (5.61) can be further written as

$$\left[\sum_{k=0}^{\infty} \frac{u^{k+m}}{(k+m)!} e_k(\rho z)\right]^L = \sum_{k=0}^{\infty} u^{Lm+k} \sum_{\substack{(i_1,i_2,\dots,i_L) \\ 0\le i_1,\dots,i_L\le k \\ i_1+\cdots+i_L=k}} \prod_{p=1}^{L} \frac{e_{i_p}(\rho z)}{(m+i_p)!}. \tag{5.63}$$

Moreover, the product in (5.63) can be expanded into

$$\prod_{p=1}^{L} \frac{e_{i_p}(\rho z)}{(m+i_p)!} = \prod_{p=1}^{L} \frac{1}{(m+i_p)!} \sum_{n=0}^{k} (\rho z)^n \sum_{\substack{(r_1,\dots,r_L) \\ 0\le r_1\le i_1 \\ \vdots \\ 0\le r_L\le i_L \\ r_1+\cdots+r_L=n}} \prod_{j=1}^{L} \frac{1}{r_j!}. \tag{5.64}$$

Next, substituting (5.63) and (5.64) into (5.61), and performing the integration, we have

$$F_{\lambda_{sc}}(u) = \left[\frac{1-\rho}{1+(L-1)\rho}\right]^m \frac{e^{-Lu}}{\Gamma(m)} \sum_{k=0}^{\infty} c_k(L,m,\rho) u^{mL+k} \tag{5.65}$$

where $c_k(L,m,\rho)$ is defined as

$$\begin{aligned} c_k(L,m,\rho) &= \sum_{\substack{(i_1,i_2,\dots,i_L) \\ 0\le i_1,\dots,i_L\le k \\ i_1+\cdots+i_L=k}} \prod_{p=1}^{L} \frac{1}{(m+i_p)!} \sum_{n=0}^{k} \frac{\rho^n \Gamma(m+n)}{[1+(L-1)\rho]^n} \sum_{\substack{(r_1,\dots,r_L) \\ 0\le r_1\le i_1 \\ \vdots \\ 0\le r_L\le i_L \\ r_1+\cdots+r_L=n}} \prod_{j=1}^{L} \frac{1}{r_j!} \\ &= \sum_{\substack{(i_1,i_2,\dots,i_L) \\ 0\le i_1\le\cdots\le i_L\le k \\ i_1+\cdots+i_L=k}} \binom{L}{l_1,\dots,l_q} \prod_{p=1}^{L} \frac{1}{(m+i_p)!} \sum_{n=0}^{k} \frac{\rho^n \Gamma(m+n)}{[1+(L-1)\rho]^n} \end{aligned}$$

$$\times \sum_{\substack{(r_1,\ldots,r_L) \\ 0\le r_1\le i_1 \\ \vdots \\ 0\le r_L\le i_L \\ r_1+\cdots+r_L=n}} \prod_{j=1}^{L} \frac{1}{r_j!}. \tag{5.66}$$

In (5.66), the multinomial coefficient $\binom{L}{l_1,\ldots,l_q}$ is defined as

$$\binom{L}{l_1,...,l_q} = \frac{L!}{l_1!\ldots l_q!} \tag{5.67}$$

and $(l_1,\ldots,l_q)$ represents the number of equal elements in $(i_1,\ldots,i_L)$. For example, suppose $k=6$ and $L=4$. If $(i_1,\ldots,i_L)=(0,1,1,4)$, then $(l_1,\ldots,l_q)=(1,2,1)$.

We then differentiate $F_{\lambda_{sc}}(u)$ with respect to u to obtain the p.d.f. of u, i.e.,

$$\begin{aligned} f_{\lambda_{sc}}(u) &= \frac{dF_{\lambda_{sc}}(u)}{du} \\ &= \left[\frac{1-\rho}{1+(L-1)\rho}\right]^m \frac{e^{-Lu}}{\Gamma(m)} \sum_{k=0}^{\infty} u^{mL+k-1}[(mL+k)c_k(L,m,\rho) - Lc_{k-1}(L,m,\rho)] \end{aligned} \tag{5.68}$$

with

$$c_{-1}(L,m,\rho) \equiv 0. \tag{5.69}$$

Finally, based on (5.60), the p.d.f. of the SC output can be obtained.

Chapter 6

Conclusions

In this concluding chapter, we summarize the major contributions of this piece of work and discuss some possible future work.

6.1 Contributions of the Thesis

6.1.1 Zero-Forcing Detector

In Chapter 2, we have derived the closed-form bit error rate (BER) expressions for MIMO systems with zero-forcing detector over correlated-Rayleigh and Rice fading channels. Based on the exponential correlation matrix at the transmit side, we observe that an increase in the value of the correlation coefficient produces a larger SNR degradation and that the symbols sent from the first and the last transmit antennas have smaller SNR degradations compared to the symbols sent from other transmit antennas.

In addition, the degradation of the systems over the Rician fading channel compared to the i.i.d. Rayleigh fading channel has been derived analytically. We find that the SNR degradation depends only on the Rician factor and the number of transmit antennas. In general, a lower Rician factor produces a higher probability of achieving a particular SNR and that the SNR degradation increases with the number of transmit antennas.

6.1.2 V-BLAST Detector

Chapter 3 has evaluated thoroughly the performance of the V-BLAST system with two transmit antennas when optimal ordering is used. The exact SNR distributions of the system in the first and second detection steps have been derived and subsequently the closed-form expressions of the BERs have been obtained. For an i.i.d. Rayleigh channel, our analytical study concludes that optimal ordering has no effect on the diversity order compared with fixed ordering. Also, at high SNR, we find that optimal ordering increases the SNR by 3 dB for the first step and decreases the SNR by $(3/r)$ dB for the second step as compared to fixed ordering.

We have also approximated the performance of the V-BLAST system over a Rician channel by that over a correlated-Rayleigh channel. Simulation results have shown that the approximation is very accurate. As a consequence, observations made for both types of channels are very similar. We find that for the correlated-Rayleigh/Rician channel, the SNR loss of the first detection step for optimal ordering increases with the transmit-correlation coefficient/Rician factor. In addition, the degradation is higher for optimal ordering compared with fixed ordering and the advantage of optimal ordering over fixed ordering diminishes with the transmit-correlation coefficient/Rician factor. Finally, the transmit-correlation coefficient/Rician factor has been found to have no effect on the performance of the second step in optimal ordering.

6.1.3 Capacity

In Chapter 4, we have shown that the capacity of MIMO Rician channels can be well approximated by that of correlated-Rayleigh MIMO channels under an intra-class correlated model. Based on the approximation, we have derived a closed-form expression for the MIMO Rician channel capacity, which is further exploited for studying the asymptotic behavior of the channel capacity. We find that at low SNR region, the minimum bit-energy-to-noise-power-spectrum-density ratio (E_b/N_0) required for a reliable communication equals -1.59 dB and is independent of the Rician factor K. At the high SNR region, for every 3 dB increase in SNR, an extra t bps/Hz of capacity will be achieved, where t denotes the number of transmit antennas. We can therefore conclude that the capacity of MIMO Rician channels increases linearly with t in the high SNR region, irrespective of the Rician factor. Finally, compared to an i.i.d. Rayleigh channel, the capacity loss of a MIMO Rician channel is found to increase with both the Rician factor and the number of transmit antenna. But the loss is upper-bounded by $\log_2(1+K)$ as t goes to infinity.

6.1.4 Antenna Selection

Finally, in Chapter 5, we have studied the performances of MIMO diversity systems using antenna selection over an intra-class correlated Rayleigh fading channel. The BER expressions of 3 antenna selection schemes, namely transmit-antenna selection (TAS), receive-antenna selection (RAS) and full complexity (FC) schemes, for correlation at the transmit side or receive side have been derived analytically. The analytical BERs are found to be very close to the simulation results, indicating that our analyses can accurately predict the BER performances of the MIMO systems with antenna selection.

In addition, the asymptotic performances of the three schemes have been evaluated and compared. We find that the diversity orders of MIMO systems employing FC, TAS and RAS schemes are identical (equal to tr) and are not affected by the correlation among the transmit antennas, or the correlation among the receive antennas. When correlation exists at the transmit (or receive) side, the asymptotic SNR degradations of FC, TAS and RAS schemes are also the same. Further, the SNR loss increases with the number of correlated (transmit or receive) antennas and the correlation coefficient, but is not affected by the number of uncorrelated (receive or transmit) antennas.

Among the 3 antenna selection schemes, TAS has been found to provide the best performance over all transmit SNR values, followed by FC, while RAS always performs worst. Moreover, at the low BER region, the differences in SNR performance between FC, TAS and RAS schemes are not related to the transmit/receive correlation coefficient, but dependent only upon the number of transmit antennas (t) and the number of receive antennas (r). In particular, the discrepancy in performance between TAS and FC has been found to increase with the number of transmit antennas and decrease with the number of receive antennas. But between FC and RAS, the discrepancy increases with both the number of transmit antennas and the number of receive antennas.

6.2 Future Work

In this thesis, it has been shown in several occasions that the Rician channel can be represented by a correlated-Rayleigh channel in statistics. As a consequence, various MIMO systems over Rician channels can be evaluated analytically. Such a technique should be further exploited to study analytically the performance of other MIMO systems over Rician channels.

Moreover, we assume a flat fading channel throughout our work. For MIMO systems over frequency selective fading channel, inter-symbol interference will occur and cause performance degradation. The performance of BLAST systems over such a channel will require further investigation.

Also, channel estimation is another important research area in MIMO systems. In our analysis, it is assumed that the characteristics of the channel are known perfectly at the receiver. In case the estimated channel characteristics differ from the actual ones, there would be performance degradation. Hence, the effect of imperfect channel estimation on the performance of MIMO systems should be investigated.

Finally, we have evaluated the performance of V-BLAST algorithms for MIMO systems with two transmit antennas over correlated Rayleigh and Rician fading channels. For V-BLAST detectors with multiple transmit antennas, our proposed technique needs multiple integrations which cannot be evaluated easily. Therefore, we should explore other techniques to study V-BLAST algorithms with an arbitrary number of transmit antennas, which is still an open problem.

Bibliography

[1] Aalo V. A., "Performance of maximal-ratio diversity systems in a correlated Nakagami-fading environment," *IEEE Transactions on Communications*, vol. 43, no. 8, pp. 2360–2369, Aug. 1995.

[2] Abramowitz M. and Stegun I. A., *Handbook of Mathematical Functions with Formulas, Graphs, and Mathematical Tables*, Dover Publications Inc., New York. 1964.

[3] Alamouti S. M., "A simple transmit diversity technique for wireless communications," *IEEE Journal on Selected Areas in Communications*, vol. 16, pp. 1451–1458, Oct. 1998.

[4] Anderson T. W., *An introduction to multivariate statistical analysis*, John Wiley & Sons, third edition, 2003.

[5] Bahceci I., Duman T. M., and Altunbasak Y., "Antenna selection for multiple-antenna transmission systems: performance analysis and code contruction," *IEEE Transaction on Information Theory*, vol. 49, no. 10, pp. 2669–2681, Oct. 2003.

[6] Catreux S., Greenstein L. J. and Erceg V., "Some results and insights on the performance gains of MIMO systems," *IEEE Journal on Selected Areas in Communications,* vol. 21, issue 5, pp. 839–847, June 2003.

[7] Chen Y. X. and Tellambura C., "Distribution functions of selection combiner output in equally correlated Rayleigh, Rician, and Nakagami-m fading channels," *IEEE Transactions on Communications*, vol. 52, no. 11, pp. 1948–1956, Nov. 2004.

[8] Chen Z., Yuan J. and Vucetic B., "Analysis of transmit antenna selection/maximal-ratio combining in Rayleigh fading channels," *IEEE Transactions on Vehicular Technology*, vol. 54, no. 4, pp. 1312–1321, July 2005.

[9] Chiani M., Win M. Z. and Zanella A., "On the capacity of spatially correlated MIMO Rayleigh-fading channels," *IEEE Transactions on Information Theory*, vol. 49, no. 10, pp. 2363–2371, Oct. 2003.

[10] Constantine A. G., "Some non-central distribution problems in multivariate analysis," *Annals of Mathematical Statistics*, vol. 34, pp. 1270–1285, 1963.

[11] Constantine A. G. and Troskie C. G., "The exact non-central distribution of a multivariate complex quadratic form of complex normal variates," *South African Statistical Journal*, no. 18, pp. 123–134, 1984.

[12] Cui X. W., Zhang Q. T., and Feng Z. M., "Generic procedure for tightly bounding the capacity of MIMO correlated Rician fading channels," *IEEE Transactions on Communications*, vol. 53, no. 5, pp. 890–898, May 2005.

[13] David H. A., *Order statistics*, NJ: John Wiley, c2003.

[14] Farrokhi F. R., Lozano A., Foschini G. J. and Valenzuela R. A., "Spectral efficiency of wireless systems with multiple transmit and receive antenna," in *Proc. IEEE International Symposium on Personal, Indoor and Mobile Radio Communications, PIMRC 2000*, London, UK, Sept. 2000, vol. 1, pp. 373-377.

[15] Farrokhi F. R., Foschini G. J., Lozano A. and Valenzuela R. A., "Link-optimal space-time processing with multiple transmit and receive antennas," *IEEE Communications Letters*, vol. 5, no. 3, pp. 85–87, Mar. 2001.

[16] Foschini G. J., "Layered space-time architecture for wireless communication," *Bell Labs Technical Journal*, vol. 1, pp. 41–59, Aug. 1996.

[17] Foschini G. J. and Gans M. J., "On limits of wireless communications in a fading environment when using multiple antennas," *Wireless Personal Communications*, vol. 6, pp. 311–335, Mar. 1998.

[18] Foschini G. J., Golden G. D., Valenzuela R. A. and Wolniansky P. W., "Simplified processing for high spectral efficiency wireless communication employing multi-element arrays," *IEEE Journal on Selected Areas in Communications*, vol. 17, no. 11, pp. 1841–1852, Nov. 1999.

[19] Gallager R. G., *Information Theory and Reliable Communcation*, J. Wiley and Sons, New York, Chapter IV, 1968.

[20] Gao H. and Smith P. J., "Exact SINR claclulations for optimum linear combining in wireless systems," *Probability in Engineering and Informational Sciences*, vol. 12, pp. 261–281, 1988.

[21] Gao H., Smith P. J., and Clark M. V., "Theoretical reliability of MMSE linear diversity combining in Rayleigh-fading additive interference channels," *IEEE Transactions on Communications*, vol. 46, pp. 666–672, May 1988.

[22] Goodman N. R., "Statistical analysis based on a certain multivariate complex Gaussian distribution (An Introduction)," *The Annals of Mathematical Statistics,* vol. 34, no. 1, pp. 152–177, Mar. 1963.

[23] Gore D., Heath R. W. Jr. and Paulraj A., "On performance of the zero forcing receiver in presence of transmit correlation," in *Proc. IEEE International Symposium on Information Theory*, Lausanne, Switzerland, June 30–July 5, 2002, p. 159.

[24] Gradshteyn I. S. and Ryzhik I. M., *Table of integral, series, and products*, sixth edition, Academic Press, 2000.

[25] Gupta A. K. and Nagar D. K., *Matrix Variate Distributions.* Boca Raton, FL: Chapman & Hall/CRC, 2000.

[26] Haustein T., Jorswieck E., Jungnickel V., Krueger U., Pohl V. and von Helmolt C., "Bit error rates for a MIMO system in Rayleigh and Rician channels," in *Proc. IEEE 54th Vehicular Technology Conference, VTC 2001 Fall,* Atlantic City, New Jersey, USA, Oct. 2001, pp. 1984–1987.

[27] *IEEE Journal of Selected Areas on Communications*, *Special issue on MIMO systems and applications: Part I*, vol. 21, Apr. 2003.

[28] *IEEE Journal of Selected Areas on Communications*, *Special issue on MIMO systems and applications: Part II*, vol. 21, June. 2003.

[29] *IEEE Transactions on Signal Processing*, *Special issue on MIMO wireless communications*, vol. 51, Nov. 2003.

[30] *IEEE Transactions Information Theory*, *Special issue on space-time transmission, reception, coding and signal processing*, vol. 49, Oct. 2003.

[31] Ivrlac M. T. and Nossek J. A., "Correlated fading in MIMO systems —- Blessing or curse?", in *Proc. 39th Annu. Allerton Conf. Communication, Control and Computing (Allerton)*, Monticello, IL, Oct. 2001, CD-ROM.

[32] Jakes W. C., *Microwave mobile communications*, IEEE Press, 1974.

[33] Winters J., "On the capacity of radio communication systems with diversity in a Rayleigh fading environment," *IEEE Journal on Selected Areas in Communications*, vol. 5, no.5, pp. 871–878, June 1987.

[34] Jayaweera S. K. and Poor H. V., "On the capacity of multiple-antenna systems in Rician fading," *IEEE Transactions on Wireless Communications*, vol. 4, no. 3, pp. 1102–1111, May 2005.

[35] Kang M. and Alouini M. S., "Impact of correlation on the capacity of MIMO channels," in *Proc. IEEE International Conference on Communications*, Alaska, USA, May 2003, pp. 2623–2627.

[36] Kang M. and Alouini M. S., "Capacity of correlated MIMO Rayleigh channels," *IEEE Transactions on Wireless Communications*, vol. 5, no. 1, pp. 143–155, Jan. 2006.

[37] Kang M. and Alouini M. S., "Capacity of MIMO Rician channels," *IEEE Transactions on Wireless Communications*, vol. 5, no. 1, pp. 112–122, Jan. 2006.

[38] Kermoal J. P., Schumacher L., Pedersen K. I., Mogensen P. E., Frederiksen F.,"A stochastic MIMO radio channel model with experimental validation," *IEEE Journal on Selected Areas in Communications*, vol. 20, no. 6, pp. 1211–1226, Aug. 2002.

[39] Khatri C. G., "Classical statistical analysis based on a certain multivariate complex Gaussian distribution," *Annals of Mathematical Statistics*, vol. 36, pp. 98-114, 1965.

[40] Kiessling M. and Speidel J., "Analytical performance of MIMO zero-forcing receiver in correlated Rayleigh fading environments", in *IEEE Workshop on Signal Processing Adavnces in Wireless Communications*, June 2003, pp. 383–387.

[41] Kiessling M. and Speidel J., “Analytical performance of MIMO MMSE receiver in correlated Rayleigh fading environments”, in *IEEE Vehicular Technology Conference*, Orlando, FL, Oct. 2003, pp. 1738–1732.

[42] Kiessling M. and Speidel J., “Unifying performance analysis of linear MIMO receivers in correlated Rayleigh fading environments”, in *ISSSTA2004*, Sydney, Australia, 30 Aug.–2 Sep. 2004, pp. 634–638.

[43] Kiessling M., “Statistical analysis and transmit prefiltering for MIMO wireless systems in correlated fading environments”, *PhD Dissertation*, 2004.

[44] Kiessling M. and Speidel J., “Exact ergodic capacity of MIMO channels in correlated Rayleigh fading environments,” in *Proc. International Zurich Seminar on Communications*, ETH Zurich, Switzerland, Feb. 18–20, 2004, pp. 128–131.

[45] Kiessling M., Speidel J., and Reinhardt M., “Unifying analysis of ergodic MIMO capacity in correlated Rayleigh fading environments,” *European Transactions Telecommunications*, vol. 16, no. 1, pp. 17–35, Jan./Feb. 2005.

[46] Kiessling M., Speidel J., and Reinhardt M., “Ergodic capacity of MIMO channels with statistical channel state information at the transmitter,” in *Proc. ITG Workshop on Smart Antennas*, Munich, Germany, March 2004, pp. 79–86.

[47] Kiessling M., Speidel J., “Asymptotics of ergodic MIMO capacity in correlated Rayleigh fading environments,” in *Proc. IEEE Vehicular Technology Conference*, Milan, Italy, May 2004, pp. 843–847.

[48] Kiessling M., Speidel J., “Mutual information of MIMO channels in correlated Rayleigh fading environments - a general solution,” in *Proc. IEEE International Conference on Communications*, Paris, June 2004, pp. 814–818.

[49] Johnson N. L. and Kotz S., *Continuous univariate Distributions*, New York: Hougton Mifflin, 1970.

[50] Kotz S., Balakrishnan N., and Johnson N. L., *Continuous Multivariate Distributions Volume 1*, second version, New York: John Wiley & Sons, Inc., 2000.

[51] Lao D. and Haimovich A., “Exact closed-form performance analysis of optimum combining with multiple co-channel interferers and Rayleigh fading,” *IEEE Transactions on Communications*, vol. 51, pp. 995–1003, June 2004.

[52] Lao D. and Haimovich A., "Exact everage sysmbol error probability of optimum combining with arbitrary interference power," *IEEE Communications Letters*, vol. 8, no. 4, pp. 226–228, April 2004.

[53] Lebrun G., Faulkner M., Shafi M. and Smith P. J., "MIMO Ricean channel capacity: An asymptotic analysis," *IEEE Transactions on Wireless Communications*, vol. 5, no. 6, pp. 1343–1350, June 2006.

[54] Lee W. C. Y., *Mobile communications design fundamentals*, John Wiley & Sons, 1993.

[55] Liberti, J. C. and Rappaport T. S., *Smart Antennas for Wireless Communications: IS-95 and Third Generation CDMA Applications*, Prentice Hall, Apr. 1999.

[56] Loyka S. and Mosig J.R., "Channel capacity of N-antennas BLAST architecture," *Electronic Letters,* vol. 26, no. 7, pp. 660–661, Mar. 2000.

[57] Loyka S., "Channel capacity of MIMO architecture using the exponential correlation matrix," *IEEE Communications Letters,* vol. 5, no. 9, pp. 369–371, Sept. 2001.

[58] Loyka S. and Gagnon F., "Performance analysis of the V-BLAST algorithm: an analytical approach," in *Proc. International Zurich Seminar on Broadband Communications Access - Transmission - Networking*, ETH Zurich, Switzerland, Feb. 2002, pp. 1–6.

[59] Loyka S. and Gagnon F., "Performance analysis of the V-BLAST algorithm: An analytical approach," *IEEE Transactions on Wireless Communications*, vol. 3, no. 4, pp. 1326–1337, July 2004.

[60] Lutkepohl H., *Handbook of matrices*, Wiley, 1996.

[61] MacKay D. J. C., *Information theory, inference, and learning algorithms*, New York: Cambridge University Press, 2003.

[62] Maiwald D. and Kraus D., "Calculation of moments of complex Wishart and complex inverse Wishart distributed matrices," *IEE Proceedings Radar, Sonar and Navigation*, vol. 147, no. 4, pp. 162–168, Aug. 2000.

[63] Mallik R. K. and Win M. Z., "Analysis of hybrid selection/maximal-ratio combining in correlated Nakagami fading," *IEEE Transactions on Communications*, vol. 50, no. 8, pp. 1372–1383, Aug. 2002.

[64] Mallik R. K., *et.al* "Bit-error probability for optimum combining of binary signals in the presence of interference and noise", *IEEE Transactions on Wireless Communications*, vol. 3, no. 2, pp. 395–407, Mar. 2004.

[65] Sellathurai M. and Haykin S., "Turbo-BLAST: Performance evaluation in correlated Rayleigh-fading environment," *IEEE Journal on Selected Areas in Communications*, vol. 21, no. 3, pp. 340–349, April 2004.

[66] McKay M. R. and Collings I. B., "General Capacity Bounds for Spatially Correlated Rician MIMO Channels," *IEEE Transactions on Information Theory*, vol. 51, no. 9, pp. 3121–3145, Sept. 2005.

[67] McKay M. R. and Collings I. B., "Improved general lower bound for spatially-correlated Rician MIMO capacity," *IEEE Communications Letters*, vol. 10, no. 3, pp. 162–164, Mar. 2006.

[68] Mestre X., Fonollosa J. R. and Pages-Zamora A., "Capacity of MIMO channels: Asymptotic evaluation under correlated fading," *IEEE Journal on Selected Areas in Communications*, vol. 21, no. 5, pp. 829–838, June 2003.

[69] Molisch A. F. and Win M. Z., "MIMO systems with antenna selection," *IEEE Microwave Magazine*, pp. 46–56, Mar. 2004.

[70] Moustakas A. L and Simon S. H.,"Random matrix theory of multi-antenna communications: the Ricean channel," *Journal of Physics A: Mathematical and General*, vol. 38, pp. 10859–10872, 2005.

[71] Muirhead R. J., *Aspects of multivariate statistical theory*, John Wiley & Sons, 1982.

[72] Nakagami M., "The m-distribution: A general formula of intensity distribution of rapid fading," in *Statistical Methods in Radio Wave Propagation*, W. C. Hoffman, Ed. New Youk: Pergamon, 1960.

[73] Prasad N. and Varanasi M. K., "Analysis of decision feedback detection for MIMO Rayleigh-fading channels and the optimization of power and rate allocations," *IEEE Transactions on Information Theory*, vol. 50, no. 6, pp. 1009–1025, Jun. 2004.

[74] Paulraj A., and Papadias C. B., "Space-time processing for wireless communications," *IEEE Signal Proceeding Magazine* vol. 14, pp. 49–83, Nov. 1997.

[75] Paulraj A., Nabar R. and Gore D., *Introduction to Space-Time Wireless Communications*, Cambridge University Press, May 2003.

[76] Proakis J. G., *Digital Communications*, third edition, McGraw-Hill Inc., 1995.

[77] Ratnarajah T., Vaillancourt R., and Alvo M., "Complex random matrices and Rayleigh channel capacity," *Communications in Information and Systems*, vol. 3, no. 1, pp. 119–138, 2003.

[78] Ratnarajah T., Vaillancourt R., and Alvo M., "Complex random matrices and Ricean channel capacity," *Problems of Information Transmission*, vol. 41, no. 1, pp. 1–22, 2003.

[79] Bohnke R., Wubben D., Kuhn V., and Kammeyer K.-D., "Reduced complexity MMSE detection for BLAST architectures," in *Proc. 2003 IEEE Global Telecommunications Conference (GLOBECOM 2003)*, San Francisco, CA, Dec. 2003, pp. 2258–2262.

[80] Sanayei S. and Nosratinia A., "Antenna selection in MIMO systems," *IEEE Communications Magazine*, pp. 68–73, Oct. 2004.

[81] Sarkar T. K., Wicks M. C., Salazar-Palma M., Bonneau R. J., *Smart Antennas*, Wiley-IEEE Press, May 2003.

[82] Shah A. and Haimovich A. M., "Performance analysis of optimum combining in wireless communicaitons with Rayleigh fading and cochannel interference," *IEEE Transactions on Communications*, vol. 46, pp. 473–479, Apr. 1998.

[83] Shah A. *et.al*, "Exact bit-error probability for optimum combining with a Rayleigh fading Gaussain cochannel interferer," *IEEE Transactions on Communications*, vol. 48, no. 6, pp. 908–912, June 2000.

[84] Shannon C. E., "A mathematical theory of communication," *The Bell System Technical Journal*, vol. 27, pp.379–423, 623–656, July, Oct., 1948.

[85] Shen H. and Ghrayeb A., "Analysis of the outage probability for MIMO systems with receive transmit selection," *IEEE Transactions on Vehicular Technology*, vol. 55, no. 4, pp. 1435–1441, July 2006.

[86] Shiu D.-S., Foschini G. J., Gans M. J. and Kahn J. M., "Fading correlation and its effect on the capacity of multielement antenna systems," *IEEE Transactions on Communications*, vol. 48, no. 3, pp. 502–513, March 2000.

[87] Simon M. K. and Alouini M.-S., *Digital communication over fading channels: a unified approach to performance analysis*, John Wiley & Sons, 2000.

[88] Steyn H. S. and Roux J. J. J., "Approximations for the non-central Wishart distributions," *Journal of South African Statist.*, vol. 6, pp. 164–173, 1972.

[89] Taroch V., Seshadri N. and Calderbank A. R., "Space-time codes for high data rates wireless communications: performance criterion and code construction," *IEEE Transactions on Information Theory,* vol. 44, pp. 744–765, Mar. 1998.

[90] Taroch V., Jafarkhani H., and Calderbank A. R., "Space-time block codes from orthogonal designs," *IEEE Transactions on Information Theory*, vol. 45, pp. 1456–1467, July 1998.

[91] Telatar I. E., "Capacity of multi-antenna Gaussian channels," *Bell Labs Technical Memorandum*, Oct. 1995.

[92] Verdu S., *Multiuser Detection*, Cambridge University Press, 1998.

[93] Viterbi A. J., "Error bounds for convolutional codes and an asymptotically optimum decoding algorithm," *IEEE Transactions on Information Theory* vol. 13, no. 2, pp. 260–269, April 1967.

[94] , Vucetic B., Yuan J., *Space-Time Coding*, Chichester: Wiley, 2003.

[95] Wang B.-Y. and Zheng W. X., "Exact BER of transmitter antenna selection/receiver-MRC over spatially correlated Nakagami-fading channels," *IEEE International Symposium on Circuits and Systems*, Greece, May 21–24, 2006, pp. 1370–1373.

[96] Wang B.-Y. and Zheng W. X., "Accurate BER of transmitter antenna selection/receiver-MRC over arbitrary correlated Nakagami fading channels," *IEEE International Conference on Acoustics, Speech, and Signal Processing*, Toulouse, France, May 14–19, 2006, pp. 753–756.

[97] Wolniansky P. W., Foschini G. J., Golden G. D. and Valenzuela R.A., "V-BLAST: an architecture for realizing very high data rates over the rich-scattering wireless channel," *in Proc. URSI International Symposium on Signals, Systems, and Electronics*, Palazzo dei Congressi, Pisa, Italy, Sept. 1998, pp. 295–300.

[98] Yang L., Tang D., and Qin J., "Performance of spatially correlated MIMO channel with antenna selection," *IEE Electronics Letters*, vol. 40, no. 20, Sept. 2004.

[99] Zanella A., Chiani M., and Win M. Z., "MMSE reception and successive interference cancellation for MIMO systems with high spectral efficiency," *IEEE Transaction on Wireless Communications*, vol. 4, no. 3, pp. 1244–1253, May 2005.

[100] Zelst A. V., "Space division multiplexing algorithms," in *Proc. IEEE 10th Mediterranean Electrotechnical Conference*, Lemesos, Cyprus, May 2000, vol. 3, pp. 1218–1221.

[101] Zheng L. and Tse D. N. C., "Diversity and multiplexing: a fundamental trade-off in multi-antenna channels," *IEEE Transactions on Information Theory*, vol. 39, no. 5, pp. 1073–1096, May 2003.